STRUCTURE, STRATIGRAPHY, AND U-PB ZIRCON-TITANITE GEOCHRONOLOGY OF THE ALEY CARBONATITE COMPLEX, NORTHEAST BRITISH COLUMBIA: EVIDENCE FOR ANTLER-AGED OROGENESIS IN THE FORELAND BELT OF THE CANADIAN CORDILLERA

by

Duncan Forbes McLeish
B.Sc., Dalhousie University, 2008

A Thesis Submitted in Partial Fulfillment
of the Requirements for the Degree of

MASTER OF SCIENCE

in the School of Earth and Ocean Sciences

SUPERVISORY COMMITTEE

Structure, stratigraphy, and U-Pb zircon-titanite geochronology of the Aley carbonatite complex, northeast British Columbia: Evidence for Antler-aged orogenesis in the Foreland Belt of the Canadian Cordillera

by

Duncan F. McLeish
B.Sc., Dalhousie University, 2008

Supervisory Committee

Dr. Stephen T. Johnston (School of Earth and Ocean Sciences, University of Victoria)
Supervisor

Dr. Dante Canil (School of Earth and Ocean Sciences, University of Victoria)
Departmental Member

Mitch G. Mihalynuk (British Columbia Geological Survey)
Outside Member

Supervisory Committee

Dr. Stephen T. Johnston (School of Earth and Ocean Sciences, University of Victoria)
Supervisor

Dr. Dante Canil (School of Earth and Ocean Sciences, University of Victoria)
Departmental Member

Mitch G. Mihalynuk (British Columbia Geological Survey)
Outside Member

ABSTRACT

The tectonic significance and age of carbonatite intrusions in the western Foreland Belt of the Canadian Cordillera are poorly constrained. Recent 1:5,000 scale field mapping of one of these carbonatite intrusions, the Aley carbonatite (NTS 94 B/5), has demonstrated that it was emplaced as a syn-kinematic sill, coeval with a major nappe-forming tectonic event. Determining the age of the Aley carbonatite therefore provides a means of directly dating tectonism related to carbonatite magmatism. A U-Pb titanite age of 365.9 +/- 2.1 Ma was obtained from the Ospika pipe, an ultramafic diatreme spatially and genetically related to the carbonatite. We interpret the Late Devonian age of the Ospika pipe to be the minimum possible age of the carbonatite and syn-magmatic nappe-forming tectonic event. The maximum possible age of the carbonatite is constrained by the Early Devonian age of the Road River Group (*ca.* 410 Ma), the youngest strata intruded by carbonatite dykes and involved in the nappe forming event. Our dating results for the Aley carbonatite closely correlate with U-Pb zircon and perovskite ages obtained for the Ice River carbonatite complex in the western Foreland Belt of the southern Canadian Cordillera, and support the interpretation of carbonatite intrusions of the western Foreland Belt as genetically linked components of an alkaline-carbonatitic magmatic province. Structural, stratigraphic, and geochronological data from the Aley area indicate that deformation was similar in style to, and coeval with, structures attributable to the Antler Orogeny, and are consistent with the Antler orogen having extended the length of Cordilleran margin from the southern United States to Alaska. Deformed alkaline-carbonatite intrusions that characterize continental suture zones in Africa and Tibet may provide an analogue for the Aley carbonatite and correlative alkaline-carbonatite complexes in the western Foreland Belt.

TABLE OF CONTENTS

LIST OF FIGURES

ACKNOWLEDGMENTS

My sincerest thanks and gratitude must foremost be extended to Dr. Stephen Johnston for his patient mentorship, enthusiastic encouragement, and, most of all, his thorough, insightful, and constructive criticism – all of which have been generously provided over the course of the past five years. Stephen, beyond your supervision, you have inspired me to think critically in every facet of life and have shown me the value of succinct, persuasive writing; I will likely spend the rest of my life trying to master these skills.

I am also indebted to my committee members, Dr. Dante Canil, for inspiring and helping me to understand the often challenging yet captivating world of alkaline rock petrology, and Mitch Mihalynuk, for showing me how to map efficiently and effectively in the mountains and for generously donating your time to finding me BCGS map data for the project. In addition Dante, Mitch, and Dr. Bernard Guest (external examiner, University of Calgary) are thanked for their thorough reviews of this thesis; their critiques have resulted in significant improvements to the text.

Dr. Jim Mortensen and Dr. Rich Friedman (UBC) are thanked for allowing me to be involved in nearly all aspects of the U-Pb dating work and patiently teaching me geochronology sample preparation and analytical techniques, all of which were a great learning experience.

Further thanks are extended to Dr. Anton Chakhmouradian (University of Manitoba), with whom I had the great fortune of mapping with on the Aley carbonatite in 2010, and with whom I had fascinating conversations on possible global analogues for the Aley carbonatite. Much gratitude is owed to Jeremy Crozier and Taseko Mines Ltd. for initiating and supporting the 2010 mapping work.

Dr. Andrew Hynes, Dr. Cees van Staal, Dr. Sandra Wyld, and Anonymous are thanked for their constructive reviews of a journal paper manuscript version of Chapter 2.

Thanks to my fellow grad students at UVic SEOS for providing good camaraderie, places to stay, academic guidance, pub discussions, and for helping build a SEOS grad social network from the ground up. Thanks to Tyler Ambrose for putting up with me for 26 straight field days in the bush. Finally, thanks to Caroline and my family for all the support, care, and understanding over the years.

Funding for this work was provided in part by NSERC grants to Dr. Johnston and a Geoscience BC award to the author.

Frontispiece: View looking south across the Aley carbonatite complex with the northern Rocky Mountain Main Ranges (Muskwa Range) in the background.

CHAPTER 1

Introduction

1.1 Motivation for study

The Neoproterozoic to Devonian succession of proximal clastic, distal shale, and platform carbonate strata of the Foreland Belt of the Canadian Cordillera is commonly interpreted to represent a Paleozoic Atlantic-style passive margin along the western edge of Laurentia (paleo-North American plate; e.g. Monger et al. 1972; Price, 1994; Miall and Blakely, 2008; Fig. 1.1). However, Middle to Upper Paleozoic strata of the western Foreland Belt contain evidence of widespread contractional deformation, including voluminous alkaline-carbonatite igneous complexes, and westerly derived coarse siliciclastic sediments (Figs. 1.1 & 1.2). Determining the implications of Middle to Late Paleozoic tectonism for conventional Foreland Belt passive margin models is made difficult by a dearth of geochronological and geological data. Limited geochronological data exist for a single carbonatite complex, and many Foreland Belt alkaline-carbonatite complexes and related volcanic sequences are known only through limited, regional-scale geological mapping. Precise geochronological constraints and detailed mapping are required in order to determine if alkaline-carbonatite magmatism was coeval with episodes of contractional deformation and coarse clastic sedimentation, and if eastern Foreland Belt passive margin sedimentation was concurrent with this magmatism.

Resolving the relationship between Paleozoic tectono-magmatic activity in the western Foreland Belt and passive margin sedimentation in the eastern Foreland is an essential step to modelling the western growth of Laurentia. Paleozoic tectono-magmatic activity in accreted terranes west of the Foreland Belt is explained by recognising them as parautochthonous or allochthonous with respect to Laurentia. In contrast, the Foreland

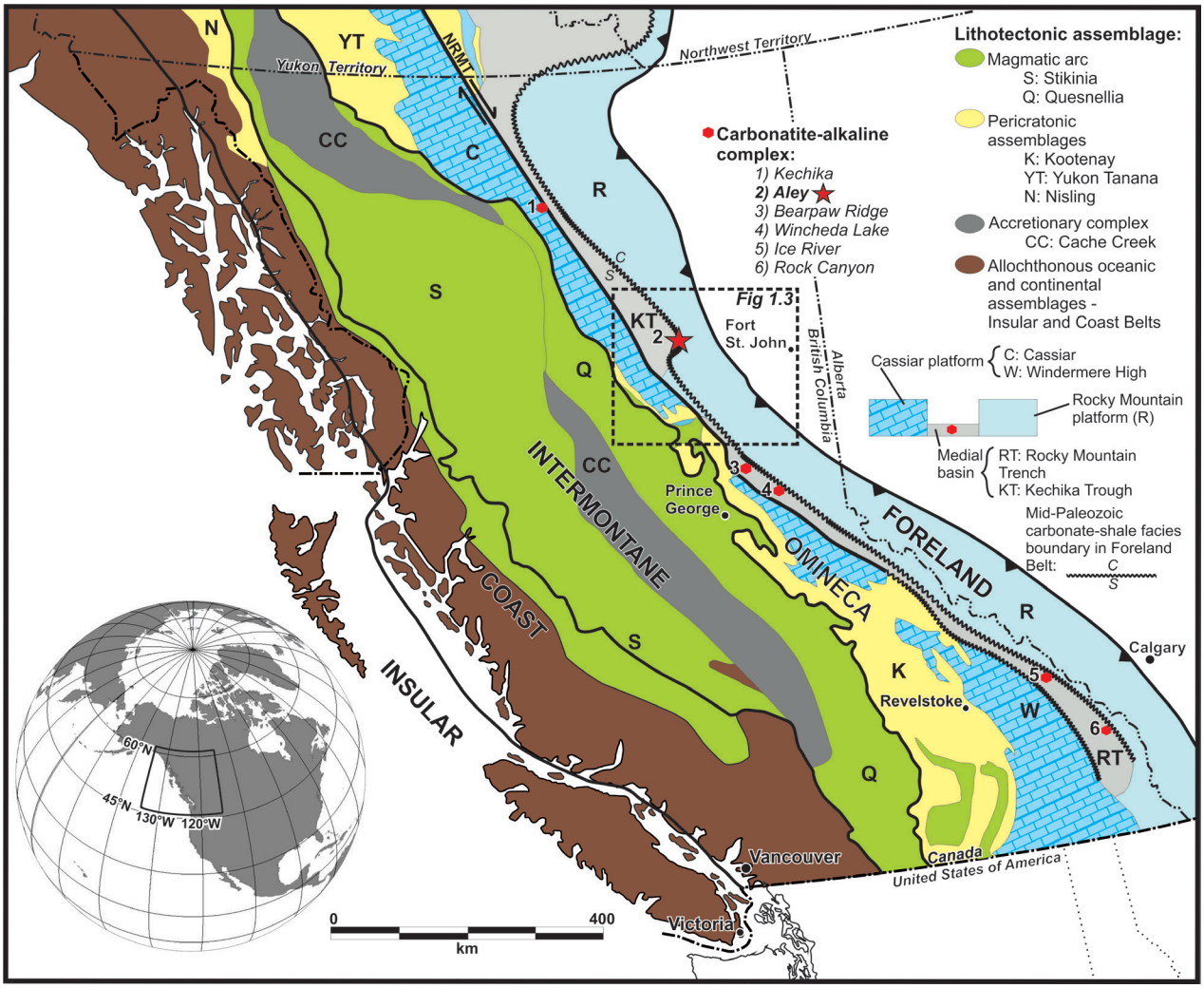

Figure 1.1: Overview map of the British Columbian segment of the Canadian Cordillera. First-order lithotectonic and morphological subdivisions and known Foreland Belt alkaline-carbonatite complexes are shown in reference to the transition of early Paleozoic continental platform and slope facies to deep-water basinal facies.

Belt is widely considered to be autochthonous with respect to Laurentia. This interpretation requires that Paleozoic tectonism and alkaline magmatism in the western Foreland Belt be explained within the context of a passive margin setting, which raises the question of whether or not passive margin models can be sufficiently modified to account for the record of mid-Paleozoic tectono-magmatic activity in the western Foreland Belt. If the tectono-magmatic record of the western Foreland Belt cannot be reconciled with the passive margin record of the east, a major structural break must exist within the central Foreland Belt, and the western Foreland Belt must be considered exotic relative to the eastern Foreland Belt.

1.2 Objectives and structure

This thesis examines one of the Foreland Belt alkaline-carbonatite complexes, the Aley carbonatite. The Aley carbonatite is among the largest and best exposed of the Foreland carbonatites; is spatially related to alkaline volcanic rock and coarse conglomerate and siliciclastic rocks that characterize its host stratigraphy; and is located just west of the Foreland Carbonate-to-Shale (C-S) facies boundary that delineates shale-dominated western and carbonate-dominated eastern provinces of the Foreland belt. Specific objectives of this thesis are:

- to map in detail the Aley carbonatite
- to determine the geometry and structure of the carbonatite
- to assess the relative timing of magmatism and deformation to constrain the age of magmatic events that characterize the Aley region, including volcanic sequences of the Skoki Formation, the Aley carbonatite and related

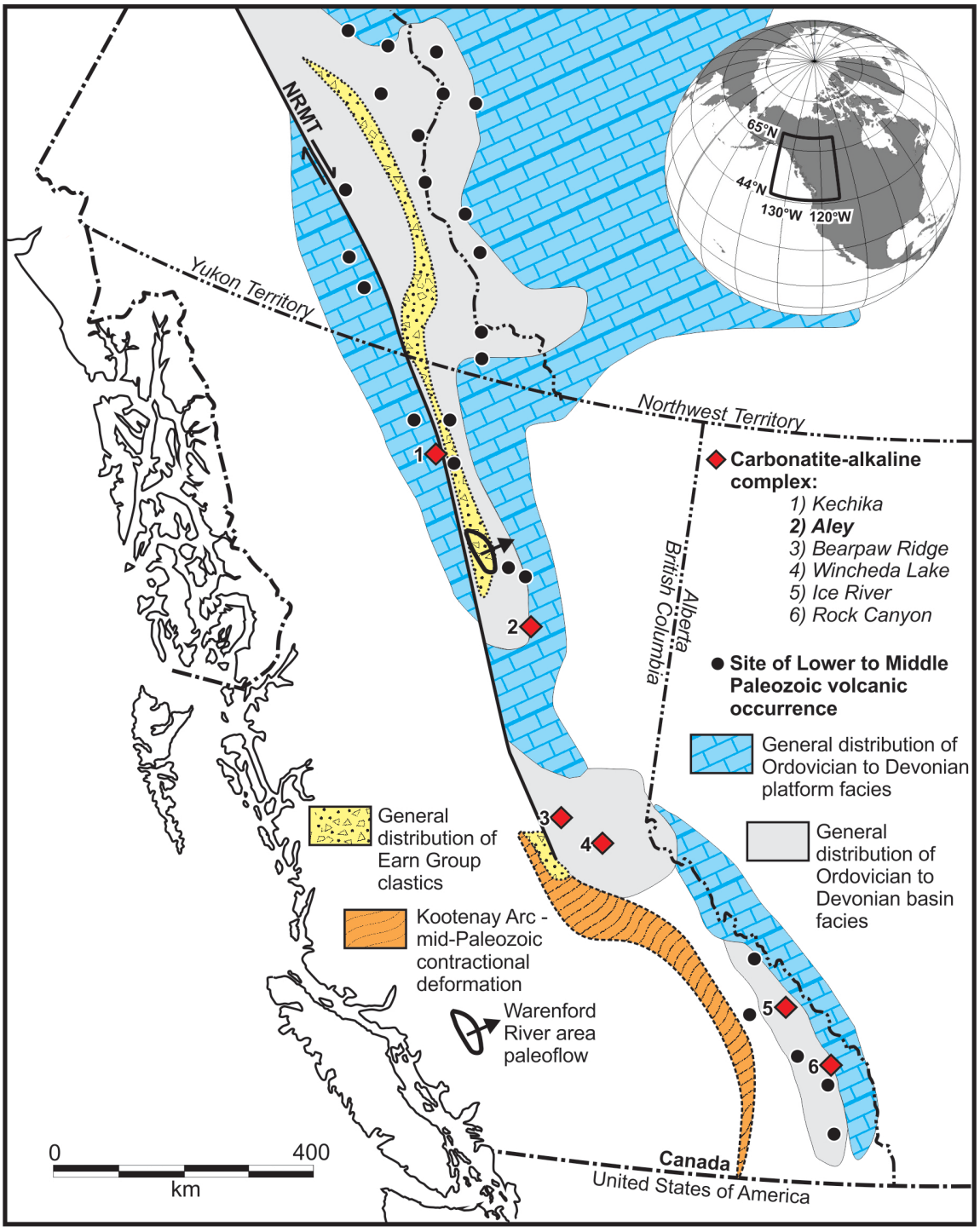

Figure 1.2: Distribution of early and mid-Paleozoic alkaline volcanic and carbonatite occurrences in the Foreland Belt of the Canadian Cordillera, revised after Goodfellow et al. (1995), shown with areas recording mid-Paleozoic deformation and/or coarse clastic sedimentation (in part after Gordey et al. 1987 and Smith et al. 1993).

lamprophyre dykes, and an intrusive diatreme pipe (the Ospika pipe) that is spatially associated with the Aley carbonatite.

- to discuss, using the geologic record of the Aley map area as a proxy, whether or not the tectonic, stratigraphic, and magmatic record of the western Foreland Belt, can be reconciled with that of the eastern Foreland Belt, and if not, examine alternative hypotheses for western Foreland Belt evolution.

These objectives are addressed in the two separate papers which comprise this thesis. Chapter 2, "The Upper Devonian Aley carbonatite complex: A product of Antler orogenesis in the western Foreland Belt of the Canadian Cordillera", presents the results of detailed structural mapping of the carbonatite complex, addresses the structural controls on emplacement and structural evolution of the carbonatite, discusses implications for the evolution of a Foreland Belt and the potential alkaline-magmatic province contained therein, and examines analogues with other syn-orogenic carbonatites worldwide. Chapter 2 was co-authored with Dr. Stephen T. Johnston.

Chapter 3, "Stratigraphy and U-Pb zircon-titanite geochronology of the Aley carbonatite complex, northeast British Columbia: Evidence for Antler-aged orogenesis in the Foreland Belt of the Canadian Cordillera", presents the results of U-Pb zircon-titanite dating efforts on the carbonatite and spatially related Ospika pipe diatreme and Skoki Formation (Lady Laurier) volcanics, in addition to investigating the host stratigraphic succession for evidence of mid-Paleozoic tectonic activity. The absolute magmatic ages obtained in the Chapter 3 study help constrain the age of syn-magmatic deformational events identified in Chapter 2 and further evaluate links between mid-Paleozoic tectono-

magmatic events in the western Foreland Belt. Chapter 3 was co-authored with Dr. Stephen T. Johnston, Dr. Richard M. Friedman, and Dr. James K. Mortensen.

Appendix A contains supplementary geochronological data and analytical methods. Appendix B provides an archive of all structural field data collected, geographically referenced with field station UTM coordinates. Appendix C and D respectively contain supplementary photomicrographs and field photos which were not suitable for inclusion in Chapter 2 and 3 papers due to publisher space restrictions. Finally, Appendix E contains two 1:5,000 scale master field maps plotted with supporting geologic data.

1.3 Location, physiography, and climate

The Aley carbonatite complex is located within the Main Ranges of the northern Canadian Rocky Mountains in northeastern British Columbia (NTS map sheets 94 B/5 and 94 B/12), 140 kilometres north-northeast of the Mackenzie, 120 kilometres northwest of Hudson's Hope, and 20 kilometres northeast of the confluence of the Ospika River and Williston Lake (Figs. 1.1 and 1.3). The carbonatite outcrops in the alpine and sub-alpine of a northwest trending ridge that bounds the southern aspects of the Aley Creek valley. Relief is significant with elevations ranging from 1300 metres in u-shaped glacial sub-alpine valleys to greater than 2200 metres on surrounding unnamed alpine peaks.

Climate in the area is typical of the northern Canadian Rocky Mountains. Weather observations of previous workers (see History) and those of the author show winter conditions, typified by heavy snow fall and cold temperatures, to persist from early October to early May. Mean temperatures increase rapidly with the onset of spring in May. South-facing sub-alpine slopes are typically snow free by late May to early June;

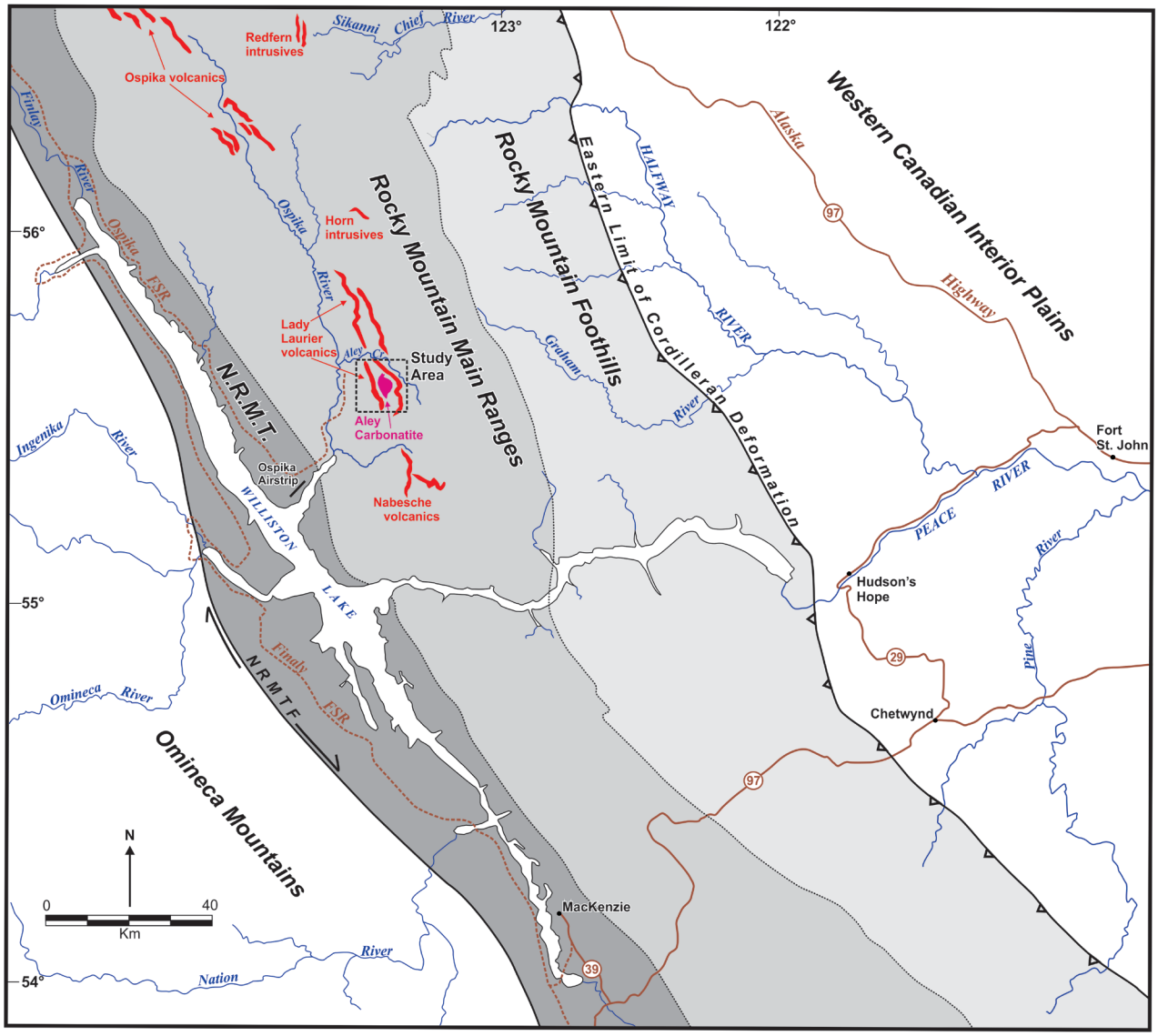

Figure 1.3: Location map showing the study area in reference to the greater Williston Lake area. First-order physiographic subdivisions of the Foreland Belt are shown in various shades of grey. Abbreviations: Northern Rocky Mountain Trench (NRMT) and Northern Rocky Mountain Trench Fault (NRMTF).

north-facing slopes and alpine areas remain snow covered until mid to late June, although peaks and avalanche paths may retain snow year-round. July and August are relatively warm and dry with most precipitation limited to short-lived, but often heavy, rain storms. Snow returns to the higher elevations in late August to early September and covers valley bottoms by late September to early October. Field seasons are consequently limited to the June-September period.

1.4 Access

Road access to within 8 kilometres of the study area is possible via a loose-surface, seasonal 4WD forest service road network that originates from the end of the provincially maintained paved Highway 39 in Mackenzie (approx. 8 hours driving from Mackenzie; Fig. 1.3). Helicopter fly-camps can be staged from cut-blocks near the end of the logging road network on the east side of the Ospika River (10 km flight), or from the fix-wing serviceable gravel airstrip at the former Ospika logging camp (30 km flight). Fixed-wing and rotary aircraft can be charted from the full-service airport in Mackenzie. At time of this writing, Taseko Mines Ltd. is evaluating plans to drive a road into the study area to service ongoing niobium exploration programs on the carbonatite.

1.5 Methods of investigation

Field work for both studies presented in this thesis was carried out from July 6 to August 4, 2009. A single fly-camp located in an alpine cirque near the centre of the carbonatite was the basis for all field mapping and sampling operations. Mapping traverses were completed by the author and Tyler Ambrose (field assistant) entirely on foot with the exception of one helicopter set-out. Additional mapping support was graciously provided by Dr. Stephen T. Johnston (Supervisor, University of Victoria) and

Mitch G. Mihalynuk (British Columbia Geological Survey) during their one week visit to the study area. Mapping was completed using a conventional station-based recording system where lithological, structural, and sampling data are collected and assigned to a GPS georeferenced waypoint with unique station ID. All GPS measurements were accurate to within ~5 metre. Representative samples were taken from all major units for structural and petrologic thin-section microscopy. All intrusive and volcanic units were sampled for U-Pb dating and a quartzite clast-bearing conglomerate unit was sampled for detrital zircon geochronology.

Digital map preparation and structural data interpretation took place at the University of Victoria using Manifold System, MapInfo Professional with Discover add-on, and GEOrient software. Following petrographic analyses at the University of Victoria, the author selected suitable samples for U-Pb geochronological analysis at the University of British Columbia (UBC). The author performed geochronological sample preparation and mineral selection at UBC under the guidance of Chapter 3 co-authors Dr. James Mortensen and Dr. Richard Friedman. U-Pb ICP-MS and ID-TIMS isotopic analyses were performed by Dr. Mortensen and Dr. Friedman respectively with support from the author. Further analytical information is available in Chapter 3 and supporting Appendix A.

The model presented in this thesis for the structural evolution of the Aley carbonatite complex and discussion of implications for the tectonic evolution of the Canadian Cordillera have been developed primarily from the mapping, data gathering, and analyses described above.

1.6 Previous work

Irish (1970) and Thompson (1989) covered the Aley Creek area in their 1:250,000 bedrock geology maps of the Halfway River region. The carbonatite is not included on either map.

The Aley carbonatite was discovered during a 1980 Cominco Ltd. (Cominco) helicopter-based base metals exploration program covering the southern Kechika Trough. In the 1970s, several prolific SEDEX Pb-Zn deposits were discovered north of the Aley Creek area. Following surface geochemical anomalies believed to be related to SEDEX deposits along strike to the south, K. R. Pride of Cominco encountered outcrops of niobate mineral-bearing dolomite rock belonging to the Aley carbonatite (P. LeCouteur, personal communication, 2010). Cominco subsequently conducted petrological and geochemical analyses on samples from the site, and staked claims covering the entire carbonatite after a second site visit in 1982. Large-scale exploration programs, including detailed mapping, prospecting, geochemical sampling, road building, geophysical survey, and diamond drilling were carried out in the summers of 1983-1986 (Pride 1983, 1985, 1987*a* and *b*). A M.Sc. thesis examining the petrography of carbonatite phases and structure of the complex was completed in conjunction with the Cominco work (Mader, 1986). Cominco did no further work on the carbonatite after 1986.

Pell (1994) provided a synthesis of work done to date on the Aley carbonatite and performed additional fieldwork and geochemical analyses as part of a review of carbonatites, kimberlites, and related alkaline rocks in British Columbia. Johnston and Pyle (2005) visited the carbonatite in 2004 and mapped the western carbonatite-wall rock contact area. A metallurgical study of the carbonatite was carried out in the fall of 2004

by Aley Corporation, who acquired the Aley claims from Cominco that year. Taseko Mines Ltd. acquired the Aley claims in 2007 and conducted limited diamond drilling on the carbonatite (Chung and Crozier, 2008). No further mapping or structural study was performed during the 2004 Aley Corp or 2007 Taseko exploration campaigns. The only previous geochronological study of the carbonatite was that of Pride et al. (1986) as part of the Cominco work.

Since fieldwork for this thesis was undertaken, Taseko Mines Ltd. has conducted three large-scale diamond drill programs on the Aley claims (2010-2012) resulting in a preliminary niobium resource estimate being released in winter of 2012 (286 million tonnes measured and indicated resource at an average grade of 0.37% Nb_2O_5 with a 0.2% Nb_2O_5 cutoff; Simpson, 2012). The company is presently attempting to advance their Aley project to the mine permitting stage.

References cited

Chung, C.J., and Crozier, J., 2008, Assessment Report on Diamond Drilling performed on the Aley Carbonatite Property: British Columbia Ministry of Energy, Mines, and Petroleum Resources, Assessment Report 30113, 194 p.

Gordey, S.P., Abbott, J.G., Tempelman-Kluit, D., and Gabrielse, H., 1987, "Antler" clastics in the Canadian Cordillera: Tectonics, v. 11, p. 1266–1287.

Goodfellow, W.D., Cecile, M.P., and Leybourne, M.I., 1995, Geochemistry, petrogenesis, and tectonic setting of lower Paleozoic alkalic and potassic volcanic rocks, northern Canadian Cordilleran miogeocline: Canadian Journal of Earth Sciences, v. 32, p. 1236–1254.

Irish, E. J. W., 1970, Geology of the Halfway River map area, British Columbia: Geological Survey of Canada, Paper 69-11, 154 p.

Mader, U.K., 1986, The Aley Carbonatite Complex [M.Sc. thesis]: Vancouver, University of British Columbia, 176 p.

Monger, J.W.H., Gabrielse, H., and Souther, J.A, 1972, Evolution of the Canadian Cordillera: a plate tectonic model: American Journal of Science, v. 272, p. 577–602.

Miall, A.D., and Blakey, R.C., 2008, The Phanerozoic Tectonic and Sedimentary Evolution of North America, *in* Miall, A.D., ed., Sedimentary Basins of the World, Volume 5: The Sedimentary Basins of the United States and Canada, Elsevier, p. 1-29.

Pell, J., 1994, Carbonatites, nepheline syenites, kimberlites and related rocks in British Columbia: British Columbia Ministry of Energy, Mines and Petroleum Resources Bulletin 88, 136 p.

Pride, K.R., 1983, Geological Survey on the Aley Claims: British Columbia Ministry of Energy, Mines, and Petroleum Resources, Assessment Report 12018, 16 p.

Pride, K.R., 1986, 1985 Year End report on the Aley Property: Private report to Cominco Ltd., 26 p. with appendices.

Pride, K.R., 1987*a*, 1986 Year End report on the Aley Property: British Columbia Ministry of Energy, Mines, and Petroleum Resources, Assessment Report 15721, 69 p.

Pride, K.R., 1987*b*, 1986 Diamond Drilling Assessment Report: British Columbia Ministry of Energy, Mines, and Petroleum Resources, Assessment Report 16484, 59 p.

Pride, K.R., LeCouter, P.C., and Mawer, A.B, 1986, Geology and mineralogy of the Aley Carbonatite: Canadian Institute of Mining and Metallurgy, 10th District 6 Meeting, Victoria, British Columbia, Abstracts, p. 32.

Simpson, R.G., 2012, Technical report on the Aley carbonatite niobium project: NI 43-101 report prepared for Taseko Mines Ltd., Vancouver, British Columbia, 66 p.

Thompson, R.I., 1989, Stratigraphy, tectonic evolution and structural analysis of the Halfway River map area (94B), northern Rocky Mountains, British Columbia: Geological Survey of Canada Memoir 425, 119 p.

CHAPTER 2

The Upper Devonian Aley carbonatite complex, northeast British Columbia: A product of Antler orogenesis in the western Foreland Belt of the Canadian Cordillera

D.F. McLeish and S.T. Johnston [1]

[1]*School of Earth and Ocean Sciences, University of Victoria, Victoria, BC, V8W 3V6*

Originally submitted to *GEOLOGY* February 28, 2012

Resubmitted to *GEOLOGY* October 15, 2012

ABSTRACT

Paleozoic continental margin strata in the western Foreland Belt of the Canadian Cordillera are characterized in part by alkaline volcanic sequences, carbonatite intrusions, coarse clastic sedimentary units, and erosional unconformities. These strata also contain a record of mid-Paleozoic contractional deformation unseen in coeval passive margin strata in the eastern Foreland Belt. In order to test potential genetic links between Paleozoic alkaline igneous activity, active margin sedimentation, and deformation in the western Foreland Belt, and better understand their implications for the evolution of the Foreland Belt as a whole, we have undertaken a detailed mapping and structural study of the Aley carbonatite intrusion and its host strata in the western Foreland Belt of northeast British Columbia. Our work demonstrates that carbonatite emplacement was coeval with a Late Devonian contractional nappe-forming tectonic event. Interpreting tectonism as associated with continental collision along a long-lived active margin provides the best explanation for our structural and stratigraphic observations, and suggests that the western Foreland Belt is far-travelled and exotic relative to coeval passive margin strata in the eastern Foreland Belt. Deformed alkaline-carbonatite intrusions that characterize continental suture zones in Africa may provide an analogue for the Aley carbonatite and correlative alkaline-carbonatite complexes in the western Foreland Belt.

2.1 Introduction

The late Neoproterozoic to Devonian stratigraphy of the Foreland Belt (Fig. 2.1) of the Canadian Cordillera includes proximal clastic strata, distal shales and platformal carbonates that together are commonly interpreted as recording rift to drift passive margin development along the western edge of Laurentia during the break up of a Neoproterozoic supercontinent, Rodinia (*e.g.* Price, 1994). A commonly proposed analogue for the development of this succession is the Jurassic-Recent growth of the Atlantic passive margins (*e.g.* Monger et al. 1972; Miall and Blakely, 2008), and 'Atlantic-type' geodynamic models have been applied to explain the evolution of Paleozoic Foreland Belt strata (*e.g.* Thompson,1989). However, three characteristics distinguish Paleozoic Foreland Belt strata from the Atlantic passive margin system: (1) lower to middle Paleozoic basinal strata of the western Foreland Belt contain alkaline-carbonatite intrusions and volcanic units that span 150 Ma, indicating that the continental margin was magmatically active throughout its evolution (Goodfellow et al., 1995); (2) the northern and central Foreland Belt contains mid-Paleozoic polymictic and chert-pebble conglomerate and coarse chert-quartz sandstone derived from the west, requiring the presence of a source terrane that lay outboard of the continental margin (Gordey et al., 1987; Smith et al., 1993); and (3) sections of the western Foreland Belt record mid-Paleozoic contractional deformation that occurred concurrently with stable subsidence in the eastern Foreland Belt (Root, 2001).

The departures of the western Foreland belt stratigraphic and structural record from that expected of an Atlantic-style margin raise two fundamental questions: (1) can a passive margin model be modified enough to accommodate the magmatic, sedimentary and structural characteristics of the western Foreland belt; and (2) what, if any, is the

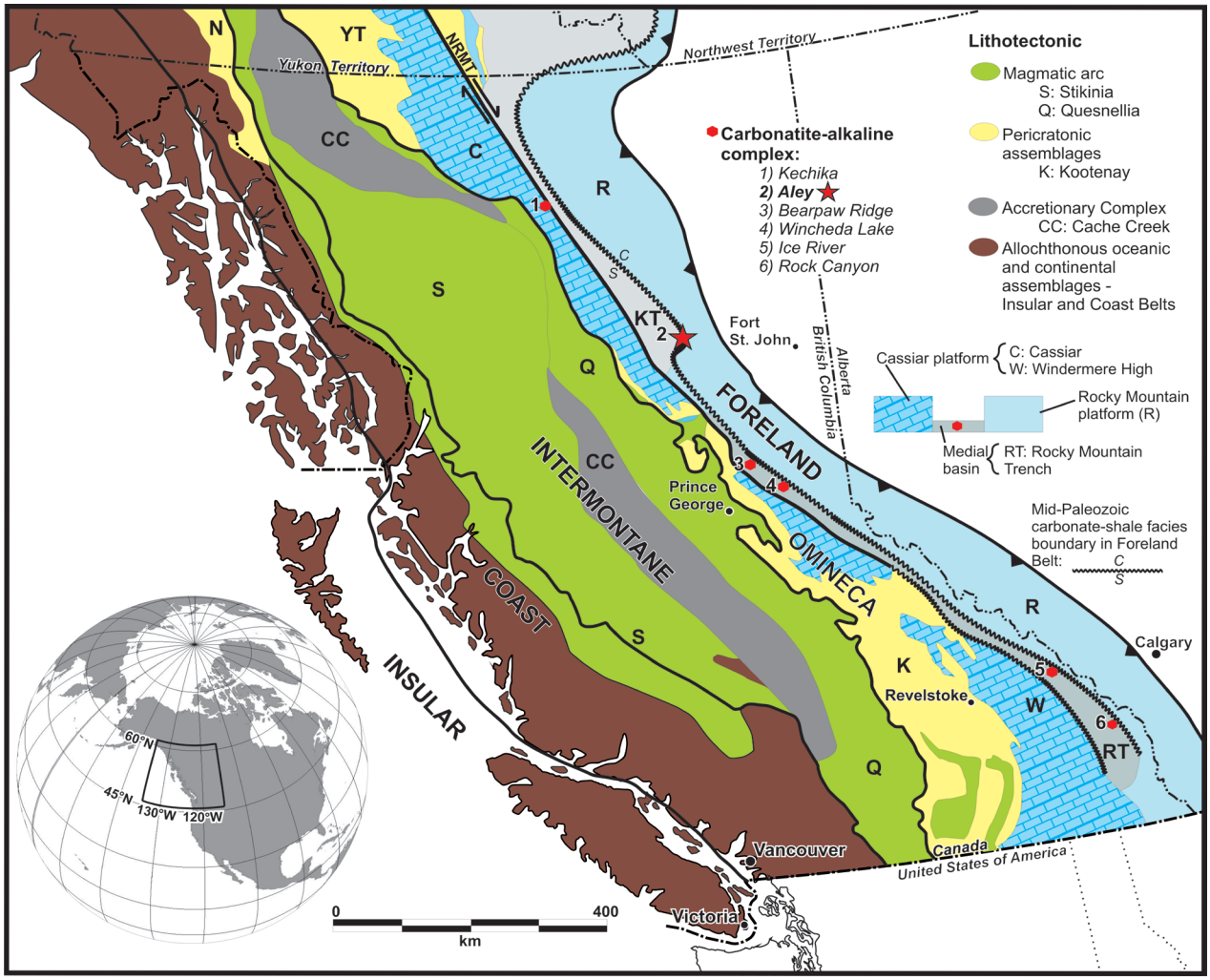

Figure 2.1: First-order morphological subdivisions of the Canadian Cordillera with known Foreland Belt alkaline complexes shown in reference to the transition of early Paleozoic continental platform and slope facies to deep-water basinal facies. This transition is also known as the Carbonate-to-Shale, or C-S, boundary. Alkaline complex localities in part after Pell (1994); facies boundary after Wheeler and McFeely (1991). The distribution of Paleozoic alkaline volcanic rocks in the Foreland Belt (not shown) closely mirrors that of the carbonatite complexes. East of the C-S boundary, the Foreland Belt contains little record of igneous activity in the early to mid-Paleozoic.

relationship between the magmatism, sedimentation and deformation within the western Foreland belt? To address these questions, we mapped and undertook a detailed structural study of one of the carbonatite intrusions of the western Foreland belt, the Aley carbonatite complex (Fig. 2.1). We demonstrate that the Aley carbonatite is a syn-kinematic sill whose emplacement was coeval with a Late Devonian contractional nappe-forming tectonic event. Our data are best explained by a model of Devonian collision along a long-lived mid-Paleozoic active margin.

2.2 General geology

The Aley region is characterized by a Lower to Middle Paleozoic stratigraphic sequence that is divisible, from oldest to youngest, into the Kechika and Skoki Formations, and the Road River Group. Igneous units include the Aley carbonatite, the Ospika pipe, and a suite of lamprophyre dykes (Fig. 2.2). The Kechika Formation is less than 1000 m thick, and consists of argillaceous limestone, calcareous siltstone and cream-coloured dolostone. Its stratigraphic base is characterized by a heterogeneous volcano/sedimentary layer that includes tuff, breccia, conglomerate and pillow lava. Conodonts from the uppermost Kechika Formation indicate an Early Ordovician age (Pyle and Barnes, 2001). The younger Skoki Formation consists of upper and lower grey dolostone layers separated by a volcanic layer, and is about 500 metre thick. Fossils constrain the age of deposition to the early Late Ordovician (Thompson, 1989). The Road River Group is more than 1000 metre thick and consists of chert rich dolostone, shale, argillaceous limestone and rare quartzite and quartz pebble conglomerate. Paleontological data indicate an age of Late Ordovician to Early Devonian (Pyle & Barnes, 2001). Regional metamorphism of these strata to lower greenschist facies is indicated by the presence of fine grained white mica in

siliciclastic units (Mader, 1986); primary sedimentary features, including bedding, graded bedding, ripple marks and scour surfaces are, however, well preserved throughout the sequence (Thompson, 1989).

The Aley carbonatite intrudes the stratigraphic sequence as indicated by the presence of a contact metasomatic aureole characterized by fenitization of the wallrocks (Mader, 1986) and by carbonatite dykes that cut the wallrocks and which root into the main intrusion (Figs. 2.3*B&D*). The carbonatite-host rock contact is everywhere parallel to bedding, and occurs at a uniform stratigraphic level located near the stratigraphic base of the Kechika Formation. These observations imply that the carbonatite intrusion was emplaced as a sill-like body. Dolomite and a volumetrically minor calcite carbonatite phase characterize the intrusion. The calcite carbonatite phase commonly occurs adjacent to the contact with the wallrocks to the intrusion. Dolomite carbonatite dykes cut calcite carbonatite dykes indicating the dolomite phase post-dates the calcite phase (Fig. 2.3*D*). Apatite is a common accessory mineral. K-Ar ages cooling ages of 349 ± 12 and 339 ± 12 Ma on phlogopite separated from samples of lamprophyre dykes that intrude and post-date the fenitized contact aureole to the carbonatite, imply an Early Mississippian or earlier age of for the intrusion (Pride et al., 1986). The Ospika pipe, a 50 metre wide ultramafic diatreme, intrudes the Skoki Formation 500 metres west of the western margin of the Aley carbonatite; Rb-Sr and K-Ar geochronological data support a temporal link between the pipe and the Aley carbonatite with mica separates from the pipe yielding cooling ages of 334 ± 7 and 323 ± 10 Ma (Pell, 1994). U-Pb titanite data indicate a 365.9 ± 2.1 Ma crystallization age for the igneous matrix of the pipe (McLeish et al., 2013).

2.3 Structural geology

2.3.1 Stratigraphic units

Geopetal features observed in the Kechika and Skoki Formations and the Road River Group indicate that the entire stratigraphic package is overturned (Fig. 2.3*H*). The distribution of the stratigraphic units corroborates an overturned orientation for the sequence (Fig.2.2*D*). Overturning of the stratigraphic sequence is explained as the result of folding (F_1). Outcrop scale, locally rootless, isoclinal folds with wavelength and amplitudes of 1 metre and 0.5 metre, respectively, are interpreted as parasitic F_1 folds (Fig. 2.3*B*). Viewed downplunge, the isoclinal folds describe an S-geometry. An axial planar cleavage (S_1) is most commonly manifested as a penetrative, bedding parallel cleavage which is best developed in more pelitic layers throughout the stratigraphic sequence. Low angle extensional shears transect S_0 and S_1, thin the stratigraphic sequence, and, because of the overturned geometry of the host strata, cut structurally down-section in the direction of transport into younger and younger strata (Fig. 2.3*E*). As described below, these shears are commonly intruded by massive to weakly foliated dolomite carbonatite.

We interpret the overturned geometry of the stratigraphic sequence, the S-geometry of F_1 outcrop scale folds, the S_1 bedding parallel cleavage and the extensional shears as products of a D_1 tectonic event. The overturned strata suggest that crust in the study area occupies the lower limb of a recumbent nappe (Fig. 2.*3L&M*). The parasitic S-geometry of the outcrop-scale F_1 folds is consistent with a nappe interpretation as is the ubiquitous, bedding parallel S_1 cleavage. In this interpretation, the extensional shears are inferred to characterize the footwall of the nappe, developing in response to and

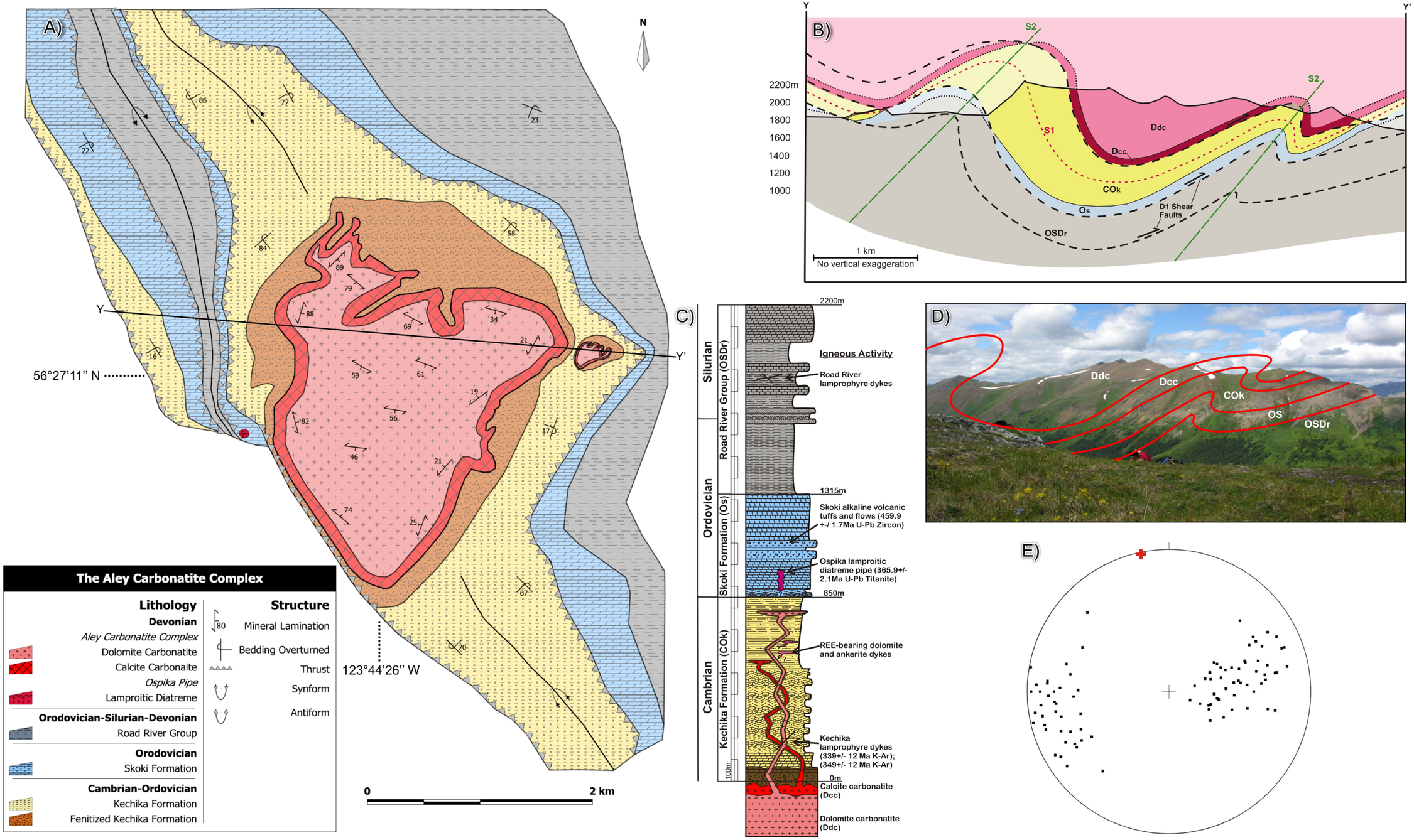

Figure 2.2: Geology and structure of the Aley carbonatite complex and host stratigraphy. (A) Geological map of complex (in part, after Mader, 1986), (B) geological cross-section, (C) idealised stratigraphic column (in part, after Pride et al., 1986), (D) east-west profile view of complex from south showing distribution of major map units, and (E) equal-angle stereonet plot of poles to bedding from cross-section transect of map area showing F_2 fold morphology. Red plus sign is calculated beta axis. Data from the hinge areas of F_1 folds are excluded from this plot.

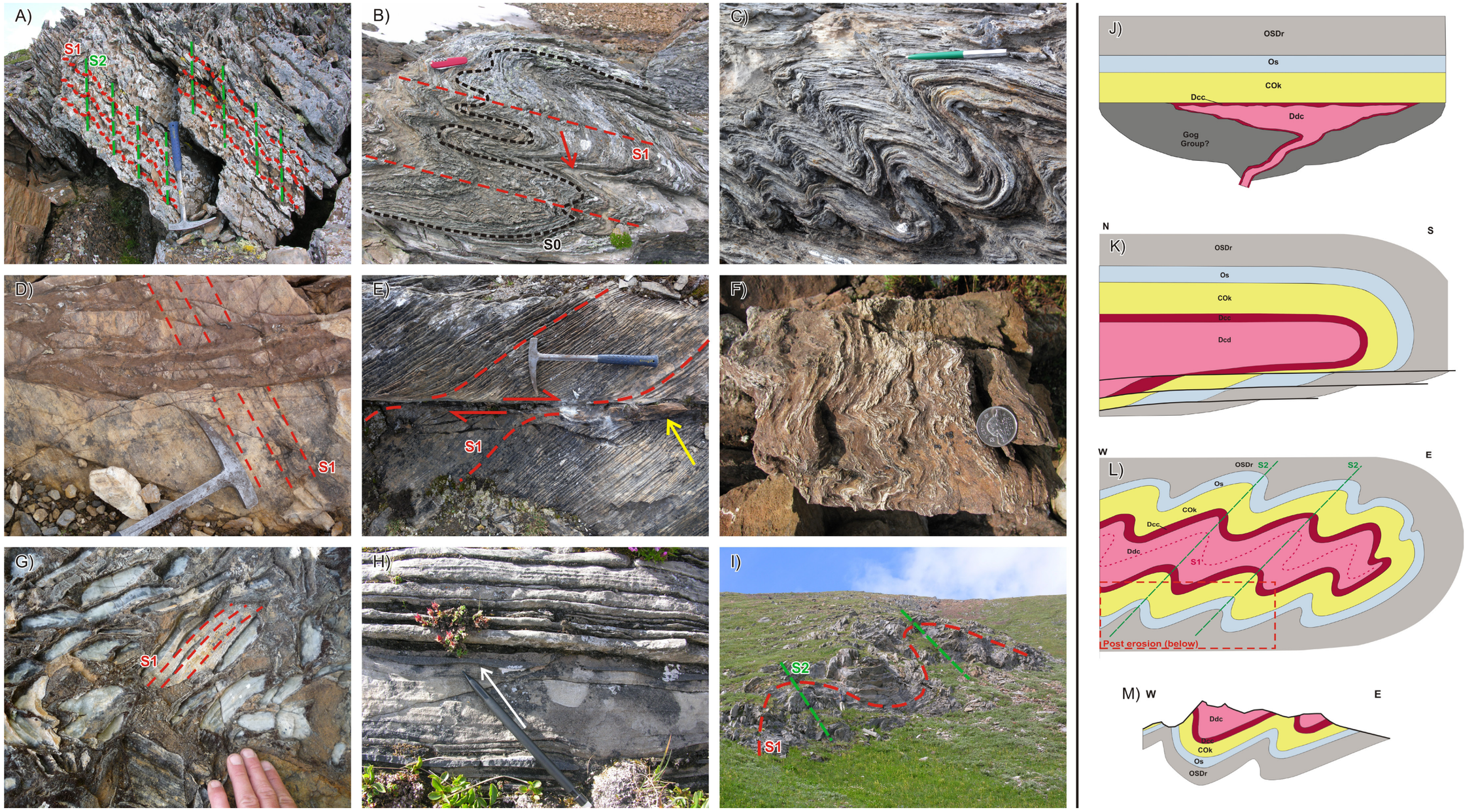

Figure 2.3: Field photographs depicting key structural relationships and schematic depiction of the evolution of the Aley carbonatite complex. (A) S_1 and S_2 foliations in fenitized Kechika Formation; (B) F_1 folds with S_1 axial planar, bedding-parallel cleavage, and concordant calcite carbonatite vein (red arrow) in fenitized Kechika Formation; (C) south-verging isoclinal F_1 folds in fenitized Kechika Formation; (D) late dolomite carbonatite veins cross-cutting S1 fabric in calcite carbonatite; (E) low-angle D_1 shear with dolomite carbonatite vein (yellow arrow) intruding along shear plane; (F) parasitic F_1 folds in dolomite carbonatite float showing characteristic S_{cd} fabric in F_1 fold hinge; (G) S_1 fabric developed in xenoliths of Road River Group in the Ospika pipe; (H) overturned scour surfaces (white arrow) in Road River Group strata indicating that host stratigraphy is overturned; and (I) F_2 folds in Road River Group strata; (J) carbonatite intrudes along the base of the Kechika Formation in the Late Devonian; (K) Late Devonian contractional deformation event (D_1) forms south-verging nappe cored by carbonatite; (L) Nappe undergoes F_2 folding during Rocky Mountain deformation; (M) Cenozoic erosion removes the upper limb of the nappe.

accommodating continued crustal shortening and late-stage translation of the overlying nappe structure (Fig. 2.3*K*).

The S_1 cleavage and D_1 extensional shears are folded. Fold axes of these younger F_2 folds are shallowly plunging and trend NNW - SSE. The folds verge east northeast, are open and asymmetric with long, shallowly dipping west limbs, short, steeply dipping east limbs and steeply west-dipping axial planes (Fig. 2.2*E*). They range in size from outcrop-to map-scale folds. A weakly-developed, spaced axial planar cleavage (S_2) is evident in and adjacent to F_2 fold hinges (Figs. 2.*3A&I*).

2.3.2 Aley carbonatite and related intrusions

The sill-like carbonatite intrusion occupies the topographically highest portions of the study area, structurally above the overturned Kechika Formation. A planar fabric, hereafter referred to as S_{cc} and S_{cd} in the calcite and dolomite phases, respectively, characterizes the carbonatite. In both phases the planar fabric is defined by a moderate to strongly-developed parallelism of mm-scale apatite layers, and by alignment of apatite mineral grains. In the calcite carbonatite phase along the margins of the intrusion, S_{cc} parallels the contact and S_0 and S_1 in the adjacent wallrocks. Centimetre to metre-scale calcite carbonatite sills are deformed into isoclinal F_1 folds together with the host wallrocks (Fig. 2.3*B*). S_{cc} is characterized by a transposition foliation, defined by centimetre-scale isoclinals folds of the apatite layers, that commonly exhibit the same S-shaped geometry as the F_1 folds observed in the adjacent wallrocks. Based on the parallelism of S_{cc} with S_1, on the presence of intrafolial folds affecting S_{cc} that mimic the F_1 folds, and by isoclinal F_1 folding of outcrop-scale calcite carbonatite sills, we interpret S_{cc} as a tectonic foliation that developed in the carbonatite early during the D_1, nappe-

forming tectonic event. Such an interpretation implies that the bedding-parallel contact between the carbonatite and the Kechika Formation is the overturned top of the sill-like intrusion (Fig. 2.3*J*).

The S_{cd} foliation in the younger dolomite phase, although broadly parallel to S_{cc} / S_0 / S_1, is locally discordant. Massive to weakly foliated dolomite phase carbonatite intrudes across and locally truncates and brecciates calcite carbonatite and its S_{cc} fabric (Fig. 2.3*D*). Massive to weakly foliated dolomite carbonatite commonly intrudes the D_1 extensional shears mapped in the wallrocks to the Aley carbonatite (Fig. 2.3*E*), and rare dolomite carbonatite dykes intrude along the S_1 cleavage in the wallrocks. We interpret these features as showing that the carbonatite magmatism was syn-kinematic with D_1 nappe and related fabric formation. Calcite carbonatite intrusion occurred early during D_1 deformation and developed an axial planar foliation (S_{cc}) that was subsequently truncated by syn- to post-kinematic dolomite carbonatite. Syn-kinematic intrusion of the bulk of the dolomite carbonatite is indicated by its overall concordant structure and fabric; post-kinematic magmatism is indicated by locally massive, non-foliated dolomite carbonatite; by truncation of S_{cc}; and by intrusion along pre-existing extensional shears and S_1 cleavage planes in the wallrocks to the Aley carbonatite.

The ultramafic matrix of the Ospika pipe (Fig 2.3*G*) is massive, and is characterized by a primary crystalline igneous texture. Abundant crustal xenoliths are randomly oriented. Bedded sedimentary xenoliths are characterized by a well-developed bedding parallel cleavage. Bedding and cleavage in the xenoliths truncates against and does not continue into the igneous matrix of the diatreme. Similarly, the well bedded Skoki Formation wallrocks to the diatreme are characterized by a bedding parallel

cleavage (S_1) that is truncated by and pre-dates the diatreme. These observations suggest that the Ospika pipe post-dates D_1 deformation, and intruded into, and incorporated xenoliths of the structurally underlying Road River Group, a deformed crustal sequence already characterized by a bedding parallel cleavage. In this interpretation, the bedding parallel cleavage observed in the randomly oriented xenoliths within the diatreme is inferred to be the S_1 cleavage observed in the wallrocks to the diatreme.

Overprinting the F_1 nappes and coeval structures are asymmetric F_2 folds observed in the wallrocks (Fig. 2.3*I*) affecting the carbonatite and the carbonatite – wallrock contact. The mapped distribution of the intrusion is attributable to F_2 folding, as the carbonatite occupies the cores of two, asymmetric ENE-verging, map-scale F_2 synforms; the main, westerly synform is cored by the largest carbonatite exposure, and is separated from a smaller, more easterly synform by wallrocks that occupy the core of the intervening antiform. F_2 folds of the S_{cc} and S_{cd} fabric in the carbonatite are geometrically indistinguishable from the F_2 folds observed in the wallrocks.

3.2.3 Constraining the timing of deformation

Strata of the Late Ordovician to Early Devonian Road River Group are overturned, occupy the lower limb of the D_1 nappe, and are characterized by the S_1 cleavage. As they are the youngest strata cut by the carbonatite, they provide a maximum age constraint for D_1. The Ospika pipe cuts the wallrocks and their contained D_1 structures, providing a minimum age constraint for D_1. Hence D_1 occurred prior to 366 Ma (Late Devonian), the crystallization age of the igneous matrix of the Ospika pipe, but after the Early Devonian as constrained by the age of the youngest strata in the deformed Road River Group. Although the syn-kinematic Aley carbonatite provides a means of

directly determining the age of D_1, no direct age determination is available for the carbonatite. Because the carbonatite is deformed it must have intruded prior to the 366 Ma intrusion of the post-tectonic Ospika pipe. We argue that the close spatial relationship, and the similar ultramafic, silica-undersaturated, alkalic nature of the Aley carbonatite, the lamprophyre dykes and the Ospika pipe imply a cogenetic relationship. Such a cogenetic relationship: (1) is consistent with the 349 Ma K-Ar phlogopite cooling age from a lamprophyre dyke that post-dates the carbonatite contact aureole; (2) requires that Ospika pipe emplacement occurred soon after the syn-tectonic intrusion of the Aley carbonatite; and (3) implies a Middle to Late Devonian age for D_1 deformation, including formation of the crustal scale nappe that produced an inverted stratigraphy in the Aley region.

F_2 folds affect the host strata, the contact, all major carbonatite fabrics (S_{cc} and S_{dc}), and the Ospika pipe, and hence post-date the carbonatite intrusion. Geometries of F_2 folds (Fig. 2.2*E*) are nearly identical to those characterising the Rocky Mountain orogeny in the region (as described by Thompson, 1989). It is therefore inferred that the F_2 folds mapped in the Aley carbonatite area are a product of Cretaceous or early Tertiary Rocky Mountain deformation.

2.4 Discussion

Our mapping shows that, in the Aley region, the western Foreland Belt of the Canadian Cordilleran is characterized by a major Upper Devonian magmatic and tectonic event. Magmatism included the Late Devonian intrusion of the Aley carbonatite as a sill at the base of the Kechika Formation. The carbonatite sill and overlying stratigraphic sequence were then folded, forming a crustal scale nappe; erosion subsequently removed

all but the overturned lower limb of the nappe (Fig. 2.3*J-M*). Carbonatite magmatism spanned nappe formation; late stage dolomite carbonatite cuts fabric in the carbonatite sill, and intrudes along S_1 cleavage planes and along extensional shears that formed along the lower limb of the nappe. Carbonatite magmatism and nappe formation had ended by 366 Ma, the age of the post-tectonic Ospika pipe diatreme. K-Ar phlogopite cooling ages from lamprophyre dykes are consistent with exhumation and cooling of the tectonized crust by the Early Mississippian. These findings cannot be reconciled with a 'passive margin' model for the western foreland belt. Crustal scale nappes are considered to be characteristic of convergent margin orogens (Price and McClay, 1981 and papers therein). If the lower Palaeozoic stratigraphic sequence of the western Foreland belt did accumulate in a passive margin setting, that margin must have been converted to an active margin by Late Devonian time. However, the stratigraphy of the western Foreland belt is characterized by abundant volcanic and coarse siliciclastic strata (Fig. 2.2*C*). The lower Kechika Formation consists of a heterogeneous volcanic unit that includes tuff, pillow basalts and volcaniclastic strata. The middle Skoki Formation is a thick and continuous volcanic unit of tuff, fragmental volcanics and pillow basalts. The Road River Group, while lacking volcanic layers, is characterized by quartzite and pebble conglomerate layers of unknown origin. In light of all these lines of evidence for Late Devonian convergent margin orogenesis, we interpret this stratigraphic sequence as a record of an active margin and infer that Late Devonian tectonism resulted from collision along the active margin.

A model of collision in the Upper Devonian explains nappe formation, but what of the syn-kinematic carbonatite magmatism, and is there a sedimentary record of

collision? Deformed alkaline-carbonatite igneous rocks are known to be associated with and characteristic of suture zones in continental collisional orogens. Burke et al. (2003) demonstrated that in Africa 90% of deformed alkaline carbonatite and nepheline syenite complexes lie along and mark known and inferred suture zones. A more modern analogue is provided by the Himalaya. There the Tertiary Indian continent - Yangtze continental block suture zone is characterized by syn-kinematic carbonatite intrusions that were emplaced in transpressional to transtensional settings within the collisional orogen (Hou et al., 2006). A sedimentary record of collisional orogenesis may be present to the north. Westerly-derived Late Devonian to Early Mississippian siliciclastic strata of the Earn Group characterize the western Foreland to the north of the Aley region (Gordey et al., 1987). Interpretation of these strata as flysch and molasse shed from a 'contractional' orogen, previously referred to as the Antler orogen (Smith et al., 1993), suggests that the Earn Group may be the stratigraphic record of the orogenic event responsible for nappe formation and magmatism observed in the Aley region. The westerly-derived Earn Group sedimentary sequence is similar to, and likely correlative with, orogenic sediments associated with the Roberts Mountain allochthon of the Antler orogen in Nevada and Idaho. Collision there is inferred to have involved west-dipping subduction of oceanic lithosphere lying west of and continuous with North American continental lithosphere which led to partial subduction of continental crust beneath a far-traveled arc (Speed and Sleep, 1982; Wright & Wild, 2006) and is consistent with our interpretation of nappe formation and magmatism in the Aley region as being a manifestation of the Antler orogeny.

Explaining Upper Devonian nappe formation and syn-kinematic carbonatite magmatism, as well as the regional westerly-derived influx of siliciclastic sediments, as the products of collisional orogenesis does present us with a dilemma. The stratigraphic record of coeval (Upper Devonian) continental margin sediments in the eastern Foreland belt and autochthon just tens of kilometers to the east of the Aley area, consists largely of shallow water carbonates and lacks volcanic layers, orogenic siliciclastic sediments or significant unconformities that might be expected in the immediate vicinity of a collisional orogen (Thompson, 1989). The implication is that the western Foreland belt is far-travelled relative to the eastern Foreland belt. No major structure separating the western and eastern portions of the Foreland Belt has been identified (Thompson, 1989); the boundary having been interpreted as a Paleozoic sedimentary facies boundary separating shallow water carbonates to the east from deeper water argillaceous strata to the west (Fig. 2.1). We suggest that what has been mapped as a facies boundary is, or lies adjacent to, a cryptic suture. Carbonatites have been shown to commonly lie along and define cryptic sutures (Burke et al., 2003) consistent with the Cordilleran Foreland distribution of carbonatites; they commonly occur along or just kilometres to the west of the mapped carbonate - shale facies boundary along the length of the orogen (Johnston, 2008). Paleontological (Orchard, 2006) and paleomagnetic (Gladwin & Johnston, 2006) studies are consistent with the western Foreland belt and correlative strata within the more westerly Omineca belt being allochthonous with respect to Laurentia. Similarly, geochronological studies of xenocrystic zircons separated from pre-Cretaceous diatremes and granitoids in the western foreland belt suggest that these intrusions passed through a young, in part Grenvillian basement, distinct from the Proterozoic and Archean Canadian

Shield basement that underpins the eastern Foreland belt and autochthon (Parrish & Reichenbach, 1991).

2.5 Conclusions

Early to Middle Palaeozoic volcanic and sedimentary strata in the Aley region of the western Foreland belt of the Canadian Cordillera record deposition in an active margin. Formation of a crustal scale nappe and syn-kinematic carbonatite magmatism is explained as a result of collision along the active margin in the Late Devonian. The westerly derived Late Devonian to Early Mississippian Earn Group that characterizes the western foreland belt to the north is inferred to consist of syn-orogenic sediments shed from the collision zone. These observations suggest that a Late Devonian collisional orogen, regionally referred to as the Antler orogen, is a characteristic of the western Foreland belt. In contrast, Palaeozoic strata of the eastern Foreland Belt lack a record of Late Devonian orogenesis, and are best explained as having been formed at a passive margin. Such an interpretation requires that the boundary between the eastern and western Foreland belts, which is mapped as a Paleozoic carbonate to shale facies boundary, is or lies immediately adjacent to a cryptic suture, and that the western Foreland belt is far-travelled and exotic relative to the eastern Foreland belt.

References cited

Burke, K., Ashwal, L.D., and Webb, S., 2003, New way to map old sutures using deformed alkaline rocks and carbonatites: Geology, v. 31, p. 391–394.

Gladwin, K., and Johnston, S.T. 2006. Mid-Cretaceous pinning of accreted terranes to miogeoclinal assemblages in the northern Cordillera: Irreconcilable with paleomagnetic data? *in* Haggart, J.W., Enkin, R.J., Monger, J.W.H., eds., Paleogeography of the North American Cordillera: evidence for and against large-scale displacements: St. John's, Newfoundland, Geological Association of Canada Special Paper 46, pp. 299–306.

Gordey, S.P., Abbott, J.G., Tempelman-Kluit, D., and Gabrielse, H., 1987, "Antler" clastics in the Canadian Cordillera: Tectonics, v. 11, p. 1266–1287.

Goodfellow, W.D., Cecile, M.P., and Leybourne, M.I., 1995, Geochemistry, petrogenesis, and tectonic setting of lower Paleozoic alkalic and potassic volcanic rocks, northern Canadian Cordilleran miogeocline: Canadian Journal of Earth Sciences, v. 32, p. 1236–1254.

Hou, Z., Tian, S., Yuan, Z., Xie, Y., Yin, S., Yi, L., Fei, H., and Yang, Z, 2006, The Himalayan collision zone carbonatites in western Sichuan, SW China: petrogenesis, mantle source and tectonic implications: Earth and Planetary Science Letters, v. 244, p. 234–250.

Johnston, S.T., 2008, The Cordilleran Ribbon Continent of North America: Annual Review of Earth and Planetary Sciences, v. 36, p. 495–530.

Mader, U.K., 1986, The Aley Carbonatite Complex [M.Sc. thesis]: Vancouver, University of British Columbia, 176 p.

McLeish, D.F., Johnston, S.T., Mortensen, J.K., and Friedman, R.M., 2013, U-Pb zircon-titanite geochronology of the Aley carbonatite complex, northeast British Columbia: Evidence for Antler aged orogenesis in the Foreland Belt of the Canadian Cordillera. Lithosphere, (in review).

Monger, J.W.H., Gabrielse, H., and Souther, J.A, 1972, Evolution of the Canadian Cordillera: a plate tectonic model: American Journal of Science, v. 272, p. 577–602.

Miall, A.D., and Blakey, R.C., 2008, The Phanerozoic Tectonic and Sedimentary Evolution of North America, *in* Miall, A.D., ed., Sedimentary Basins of the World, Volume 5: The Sedimentary Basins of the United States and Canada, Elsevier, p. 1-29.

Orchard, M.J, 2006, Late Paleozoic and Triassic conodont faunas of Yukon and northern British Columbia and implications for the evolution of the Yukon–Tanana terrane, *in* Colpron, M., and Nelson, J.L., eds., Paleozoic evolution and metallogeny of pericratonic terranes at the ancient Pacific margin of North America, Canadian and Alaskan Cordillera: St. John's, Newfoundland, Geological Association of Canada Special Paper 45, p. 229–260.

Parish, R.R., and Reichenback, I., 1991, Age of xenocrystic zircon from diatremes of western Canada: Canadian Journal of Earth Sciences, v.28, p. 1232-1238.

Pell, J., 1994, Carbonatites, nepheline syenites, kimberlites and related rocks in British Columbia: British Columbia Ministry of Energy, Mines and Petroleum Resources Bulletin 88, 136 p.

Price, N.J., McClay, K.R. eds., 1981, Thrust and Nappe Tectonics: London, Geological Society, Special Publication 9, 528 p.

Price, R.A. 1994. Cordilleran Tectonics and the evolution of the Western Canada Sedimentary Basin, *in* Mossop, G. And Shetsen, I., eds., Geological atlas of the Western Canada Sedimentary Basin: Calgary, Alberta, Canadian Society of Petroleum Geologists and Alberta Research Council, p. 13–24.

Pride, K.R., LeCouter, P.C., and Mawer, A.B, 1986, Geology and mineralogy of the Aley Carbonatite: Canadian Institute of Mining and Metallurgy, 10th District 6 Meeting, Victoria, British Columbia, Abstracts, p. 32.

Pyle, L.J., and Barnes, C.R., 2001, Conodonts from the Kechika Formation and Road River Group (Lower to Upper Ordovician) of the Cassiar Terrane, northern British Columbia: Canadian Journal of Earth Sciences, v. 38, p. 1387–1401.

Root, K., 2001, Devonian Antler fold and thrust belt and foreland basin development in the southern Canadian Cordillera: implications for the Western Canada Sedimentary Basin: Bulletin of Canadian Petroleum Geology, v. 49, p. 7–36.

Smith, M.T., Dickinson, W.R., and Gehrels, G.E. 1993. Contractional nature of Devonian–Mississippian Antler tectonism along the North American continental margin: Geology, v. 21, 21–24.

Speed, R.C, and Sleep, N.H., 1982, Antler orogeny and foreland basin: A model: Geological Society of America Bulletin, v. 93, p. 815-818.

Thompson, R.I., 1989, Stratigraphy, tectonic evolution and structural analysis of the Halfway River map area (94B), northern Rocky Mountains, British Columbia: Geological Survey of Canada Memoir 425, 119 p.

Wheeler, J.O., and McFeely, P., 1991, Tectonic Assemblage Map of the Canadian Cordillera and Adjacent Parts of the United States of America: Geological Survey of Canada Map 1712A, scale 1:2,000,000, 2 sheets.

Wright, J.E., and Wyld, S.J., 2006, Gondwana, Iapetan, Cordilleran interactions: A geodynamic model for the Paleozoic tectonic evolution of the North American Cordillera: *in* Haggart, J.W., Enkin, R.J., and Monger, J.W.H., eds., Paleogeography of the North American Cordillera: Evidence for and against Large-Scale Displacements: St. John's, Newfoundland, Geological Association of Canada Special Paper 46, p. 377-408.

CHAPTER 3

U-Pb zircon-titanite geochronology of the Aley carbonatite complex, northeast British Columbia: Evidence for Antler aged orogenesis in the Foreland Belt of the Canadian Cordillera

D.F. McLeish[1], S.T. Johnston[1], R.M. Friedman[2], and J.K. Mortensen[2],

[1]*School of Earth and Ocean Sciences, University of Victoria, Victoria, BC, V8W 3V6*

[2]*Department of Earth and Ocean Sciences, University of British Columbia, Vancouver, BC, V6T 1Z4*

Submitted to *LITHOSPHERE* December 21, 2012

ABSTRACT

The tectonic significance and age of carbonatite intrusions in the central Foreland Belt of the Canadian Cordillera are poorly constrained. Recent work has demonstrated that one of these carbonatite intrusions, the Aley carbonatite, was emplaced as a syn-kinematic sill, coeval with a major nappe-forming tectonic event. Determining the age of the Aley carbonatite thus provides a means of directly dating syn-magmatic tectonism. Attempts at dating carbonatite units failed due to low U-Pb content in sampled zircons; however, a U-Pb titanite age of 365.9 +/- 2.1 Ma was obtained from the Ospika pipe, an ultramafic diatreme spatially and genetically related to the carbonatite. This U-Pb titanite age is further supported by respective $^{40}Ar/^{39}Ar$ phlogopite ages of 359.4 +/- 3.4 Ma and 353.3 +/- 3.6 Ma for the pipe and a lamprophyre dyke spatially associated with the pipe. We interpret the Late Devonian age of the Ospika pipe to be the minimum possible age of the carbonatite and syn-magmatic nappe-forming tectonic event. The maximum possible age of the carbonatite is constrained by the Early Devonian age of the Road River Group, the youngest strata intruded by carbonatite dykes and involved in the nappe forming event. Our dating results for the Aley carbonatite closely correlate with U-Pb zircon and perovskite ages obtained for the Ice River carbonatite complex in the central Foreland Belt of the southern Canadian Cordillera, and support the interpretation of carbonatite intrusions of the western Foreland Belt as genetically linked components of an alkaline-carbonatitic magmatic province. Structural, stratigraphic, and geochronological data from the Aley area indicate that deformation was similar in style to, and coeval with, structures attributable to the Antler Orogeny, and are consistent with the Antler orogen having extended the length of Cordilleran margin from the southern United States to Alaska.

3.1 Introduction

Paleozoic strata in the western Foreland Belt of the Canadian Cordillera are characterized by widely spaced carbonatite and silica-undersaturated alkali intrusive and volcanic complexes (Fig. 3.1). A detailed structural study of one of the carbonatite complexes, the Aley carbonatite of the Rocky Mountains of northeast British Columbia (McLeish and Johnston, 2013) demonstrated that the carbonatite: (*1*) forms a sill intruded near the base of a Lower to Middle Paleozoic stratigraphic sequence that includes, from oldest to youngest, the Kechika and Skoki Formations and the Road River Group; and (*2*) is, together with its wallrocks, overturned, forming the lower limb of a syn-magmatic crustal-scale recumbent nappe. McLeish and Johnston (2012) interpreted the carbonatite and syn-magmatic nappe as manifestations of collisional orogeny along an active convergent margin.

Questions arising from these findings include: (*1*) are other Cordilleran carbonatite complexes attributable to the same collisional event?; (*2*) was the collisional orogenic event of continental scope; and, if so (*3*) can we distinguish correlative structures and identify sedimentary, igneous and metamorphic rocks attributable to the same event elsewhere in the foreland of the Cordillera? Answering these questions requires that we constrain the timing of deformation and syn-kinematic magmatism in the Aley region. Toward this goal, we conducted an integrated field stratigraphic and geochronological study of the Aley carbonatite complex and its wall rocks, including a post-kinematic diatreme pipe, the Ospika pipe diatreme; the Lady Laurier volcanic unit, part of the Ordovician Skoki Formation; and a volcano-sedimentary member of the Kechika Formation. By constraining the age of the syn-kinematic Aley carbonatite, we

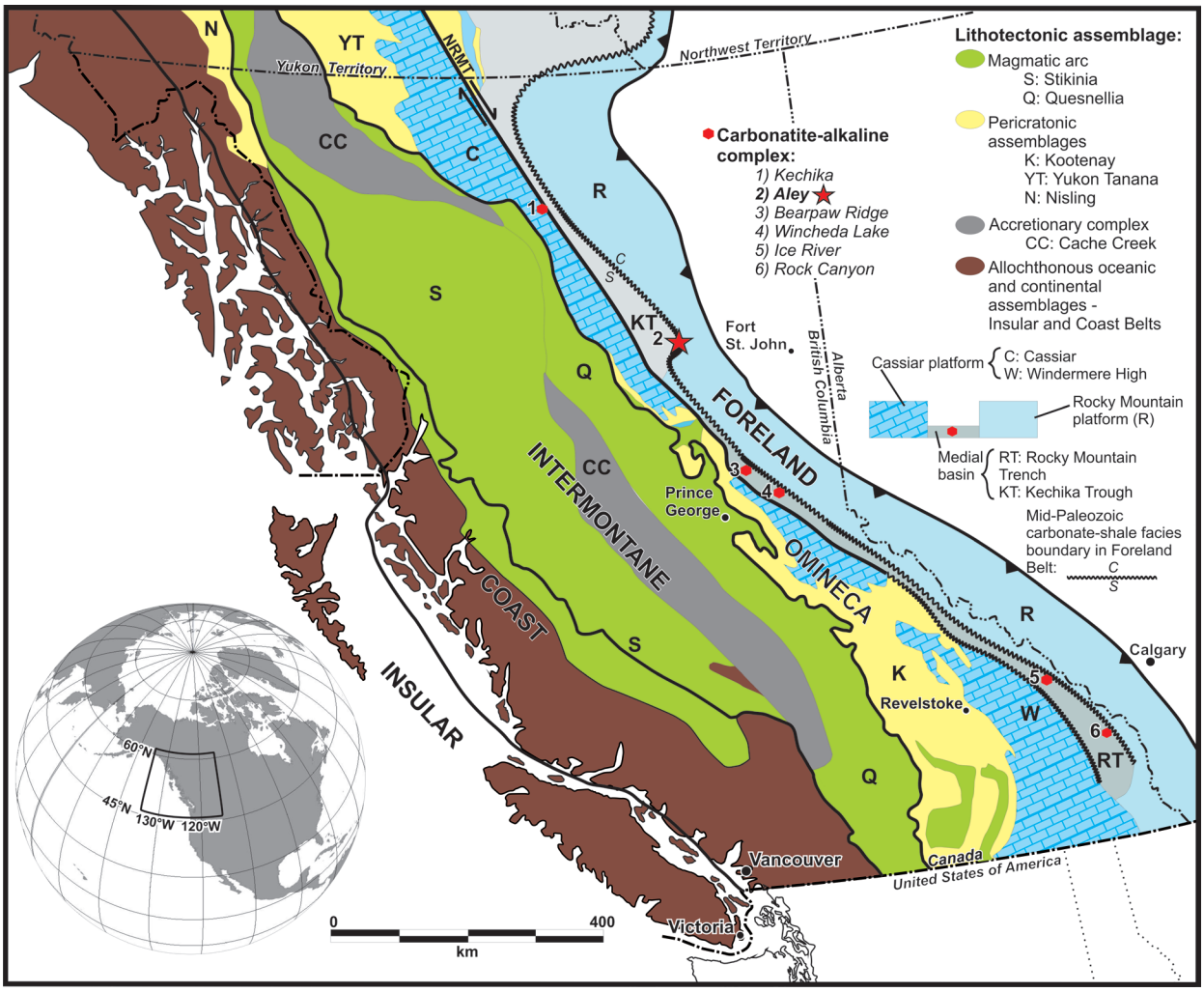

Figure 3.1: First-order morphological subdivisions of the Canadian Cordillera with known Foreland Belt alkaline-carbonatite complexes shown in reference to the transition of early Paleozoic continental platform and slope facies to deep-water basinal facies. This transition is also known as the Carbonate-to-Shale, or C-S, boundary. Alkaline complex localities in part after Pell (1994); facies boundary after Wheeler and McFeely (1991). The distribution of Paleozoic alkaline volcanic rocks in the Foreland Belt (not shown) closely mirrors that of the carbonatite complexes.

constrain the age of the coeval tectonic event responsible for nappe formation. In addition, constraining the age of the Aley carbonatite, the Ospika pipe diatreme, lamprophyre dykes, and the Lady Laurier volcanics of the Skoki Formation, is necessary to determine if these spatially related silica-undersaturated to alkalic igneous units share a genetic relationship. Finally, detrital zircons in quartzite clasts separated from conglomerate in the volcano-sedimentary member of the Kechika Formation constrains the maximum age and provenance of the oldest unit in this portion of the western Foreland belt. Here we review the geological setting of the Aley carbonatite and its wall-rocks, present the results of our geochronological studies, and attempt, using these data, to address the questions posed above.

3.2 Geology of the Aley region of the Rocky Mountains of Northeast B.C.

The study area lies within the Williston Lake area of the western Foreland belt of the Rocky Mountains and is characterized by Early to Middle Paleozoic deep water carbonates and shales (Figs. 3.1 and 3.2). These slope to off-shelf deep water strata define the paleogeographic Kechika Trough. In the Aley region, the north-south trending, 50 kilometre wide trough is bound to the west by the Northern Rocky Mountain Trench, which is host to an Eocene dextral strike-slip fault interpreted to have accommodated >400 kilometres of dextral strike-slip displacement (Gabrielse, 1985); and to the east by a facies boundary defined by the western limit of shallow water carbonates of the MacDonald Platform. This facies boundary constitutes the boundary between the western and eastern portions of the Foreland Belt. North of 59 degrees N Latitude, the Kechika Trough widens into the Selwyn Basin. The trough terminates immediately south of the Aley region, where the facies boundary marking the east margin of the trough

curves around to the west, and is truncated against the Northern Rocky Mountain Trench fault. Thompson (1989) established the regional stratigraphic framework of the MacDonald Platform and Kechika Trough. Additional stratigraphic studies of the Aley region include Pride (1983) and Pyle and Barnes (2001). Intrusive into the Kechika Trough stratigraphic sequence are the Aley carbonatite, the Ospika pipe diatreme and lamprophyre dykes (Fig. 3.3*D*). Within the study area, the stratigraphic sequence and the Aley carbonatite intrusion all lie within and define the overturned lower limb of a crustal scale nappe (McLeish and Johnston, 2013).

3.3 Stratigraphic units

3.3.1 Kechika Formation

The Kechika Formation is divisible into a lower volcano-sedimentary member, and an upper carbonate and siliciclastic member. The heterogeneous lower volcano-sedimentary member consists of interlayered conglomerate, pillow basalt, tuff, volcaniclastic rocks and fragmental volcanic layers. The pebble to boulder conglomerate layers are discontinuous and are of variable thickness. Quartzite, siltstone, granitoid and dolostone clasts are rounded to well rounded. Volcanic layers weather dark to light green. Well preserved pillows are rare; fragmental volcanic layers, tuff and immature, volcaniclastic sedimentary rocks, are more common. The thickness of this member is difficult to constrain as its base has been intruded by the Aley carbonatite, and nowhere in the map area is the contact with regionally underlying Cambrian quartzite exposed. Extension along the lower overturned limb of the nappe during its development structurally thinned all units in the Kechika-Road River host succession (McLeish and Johnston, 2013). Assuming the Aley carbonatite intruded along the contact between

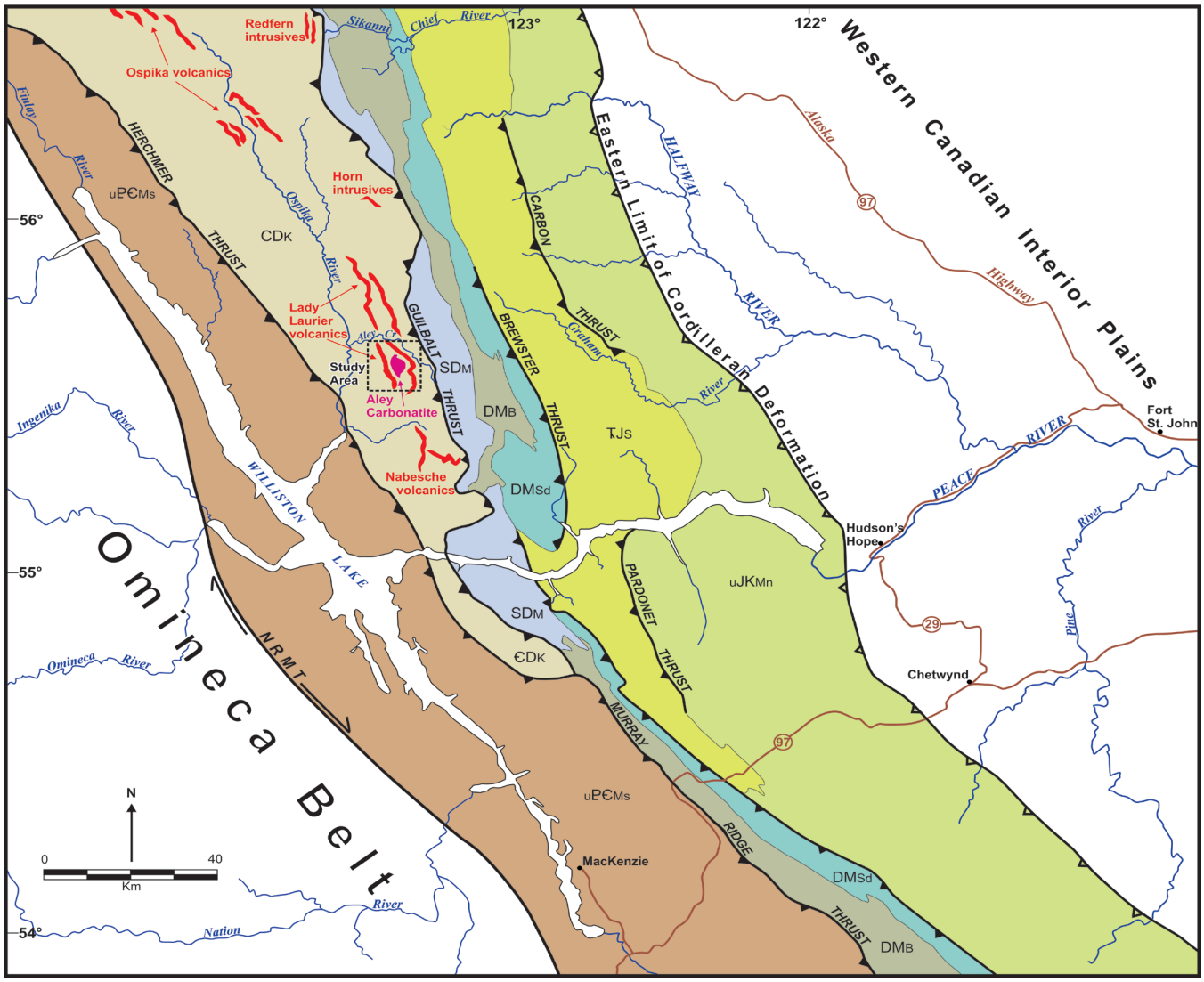

Rocky Mountains Subprovince

SDM — *SOUTHERN MUSKWA: Passive continental margin sediments. Includes massive to thick-bedded dolomite and limestone with black chert lenses, minor interbedded shale and dolomitic sandstone of Nonda, Muncho-McConnell, Stone, and Dunedin Formations*

CDK — *KECHIKA: Mainly offshelf sediments of an active continental margin undergoing to periodic rifting, contraction, volcanism, and carbonatite magmatism. Includes shale, siltstone, thin-thickly bedded argillaceous carbonate, westerly-derived siliclastics, and alkaline and potassic basalt flows, and tuff of the Kechika and Skoki Formations and Road River and Earn Groups*

uPЄMs — *MISINCHINKA: Clastic continental margin sediments with Cambrian rift-related sediments at top of assemblage. Includes phyllitic and schistose pelite, quartz-feldspar grit, quartzite, and massive limestone of the Misinchinka Group*

Foothills Subprovince

uJKMn — *MINNES: Fordeep clastic wedge of the Rocky Mountain orogen. Includes marine sandstone and shale grading westward into prograding deltaic sandstone, massive conglomerate, and coal of the Monteith, Beattie Peaks, Monach, Bickford Formations and Bullhead Group*

TJS — *SPRAY RIVER: Passive continental margin prism. Includes phosphatic and chert rich limestone, organic rich shale, marine siltstone, dolomite, and calcareous sandstone*

DMSd — *STODDART: Continental shelf carbonate and shale. Includes platform and reef limestone and dolomite, massive chert, and minor shale and dolomitic quartz sandstone of the Stoddart Group and Prophet Formation*

DMB — *BESA: marginal basin fine-grained clastic sediments. Includes mainly deep water shales and chert of the Besa River Formation*

Figure 3.2: Simplified geological map of the Williston Lake area of northeast British Columbia showing key tectono-stratigraphic divisions (after Wheeler and McFeely, 1991). Several alkaline volcanic occurrences (red) and the Aley carbonatite complex (magenta) define a strike-parallel belt of Paleozoic igneous activity unseen in Paleozoic continental shelf and margin strata to the east.

the lower volcano-sedimentary member and the Cambrian quartzite without significant structural thinning, the minimum thickness of the member is 200 metre. Correlative volcanic layers within the lower Kechika Formation (Fig. 3.2) have been documented 100 kilometres north of the Aley region in the Redfern Lake (Taylor and Scott, 1973; Taylor, 1979) and Ospika River areas (Taylor et al., 1979; MacIntyre, 1998).

Carbonate and siliciclastic strata of the upper sedimentary member of the Kechika Formation include tan-brown and grey planar laminated argillaceous limestone; wavy, banded orange-brown calcareous siltstone; and massive, cream-coloured dolostone. These strata are interpreted to have been deposited in a deep water, slope to off-shelf environment (Pyle and Barnes, 2001). Siliciclastic strata are phyllitic, have a bedding parallel cleavage, and record low grade metamorphism. The maximum thickness of the upper member in the map area is 800 metre (Fig. 3.3*D*).

Age constraints on the Kechika Formation are few. No direct age constraints on the volcano-sedimentary member are available. Few fossils are preserved in the upper sedimentary member. Conodonts recovered from the uppermost member to the north of the Aley region indicate an Early Ordovician age (Pyle and Barnes, 2001).

3.3.2 Skoki Formation

The Skoki Formation is divisible into three members; lower and upper dolostone members are separated by a distinct volcanic member informally referred to as the Lady

Figure 3.3 (next page): Geology and structure of the Aley carbonatite complex and host stratigraphy. (A) Geological map of complex (in part, after Mader, 1986); (B) east-west profile view of complex from south showing distribution of major map units; (C) geological cross-section; (D) idealised stratigraphic column (in part, after Pride et al., 1986).

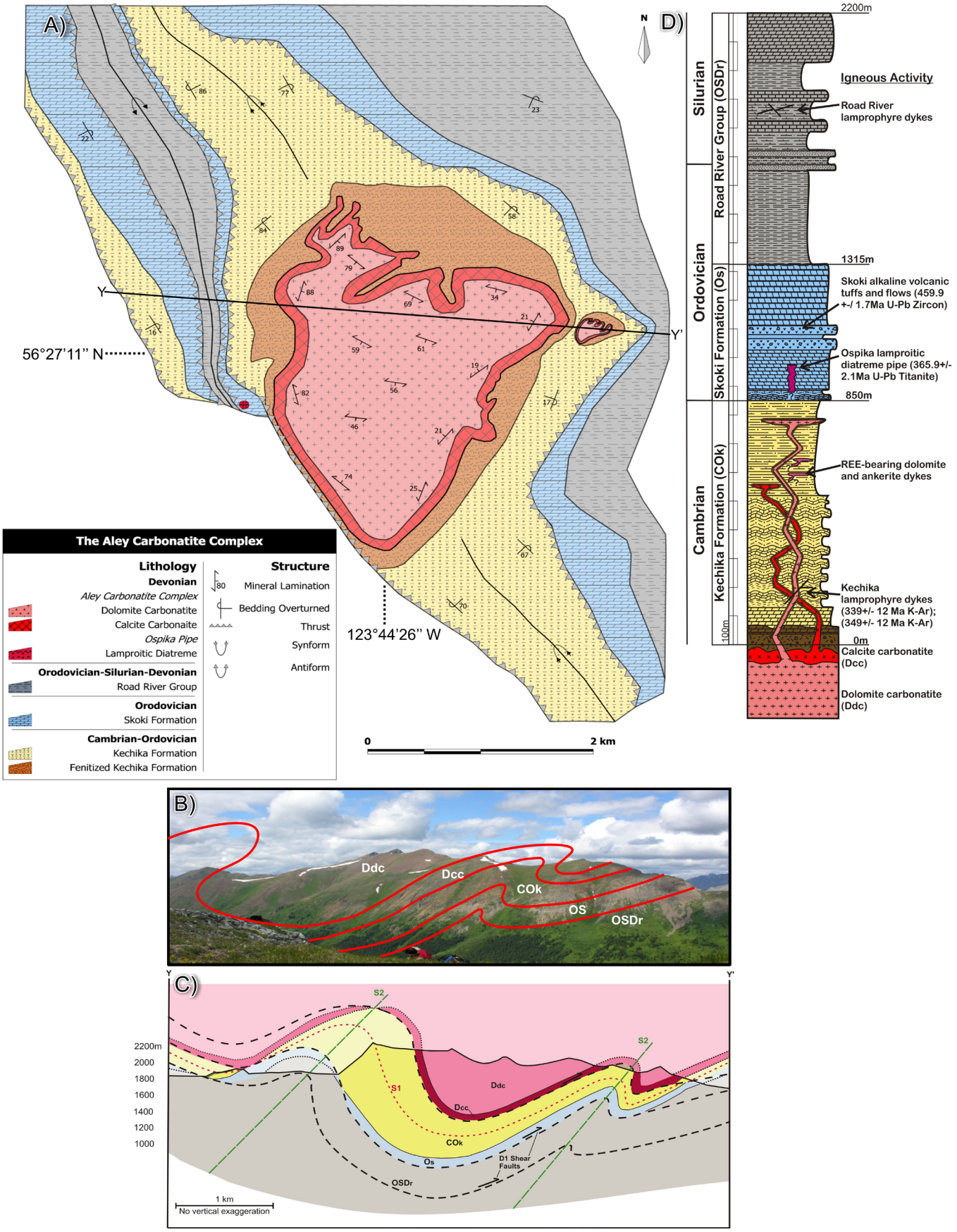
A)
Y
Y'
56°27'11" N
123°44'26" W
0
2 km
The Aley Carbonatite Complex
Lithology
Devonian
Aley Carbonatite Complex
Dolomite Carbonatite
Calcite Carbonatite
Ospika Pipe
Lamproitic Diatreme
Orodovician-Silurian-Devonian
Road River Group
Orodovician
Skoki Formation
Cambrian-Ordovician
Kechika Formation
Fenitized Kechika Formation
Structure
Mineral Lamination
Bedding Overturned
Thrust
Synform
Antiform
D)
N
Silurian
Ordovician
Cambrian
Road River Group (OSDr)
Skoki Formation (Os)
Kechika Formation (COk)
100m
2200m
Igneous Activity
Road River lamprophyre dykes
1315m
Skoki alkaline volcanic tuffs and flows (459.9 +-/ 1.7Ma U-Pb Zircon)
Ospika lamproitic diatreme pipe (365.9+/- 2.1Ma U-Pb Titanite)
850m
REE-bearing dolomite and ankerite dykes
Kechika lamprophyre dykes (339+/- 12 Ma K-Ar); (349+/- 12 Ma K-Ar)
0m
Calcite carbonatite (Dcc)
Dolomite carbonatite (Ddc)
B)
Ddc
Dcc
COk
OS
OSDr
C)
Y
Y'
S2
S1
Ddc
Dcc
COk
Os
OSDr
D1 Shear Faults
2200m
2000
1800
1600
1400
1200
1000
1 km
No vertical exaggeration

Laurier volcanics. The dolostone members consist of cliff-forming, grey weathering, medium to thick-bedded, mottled grey dolostone. The dolostone is massive to cross-bedded bioclastic limestone. Fossiliferous layers contain crinoid ossicles and gastropods. Planispiral gastropods (Maclurites) have been described from the upper dolostone member (Mader, 1986). Chert lenses and oncolites are rare in the lower dolostone member, but are common toward the top of the upper dolostone member adjacent to the contact with the stratigraphically overlying Road River Group.

Argillaceous, wavy bedded dolostone is present in the lower dolostone member near the contact with the underlying Kechika Formation. The contact between the lower member and the Kechika Formation is commonly faulted; low angle faults that developed along the overturned lower limb of the nappe during nappe formation, cut structurally downsection, stratigraphically up-section, from the upper Kechika Formation into the lower dolostone of the Skoki Formation, thinning the overturned stratigraphic sequence (McLeish and Johnston, 2013). The true thickness of the lower dolostone member is therefore difficult to assess, but we estimate it to be 150 metres based on exposures in the northwest of the map area where the lower contact with the Kechika is little modified by faults and the contact with the volcanic member is sharp. The thickness of the upper dolostone member is 200 metre as constrained by a complete section exposed in the southeast of the map area (Fig. 3.3*D*).

The 10 to 100 metre thick middle (Lady Laurier) volcanic member of the Skoki Formation consists of fine grained, marine tuffs that pass upward into agglomerate and volcaniclastic layers. Thin (10-20 m) exposures of this member are likely attributable to structural thinning by faults similar to those observed in the lower dolostone member.

Metre thick layers of dark green shale are common. Pillow basalt is rare. Carbonatite ocelli have been observed in agglomeratic layers of this member (D. Canil, personal communication, 2009). Dolostone layers interfinger with volcanic layers near the top of the volcanic member, and the contact with the overlying dolostone is gradual. The Skoki Formation, including the Lady Laurier volcanic member, is continuous throughout the Halfway River region (Thompson, 1989). Paleontological studies constrain the age of the formation to Early to Late Ordovician (Cecile and Norford, 1979; Thompson, 1989; Pyle and Barnes, 2001). No direct age determination is available for the volcanic member.

3.3.3 Road River Group

The Road River Group consists of a >1 kilometre thick sequence of off-shelf clastic and lesser carbonate rocks. The contact with the Skoki Formation is sharp, possibly unconformable, and is marked by an abrupt transition from thickly bedded, resistant, chert rich dolostone to recessive shale. Within the map area, the Road River Group can be divided into two shale-dominated members that are separated by a quartzite unit. The lower member consists of fissile, graptolitic shale and planar-laminated to thinly-bedded, grey-weathering siltstone and argillaceous limestone. At least four, 10-20 metre thick quartzite beds are found 175 to 300 metres above the contact with the underlying Skoki Formation. The quartzites are massive, fine- to medium-grained and homogenous and form a distinctively resistant section that can be traced throughout the map area; they are regionally recognised as a distinct unit by Thompson (1989). The upper member consists of graptolitic shale and laminated siltstone, but also contains metre-thick dolostone beds with chert lenses. Pride (1983) also described an additional dolomitic quartzite unit at the top of the Road River Group. Paleontological collections of

Cecile and Norford (1979) and Norford (1979) indicate the age range of the Road River Group in the region to be Late Ordovician to Early Devonian.

3.4 Intrusive rocks

Exposures of intrusive rocks in the Aley Creek area include: (1) the Aley carbonatite sill; (2) the Ospika diatreme pipe; and (3) ultrabasic lamprophyre dykes and sills (Fig. 3.3). The carbonatite has been described by Pride (1983,1986), Mader (1986), and Pell (1994). Pell (1994) also reported petrological and geochronological data for the Ospika pipe.

3.4.1 Aley carbonatite

The Aley carbonatite intruded as a 1.5 kilometre thick, layer-parallel sill beneath the volcanic sequence in the lower Kechika Formation (McLeish and Johnston, 2013). The carbonatite now lies structurally above the host statigrahic sequence. Its main exposure lies in the core of an asymmetric, Rocky Mountain deformation-related F_2 synform with a steeply dipping to vertical west-limb and a shallowly west-dipping east-limb (Fig 3.3*C*). To the east, 0.5 kilometres from the eastern margin of the main exposure, a separate 300 metre wide exposure of the carbonatite sill crops out in a smaller parasitic F_2 synform. Three principal units within the carbonatite have been identified: (1) a volumetrically dominant fersmite- and pyrite-bearing dolomite-apatite carbonatite unit that forms the core of the sill; (2) a magnetite, pyrochlore, phlogopite-bearing calcite-apatite carbonatite unit that forms the margins of the sill where it is in contact with the Kechika Formation; and (3) a banded magnetite-apatite unit in the dolomite core (Kressall et al., 2010).

Variably developed apatite mineral bands within the calcite and dolomite carbonatite units define an S_1 foliation interpreted to have developed as a result of large rheological variations between carbonate, phosphate, and oxide mineral phases during stress-induced plastic flow and kinematic differentiation associated with the D_1 event (McLeish et al., 2010). The S_1 foliation in the carbonatite is largely concordant with the bedding-parallel S_1 cleavage in the country rock and is cut by late phase dolomite carbonatite dykes, indicating that intrusion of the carbonatite was syn-kinematic with D_1 nappe formation (McLeish and Johnston, 2013). The banded magnetite-apatite unit is conformable with the S_1 fabric and may represent a distinct primary cumulate phase of the carbonatite. Locally, calcite and dolomite carbonatite units contain xenoliths of heavily fenitized siltstone country rock, likely belonging to the Kechika Formation. The abundance of xenoliths increases towards the margin of the sill, with the peripheral calcite carbonatite unit containing the highest concentration. Numerous dykes and sills of calcite and dolomite carbonatite intrude the Kechika Formation in the fenitized contact aureole where cross-cutting relationships show that the intrusion of the calcite carbonatite intrusion largely preceded intrusion of the dolomite carbonatite (McLeish and Johnston, 2013).

A metasomatic fenite aureole extends out from the carbonatite-Kechika Formation contact into the upper sedimentary member of the Kechika Formation (Fig. 3.3*A*). Fenite metasomatization is indicated by replacement of the primary igneous minerals by sodic amphibole and sodic pyroxenes (arfvedsonite, richterite, aegirine and lorenzenite), and decreases gradationally in intensity outwards from the contact (Mader 1986, Pell 1994). Metasomatization is therefore interpreted to have occurred during, and

is attributable to, intrusion of the Aley carbonatite. Fenitized volcano-sedimentary rocks in the lower member explains previous mapping and interpretation of the lower member as 'amphibolite' (*cf.* Mader, 1986; Pride, 1986; Pell, 1994; McLeish and Johnston, 2013).

Pre-existing geochronological data for the carbonatite is limited to a single K-Ar date of 339 +/- 12 Ma on phlogopite from a sample of amphibolitized, siltstone xenolith-bearing calcite carbonatite breccia from the western margin of the main carbonatite exposure (Pride et al., 1986). U-Pb dating of zircon separates from the dolomite carbonatite was also attempted by Pride et al. (1986) but failed due to low U-Pb content in sampled zircons.

3.4.2 Lamprophyre dykes

Multiple thin (0.5-2.0 m) ultrabasic sills and dykes, including some that are enriched in rare-earth carbonate minerals and which bear distinct purple fluorite, occur throughout the map area in the host stratigraphy (Fig. 3*D*) but are most common in the metasomatic fenite aureole peripheral to the carbonatite. Similar dykes intrude the dolomite carbonatite phase near the core of the complex (A. Chakhmouradian, personal communication, 2010). The sills and dykes range in colour from reddish-orange to deep chocolate-brown and are primarily composed of ankerite (Pell, 1994). The dykes cut bedding (S_0) and the bedding parallel cleavage (S_1), and truncate and post-date the fenite metasomatized rocks of the carbonatite contact aureole, indicating that the ultrabasic intrusions post-date D_1 tectonism and carbonatite magmatism. A single K-Ar date of 329 +/- 12 Ma was obtained from a sample of biotite lamprophyre talus collected near the carbonatite Kechika Formation contact (Pride, 1986).

3.4.3 Ospika pipe diatreme

The Ospika pipe is a 50 metre wide ultramafic diatreme pipe intruding the Skoki Formation 500 metres west of the western margin of the main carbonatite sill. The pipe weathers a distinct maroon brown, is roughly circular in plan view, and contains both massive and breccia phases. The breccias contain 5-30% subangular to subrounded, randomly-oriented xenoliths of siltstone from the underlying Road River Group that range from sub-centimetre to sub-metre in size and which are characterized by the bedding-parallel S_1 cleavage. The cleaved wallrock xenoliths indicate that the diatreme pipe post-dates D_1 deformation that was coeval with carbonatite magmatism. Mineralogically, the pipe is characterized by a phlogopite-dominated, phlogopite-clinopyroxene-olivine macrocryst mineral assemblage hosted in a very fine-grained, hypidiomorphic dolomite-chlorite matrix. Geochemical analyses of the diatreme pipe are consistent with its classification as an aillikite (Pell, 1994). A geochronological study of phlogopite separates from the matrix yielded Rb-Sr and K-Ar ages of 334 +/- 7 and 323 +/- 10 Ma respectively (Pell, 1994). These age determinations are similar to the K-Ar ages reported for the lamprophyre dykes and sills (Section 3.4.2).

3.5 Geochronology

3.5.1 Analytical methods

Igneous units were sampled during mapping for U-Pb zircon, U-Pb titanite, and Ar-Ar phlogopite geochronological analyses at the Pacific Centre for Isotopic and Geochemical Research (PCIGR) at the University of British Columbia, Vancouver, Canada. Zircon and titanite were isolated from 5-10 kg samples using standard rock crushing, grinding, and Wilfley table methods, followed by heavy liquid, and magnetic

separation. Zircon and titanite fractions were handpicked based on differences in crystal quality, size, magnetic susceptibility, and morphology.

Zircon was dated via Laser Ablation (LA) ICP-MS methods described in Tafti et al. (2009) and Beranek and Mortensen (2011). The $^{206}Pb/^{238}U$ age is the most precisely determined age for Phanerozoic zircons and is interpreted as the best estimate for the crystallization age of the samples. Assigned ages are based on a weighted average of overlapping, concordant $^{206}Pb/^{238}U$ ages of individual analyses for each sample. Error ranges for all samples are quoted at the 2σ level. A detailed summary of the (LA) ICP-MS analytical methods can be found in Appendix A-1. Titanite was dated via Isotope Dissolution Thermal Ionization Mass Spectrometry (ID-TIMS) methods described in Appendix A-2 of the data repository. Analytical data for all dated samples discussed in this report are available in Appendix A-3.

Samples dated by $^{40}Ar/^{39}Ar$ methods were prepared by handpicking phlogopite from crushed, ground mineral separates that had been reduced on a Wilfley table. Phlogopite extracts were washed in acetone, dried, wrapped in aluminum foil, and stacked in an irradiation capsule with similar-aged samples and neutron flux monitors. Extracts were then irradiated at the McMaster Nuclear Reactor in Hamilton, Ontario, for 90 MWh, with a neutron flux of approximately 3 by 1016 neutrons/cm^2/s. Analyses (n = 57) of 19 neutron flux monitor positions produced errors of <0.5% in the J value. The samples were an analyzed at the Noble Gas Laboratory at PCIGR. The mineral separates were step-heated at incrementally higher powers in the defocused beam of a 10 W CO_2 laser (New Wave Research MIR10) until fused. The gas evolved from each step was an analyzed by a VG5400 mass spectrometer equipped with an ion-counting electron

multiplier. All measurements were corrected for total system blank, mass spectrometer sensitivity, mass discrimination, radioactive decay during and subsequent to irradiation, as well as interfering Ar from atmospheric contamination and the irradiation of Ca, Cl and K.

3.5.2 Results

Aley carbonatite

Zircon fractions obtained from a sample of dolomite carbonatite (MA096) contained near-zero ppm concentrations of radiogenic Pb and therefore could not be used to determine a U-Pb crystallization age of the carbonatite. The sampling locality, an outcrop near the centre of the dolomite core of the intrusion, is characterized by banded to massive fersmite- and pyrite-bearing dolomite-apatite carbonatite typical of the core dolomite carbonatite phase. The zircons analyzed were tan-brown to beige, translucent, euhedral, stubby dipyramids and displayed significant resorption and zonation textures in cathode-luminescence light (see images in Appendix A-1). Whole rock geochemistry of Mader (1986) shows all phases of the carbonatite to have anomalously low U content which suggests that the low Pb content of the zircons is due to a lack of U in the parent magma rather than post-crystallization Pb loss.

Skoki (Lady Laurier) volcanics

Twenty light pink, translucent, elliptical zircons were isolated from a sample collected from a 1 metre thick agglomeratic tuff bed, 15 metres from the top of the Skoki volcanic member (sample MA064). The sampling locality lies 800 metres northwest of the west margin of the carbonatite. Weakly developed growth zonation was observed in all grains under cathode-luminescent light. Sixteen of the twenty $^{206}Pb/^{238}U$-

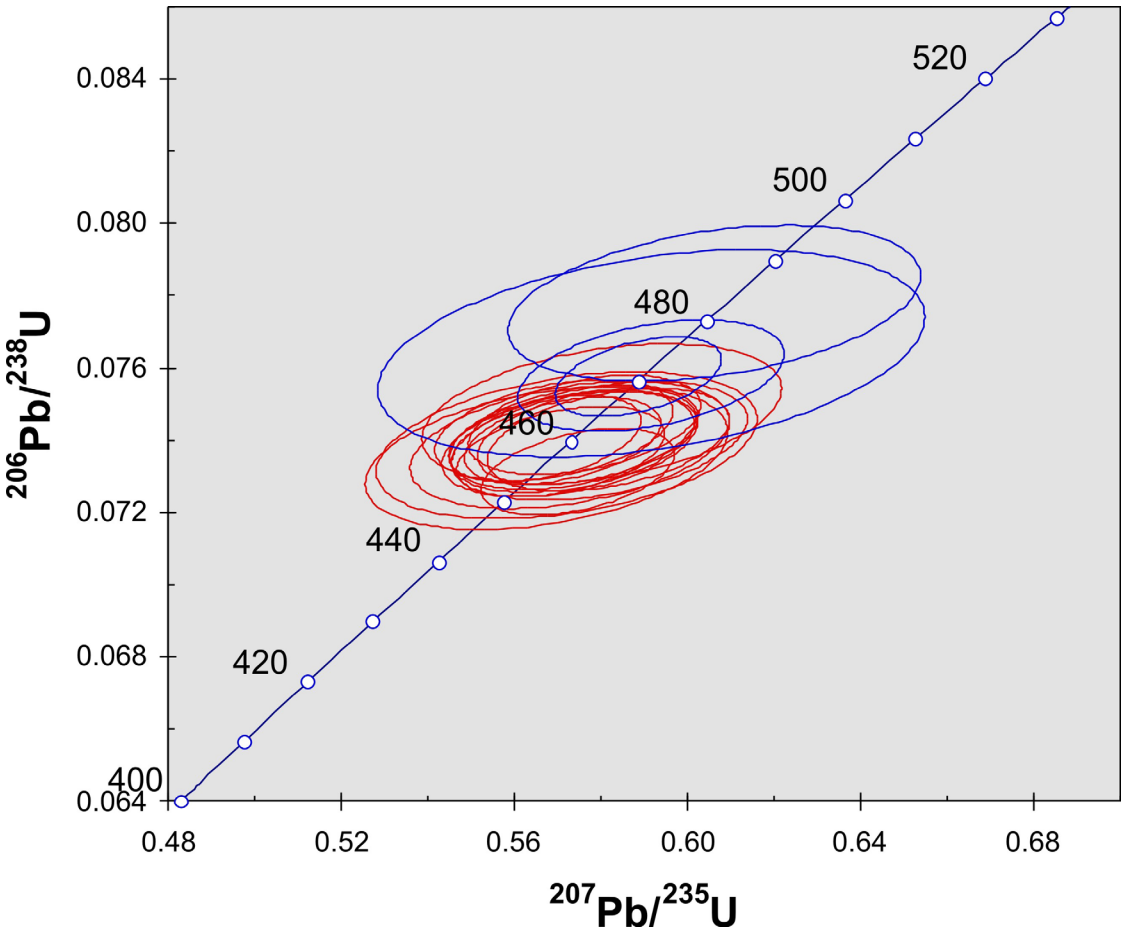

Figure 3.4: Conventional U-Pb concordia diagram for the Skoki agglomerate tuff (MA064). Data ellipses in red were used to calculated a weighted average $^{206}Pb/^{238}U$ age of 459.9 +/- 1.7 Ma (MSWD = 0.37).

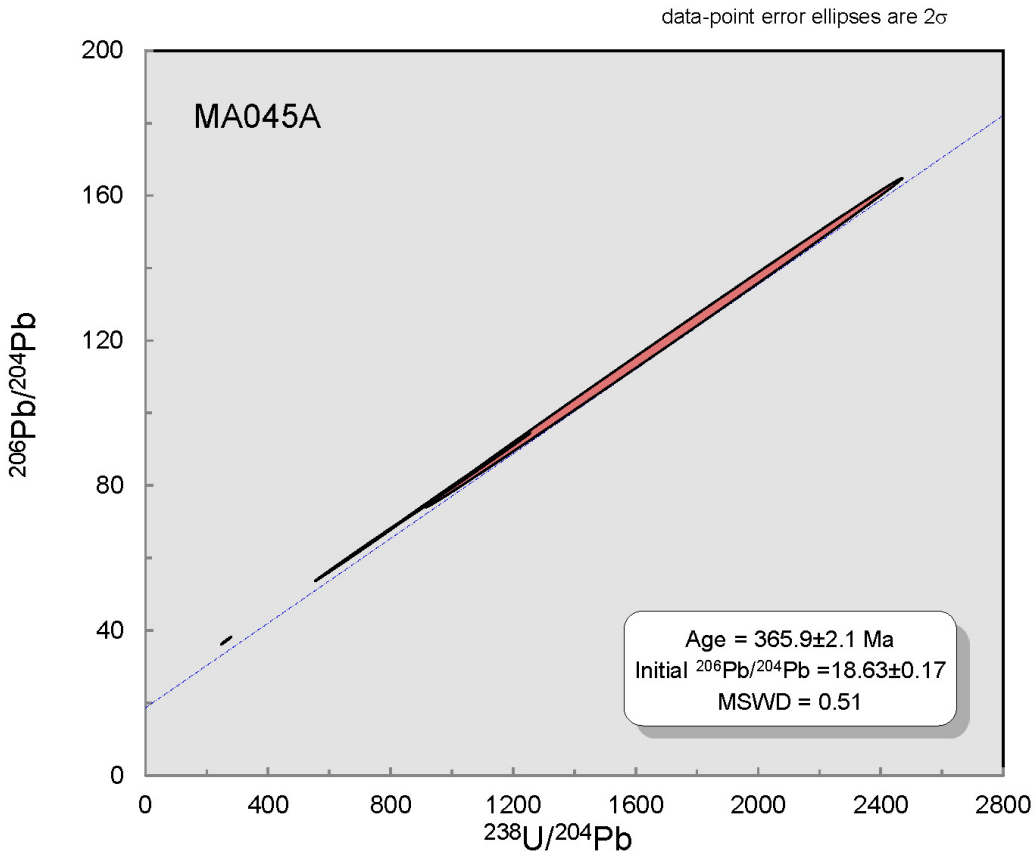

Figure 3.5: U-Pb analyses of titanites from the Ospika pipe define four-point isochron of 365.9 +/- 2.1 Ma (MSWD = 0.51).

$^{207}Pb/^{235}U$ data points plot as a tight cluster along the concordia curve at 460 Ma with the remaining four scattered between 470 and 480 Ma (Fig. 3.4). A weighted average of $^{206}Pb/^{238}U$ ages for the cluster of 16 analyses is 459.9 +/- 1.7 Ma (MSWD=0.37), which is interpreted as the crystallization age of the volcanic unit. This age is in close agreement with a Middle Ordovician age for the Skoki Formation as determined by paleontological investigations (Pyle, 2001), and is interpreted as the age of volcanism.

Ospika Pipe Diatreme

Titanite grains for single-grain ID-TIMS dating were isolated from a sample of the massive diatreme phase exposed near the core of the pipe (MA045A). The sample was free of visible country rock xenoliths and contained 15% phlogopite megacrysts similar to those dated by Pell (1994). The titanite grains were translucent, pale yellow-coloured, and displayed characteristic wedge-shaped igneous crystal habit. In total, five grains were analyzed and four yielded usable results, which together define a $^{206}Pb/^{238}U$ isochron age of 365.9 +/- 2.1 Ma (MSWD = 0.51; Fig. 3.5). The titanite age is in reasonable agreement with the *ca.* 330 Ma K-Ar and Rb-Sr phlogopite dates of Pell (1994), provided the latter two are considered as cooling ages and the titanite age as the igneous crystallization age.

Phlogopite grains isolated from MA045A were dated with $^{40}Ar/^{39}Ar$ step-heating techniques to further constrain the cooling history of the Ospika pipe. Two attempts were made to date phlogopite separates; both yielded continuously rising age spectra. We interpret the oldest step in each attempt, 359.4 +/- 3.4 Ma and 340.6 +/- 3.4 Ma in first and second attempts respectively, as a minimum cooling ages for the phlogopites, and as consistent with a *ca.* 365 Ma emplacement age (Fig. 3.6).

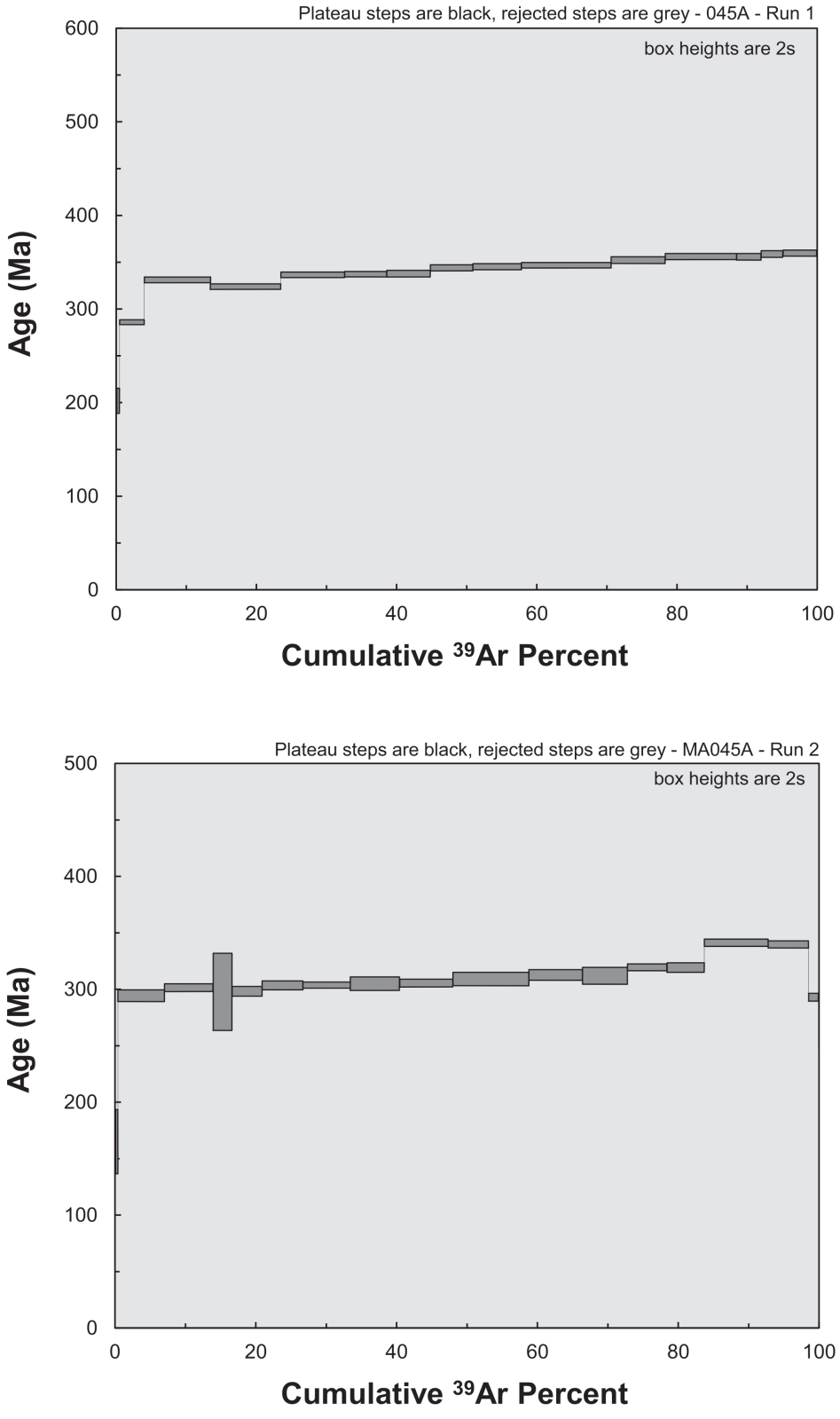

Figure 3.6: $^{40}Ar/^{39}Ar$ step heating results for MA045A runs 1 and 2.

Quartzite clasts from the volcano-sedimentary member of the Kechika Formation

Two cobble-sized quartzite clasts were cut out of two separate 25 kilogram loose boulder-sized talus (float) samples of fenitized conglomerate (MA076 and MA190) and processed for U-Pb detrital zircon geochronology. The talus samples were identical to the conglomerate documented in volcano-sedimentary member at the base of the Kechika Formation. The quartzite clasts sampled for dating were near-pure quartz with accessory concentrations of zircon and opaque minerals. The majority of the zircon grains isolated from the quartzite clasts were too fine-grained to be suitable for LA-ICP-MS analysis; however, 13 and 18 of the near-spherical pink zircon grains were deemed large enough and analysed from MA076 and MA190 respectively. Nearly 40% of the zircons analysed showed significantly large (>10%) discordance due to Pb loss and were removed from the age determination results. No statistically significant difference was found between the age populations of the two samples; both age populations ranged from 1.7 to 2.6 Ga with major age probability peaks at 1.8 and 2.4 Ga. A zircon grain from MA076 was the only outlier from the two populations with an age of 2.8 Ga. A MA076-MA190 composite cumulative probability plot was therefore constructed to increase the sample size (Fig. 3.7) and facilitate comparison with the detrital zircon signature of potential parent units (*e.g.* Gog Group, as postulated by Mader, 1986). The extensive Pb loss displayed by many of the zircons is likely due to the extensive metasomatic alteration of the host conglomerate unit during intrusion of the carbonatite.

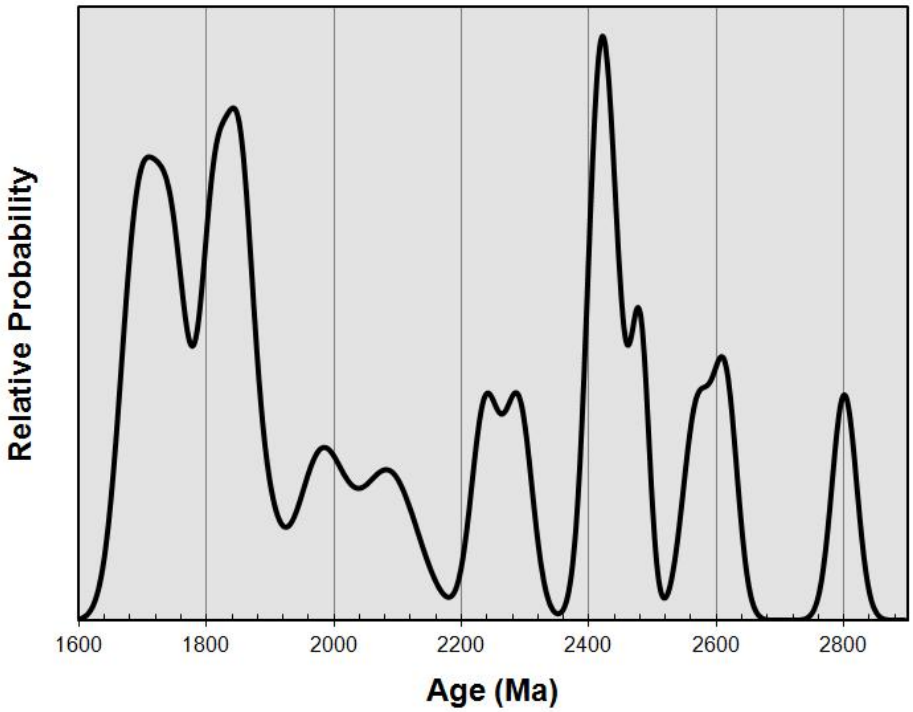

Figure 3.7: Cumulative probability density plot of $^{206}Pb/^{238}U$ zircon ages analyses (n=19) that were <10% discordant for detrital zircons sampled from quartzite clasts of the basal Kechika Formation. See text for further discussion.

Lamprophyres

A 0.5 metre wide lamprophyre dyke that intrudes the Skoki Formation, cutting across bedding in a dark-grey, fenitized, massive argillaceous dolostone of the Skoki Formation was sampled from the wall rocks of the Ospika pipe for Ar-Ar phlogopite analysis. The dyke sampled is characterised by a very fine-grained calcareous, beige- to orange-coloured 'rock-flower' matrix hosting phlogopite megacrysts. Sample MA045D yielded coarse, dark honey-brown phlogopite. Two attempts at dating separates both yielded continuously rising age spectra. The oldest step in each attempt, 353.3 +/- 3.6 Ma and 352.6 +/- 3.5 Ma in the first and second attempts respectively, are interpreted as the minimum age for cooling of the phlogopite (Fig. 3.8).

3.6 Discussion

The Aley carbonatite, the lamprophyre dykes and the Ospika pipe share similar 360-340 Ma K-Ar and Ar-Ar cooling ages; all therefore are interpreted as having intruded and crystallized prior to 340 Ma. Because carbonatite intrusions are commonly spatially and genetically associated with coeval alkaline intrusive rocks, we argue that the carbonatite, the Ospika pipe and the lamprophyre dykes are attributable to a single magmatic event. The 366 Ma (Late Devonian) U-Pb age for magmatic titanite from the Ospika pipe yields the age of intrusion of the diatreme, and is therefore the minimum possible age of the Aley carbonatite and the D_1 tectonic event, including nappe formation and cleavage development. The maximum possible age of the Aley carbonatite is constrained by the Early Devonian age of the Road River Group, the youngest strata intruded by carbonatite dykes and involved in the syn-magmatic D_1 nappe forming event. Hence carbonatite magmatism, and the coeval D_1 event, is constrained to have occurred

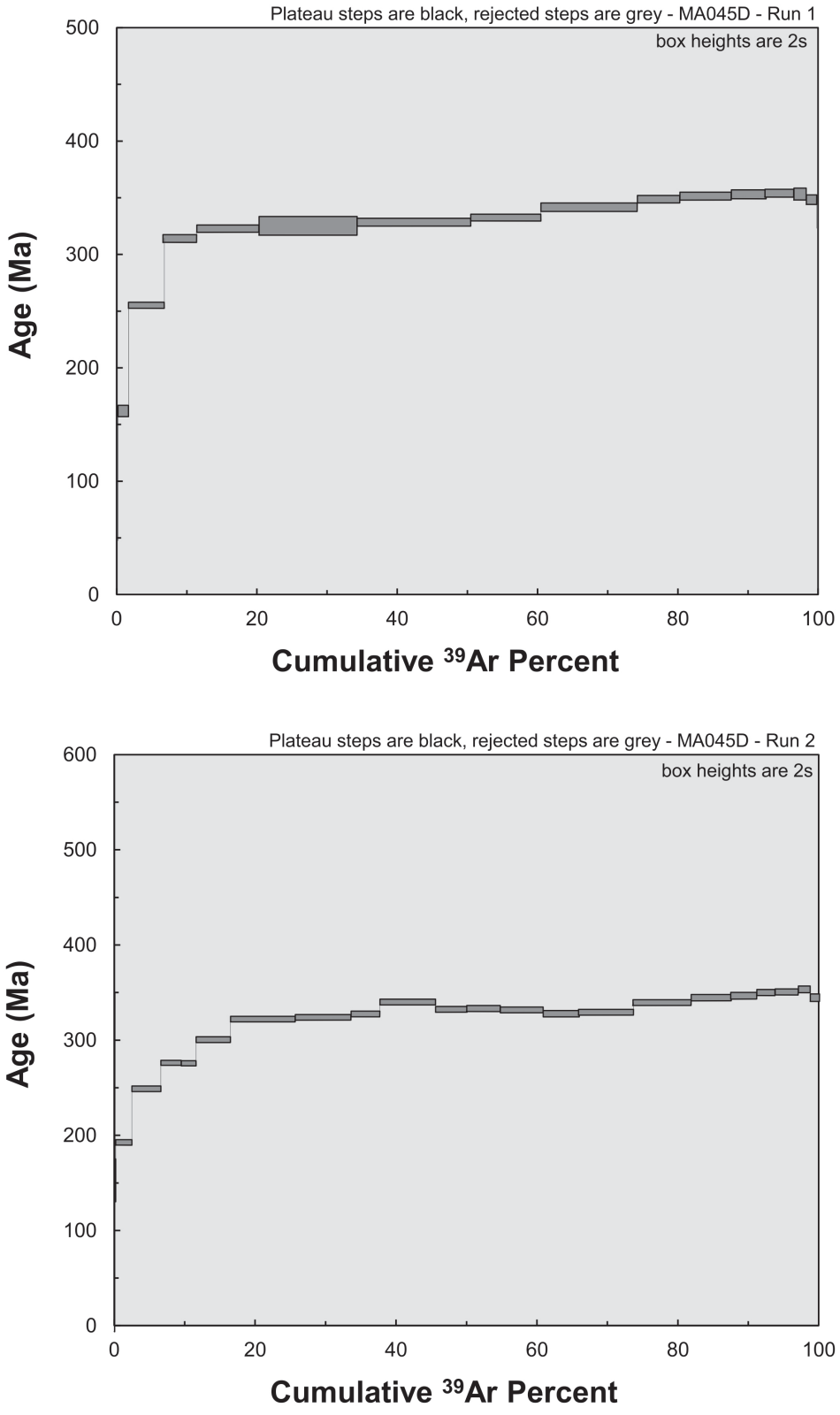

Figure 3.8: $^{40}Ar/^{39}Ar$ step heating results for MA045D runs 1 and 2.

between about 400 Ma, the age of the youngest Road River Group intruded by carbonatite dykes, and 366 Ma, the emplacement age of the Ospika pipe, an interval of just over 30 million years. The contractional D_1 tectonic event, responsible for syn-magmatic nappe formation and the development of the bedding parallel cleavage, is therefore constrained to have occurred in the Late Devonian close to but before 366 Ma.

The 460 Ma U-Pb zircon crystallization age of the Lady Laurier volcanic member of the Skoki Formation is consistent with the paleontological Upper Ordovician age of the Skoki dolostone members. The Lady Laurier volcanic member of the Skoki Formation, despite being characterized by alkaline magmatism (Goodfellow et al. 1995, pre-dated intrusion of the Aley carbonatite by 90 million years, and constituted a distinct magmatic event unrelated to the Aley carbonatite.

Detrital zircon data from quartz clasts of the Kechika Formation volcano-sedimentary member indicate that the quartzite has a maximum age of 1680 Ma (late Paleoproterozoic). This data for the Aley area quartzites closely correlate with those from sandstone and quartzite of the Cambrian Atan Group, the northernmost British Columbia Foreland Belt equivalent of the Hamil-Gog Groups, but differ from those from quartzite of the Ordovician Monkman Formation, located to the immediate south of Aley, in that they do not contain Grenvillian-aged zircons (Gehrels and Ross, 1998).

Paleozoic alkaline volcanic centres and alkaline-carbonatite intrusive complexes are known along the length of the Cordilleran Foreland belt (Fig. 3.9). However, whether or not these alkaline igneous suites and complexes, including the Aley, constitute coeval components of a margin-wide, syn-tectonic alkaline magmatic province has remained

unclear due to a lack of data. Geochronological data for the alkaline-carbonatite complexes are limited; geochronological data exists for only one other carbonatite complex, the Ice River of the southern Rocky Mountains of Alberta (Fig. 3.9). Parrish (1987) obtained U-Pb ages of 363.1 +/- 2.2 on zircon and 368.8 +/- 7.0 on titanite from the Ice River Complex. More recently Tappe and Simonetti (2012) obtained a 361.7 +/- 1.0 Ma U-Pb age on perovskite from the Ice River complex. Available geochronological data are, therefore, consistent with interpretation of the Aley and Ice River complexes as having intruded during, and being correlative components of, a major carbonatitic magmatic event that affected the western Foreland belt. Furthermore, field relationships constrain the undated alkaline-carbonatite complexes to emplacement in the Late Devonian to Early Mississippian (Pell, 1994). Available geological and geochronological constraints are therefore consistent with coeval carbonatite magmatism in the Upper Devonian along the length of the western Foreland Belt of the Canadian Cordilleran.

Similarities exist in the stratigraphy that are host to the five alkaline-carbonatite complexes; all intrude shelf-slope carbonates and clastic rocks proximal to the carbonate-shale facies boundary that separates and distinguishes the eastern and western subprovinces of the Foreland Belt. Detailed structural data and mapping at Aley has established that carbonatite magmatism was syn-kinematic with a major collisional tectonic event that gave rise to crustal scale nappes and a related bedding parallel cleavage. Currie (1975) demonstrated that the Ice River complex has, like Aley, undergone complex polyphase deformation and that its wall rocks are similarly characterized by an S_1 bedding parallel cleavage. However, the age of fabrics and folds

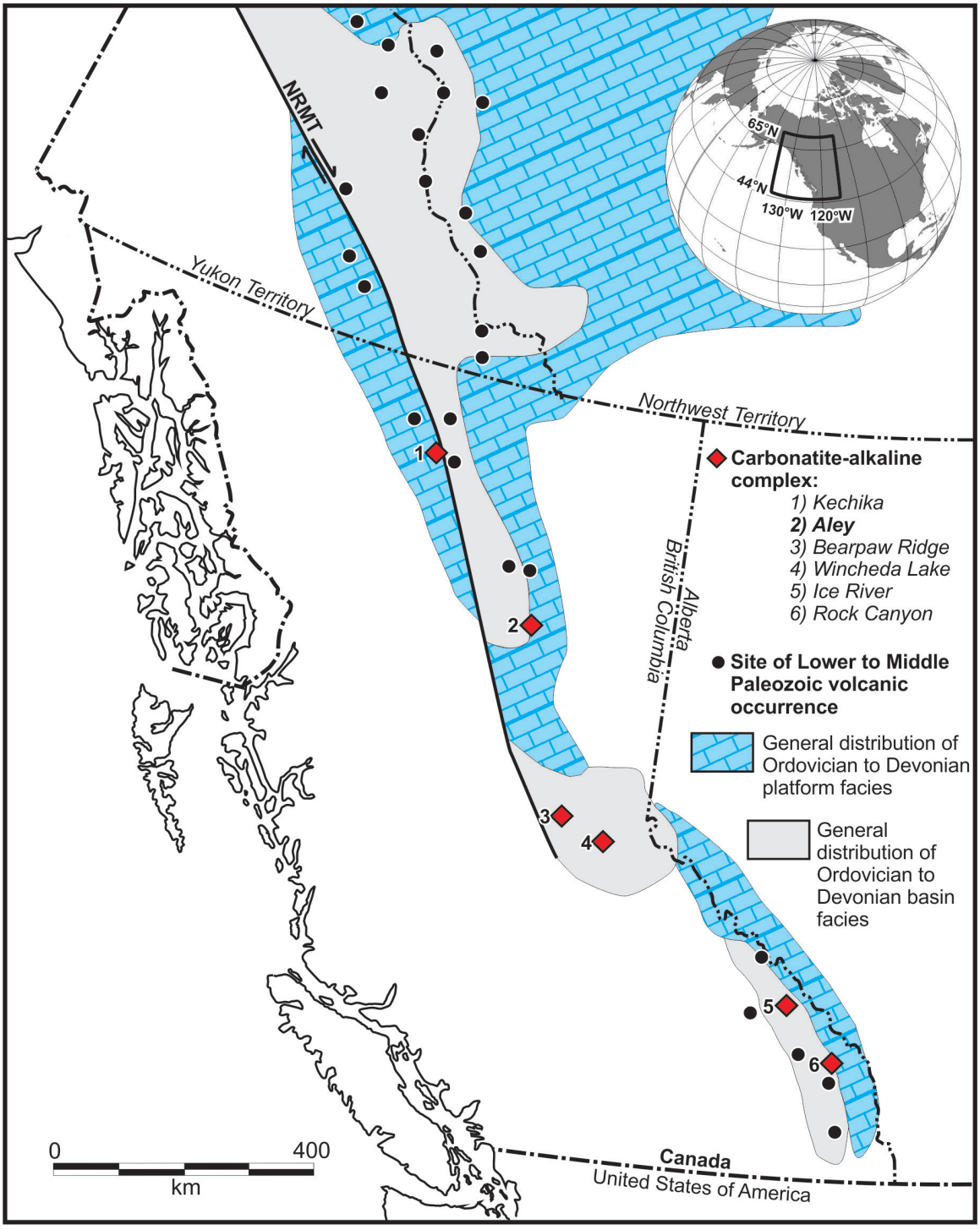

Figure 3.9: Distribution of early and mid-Paleozoic alkaline volcanic and carbonatite occurrences in the Foreland Belt of the Canadian Cordillera, revised after Goodfellow et al. (1995) with additional data from Hunt (2002).

at Ice River are poorly constrained, and they have commonly been interpreted to all be products of Cretaceous Rocky Mountain deformation (Currie, 1975). Our findings suggest that the bedding parallel cleavage that characterizes the wall rocks of the Ice River complex and other carbonatite complexes of the western Foreland belt, may have resulted from Upper Devonian deformation. Demonstrating syn-magmatic tectonism during emplacement of the other Foreland carbonatite complexes constitutes a test of our interpretation of the foreland carbonatite complexes as comprising a syn-tectonic alkaline magmatic province.

Structural and stratigraphic data from along the length of the Cordilleran orogen are consistent with a continental scale Upper Devonian collisional orogenic event. This event was originally recognised as the Antler Orogen in north-central Nevada (Roberts Mountain area) where large-scale Upper Devonian to Early Mississippian folding, nappe formation and thrust sheet emplacement produced a major angular unconformity (Roberts et al., 1958). Johnson (1971) proposed that Antler orogeny affected the entire North American Cordillera based in part on the recognition by Gabrielse (1963, 1967) of similar contractional structures and unconformities in the Cariboo and Cassiar districts of British Columbia and Yukon. In the United States, Antler orogenesis has been attributed to arc-continent collision involving west-dipping subduction of oceanic lithosphere lying west of and continuous with North American continental lithosphere, leading to partial subduction of continental crust beneath a far-traveled arc. Obduction of the arc formed the Roberts Mountain allochthon along the Roberts Mountain thrust (Johnson and Pendergast, 1981; Speed and Sleep, 1982; Dickinson, 2004). In Canada, the Antler Orogeny is manifest by Middle Devonian contractional deformation in the Purcell and

southern Rocky Mountains (Root, 2001); Upper Devonian to Early Mississippian erosional unconformities in the Cariboo Mountains and Kootenay Arc (Klepacki, 1985; Struik, 1986); volcanism and alkaline magmatism along the length of the western Foreland Belt (Goodfellow et al. 1995); and Devono-Mississippian coarse clastic sedimentation in northern British Columbia and Yukon (e.g. Earn Group, Gordey et al. 1987). Paleocurrent indicators suggest that Earn Group was derived from an uplifted landmass that lay to the west of the Cordillera and which shed clastic sediments to the east (Gabrielse, 1977). Smith et al. (1993) proposed that Devonian-Mississippian orogenesis characterized the entire Cordilleran margin; that it resulted from continent-arc collision; and that the resulting orogenic welt shed clastic detritus eastward into a foreland basin as exemplified by the westerly-derived Earn Group.

The syn-magmatic deformation at Aley Creek appears to have been synchronous with the *ca.* 370 Ma (Oldow et al., 1989) Antler Orogeny. Observations from the stratigraphic, structural, and magmatic record in our study area indicate that the D_1 event affecting the Aley area is consistent with Antler-style orogenesis: (1) the quartzites observed in the Ordovician-Devonian Road River Group are similar to coarse clastic sediments of the Antler-linked Earn Group exposed to the north of the Aley Creek area (Fig. 3.2); and (2) the syn-magmatic D_1 deformation, including tight folding and nappe formation, is similar to Antler deformation observed in the Kootenay and Cariboo Mountains of southern and central British Columbia.

3.7 Conclusions

Our geochronological data demonstrate that the Aley carbonatite and associated alkaline intrusives were emplaced at *ca.* 365 Ma, coeval with the *ca.* 362 Ma Ice River

carbonatite complex, and support interpretation of the carbonatite intrusions of the western Foreland Belt as genetically linked components of an alkaline-carbonatitic magmatic province. Syn-magmatic contractional deformation at Aley suggests that the Foreland Belt carbonatite intrusions are magmatic manifestations of a Late Devonian orogenic event of continental scope. Structural, stratigraphic, and geochronological data from the Aley area indicate that deformation was similar in style to and coeval with structures attributable to the Antler Orogeny, supporting the interpretation of the Antler orogen having extended the length of Cordilleran margin from the southern United States to Alaska. Further structural, stratigraphic, and geochronological investigations of the other five alkaline-carbonatite complexes in the Foreland Belt are required to further test this hypothesis.

References cited

Beranek, L.P., Mortensen, J.K., 2011, The timing and provenance record of the Late Permian Klondike orogeny in northwestern Canada and arc-continent collision along western North America: Tectonics, v. 30, p. TC5017.

Cecile, M.P., and Norford, B.S., 1979, Basin to platform transition, Lower Paleozoic strata of Ware and Trutch map areas, northeastern British Columbia, *in* Current Research, part A: Geological Survey of Canada Paper 79-1A, p. 219–226.

Currie, K.L., 1975, The geology and petrology of the Ice River alkaline complex, British Columbia. Geological Survey of Canada Bulletin, 245, 68 p.

Dickinson, W.R., 2004, Evolution of the North American Cordillera: Annual Reviews in Earth and Planetary Sciences, v. 32, p. 13-45.

Gabrielse, H., 1963, McDame map area, British Columbia: Geological Survey of Canada Memoir 319, 138 p.

Gabrielse, H., 1967, Tectonic evolution of the northern Canadian Cordillera: Canadian Journal of Earth Sciences, v.4, p. 271-298.

Gabrielse, H., Dodds, C.J., and Mansy, J.L., 1977, Operation Finlay, British Columbia, *in* Report of activities, part A: Geological Survey of Canada Paper 77-1A, p. 243-246.

Gabrielse, H., 1985, Major dextral transcurrent displacements along the Northern Rocky Mountain Trench and related lineaments in north-central British Columbia: Geological Society of America Bulletin, v. 96, p. 1-14.

Gehrels, G.E., and Ross, G.M., 1998, Detrital zircon geochronology of Neoproterozoic to Permian miogeoclinal strata in British Columbia and Alberta: Canadian Journal of Earth Sciences, v. 35, p. 1380-1401.

Goodfellow, W.D., Cecile, M.P., and Leybourne, M.I., 1995, Geochemistry, petrogenesis, and tectonic setting of lower Paleozoic alkalic and potassic volcanic rocks, northern Canadian Cordilleran miogeocline: Canadian Journal of Earth Sciences, v. 32, p. 1236–1254.

Gordey, S.P., Abbott, J.G., Tempelman-Kluit, D., and Gabrielse, H., 1987, “Antler” clastics in the Canadian Cordillera: Tectonics, v. 11, p. 1266–1287.

Hunt, J.A., 2002, Volcanic-associated massive sulfide (VMS) mineralization in the Yukon-Tanana Terrane and coeval strata of the North American miogeocline, in the Yukon and adjacent areas: Exploration and Geological Services Division, Yukon Region, Indian and Northern Affairs Canada, Bulletin 12, 107 p.

Johnson, J.G., 1971, Timing and coordination of orogenic, epeirogenic, and eustatic events: Geological Society of America Bulletin, v. 82, p. 3263-3298.

Johnson, J.G., and Pendergast, A., 1981, Timing and mode of emplacement of the Roberts Mountain allochthon, Antler orogeny: GSA Bulletin, v. 92, p. 648-659.

Klepacki, D.W., 1985, Stratigraphy and structural geology of the Goat Range area, southeastern British Columbia [Ph.D. thesis]: Cambridge, Massachusetts, U.S.A., Massachusetts Institute of Technology, 268 pages.

Kressall, R., McLeish, D.F., Crozier, J., and Chakhmouradian, A.R., 2010, The Aley carbonatite complex: petrogenesis of a Cordilleran niobium deposit: Geology of Rare Metals International Workshop, British Columbia Geological Survey Open File 2010-10, p. 25-26.

MacIntyre, D.G., 1998, Geology, geochemistry and mineral deposits of the Akie River Area, northeast British Columbia: British Columbia Ministry of Energy and Mines Bulletin 103, 91 p.

Mader, U.K., 1986, The Aley Carbonatite Complex [M.Sc. thesis]: Vancouver, University of British Columbia, 176 p.

McLeish, D.F., and Johnston, S.T., 2013, The Upper Devonian Aley carbonatite complex: A product of Antler orogenesis in the western Foreland Belt of the Canadian Cordillera: Geology, (in review).

Norford, B.S., Lower Devonian graptolites in the Road River Formation, northern British Columbia, *in* Current Research, part A: Geological Survey of Canada Paper 79-1A, p. 383-384.

Oldow, J.S., Bally, A.W., Avé Lallement, H.G., Leeman, W.P., 1989, Phanerozoic evolution of the North American Cordillera, United States and Canada, *in* Bally, A.W., Palmer, A.R., eds., The Geology of North America – An Overview: Boulder, Colorado, Geological Society of America, v. A, p. 139–232.

Parrish, R.R., Heinrich, S., and Archibald, D., 1987, Age of the Ice River complex, southeastern British Columbia. Geological Survey of Canada Paper 87-2, p. 33-37.

Pell, J., 1994, Carbonatites, nepheline syenites, kimberlites and related rocks in British Columbia: British Columbia Ministry of Energy, Mines and Petroleum Resources Bulletin 88, 136 p.

Pride, K.R., 1983, Geological Survey on the Aley Claims, Omineca Mining Division, British Columbia: British Columbia Ministry of Energy, Mines and Petroleum Resources Assessment Report 12018.

Pride, K.R., LeCouter, P.C., and Mawer, A.B, 1986, Geology and mineralogy of the Aley Carbonatite: Canadian Institute of Mining and Metallurgy, 10th District 6 Meeting, Victoria, British Columbia, Abstracts, p. 32.

Pyle, L.J., and Barnes, C.R., 2001, Conodonts from the Kechika Formation and Road River Group (Lower to Upper Ordovician) of the Cassiar Terrane, northern British Columbia: Canadian Journal of Earth Sciences, v. 38, p. 1387–1401.

Roberts, R.J, Ferguson, H.G., Gilluly, J., and Hotz, P.E., 1958, Paleozoic rocks of northcentral Nevada: Bulletin of the American Association of Petroleum Geologists, v.42, p. 2813-2857.

Root, K., 2001, Devonian Antler fold and thrust belt and foreland basin development in the southern Canadian Cordillera: implications for the Western Canada Sedimentary Basin: Bulletin of Canadian Petroleum Geology, v. 49, p. 7–36.

Smith, M.T., Dickinson, W.R., and Gehrels, G.E. 1993. Contractional nature of Devonian–Mississippian Antler tectonism along the North American continental margin: Geology, v. 21, 21–24.

Speed, R.C, and Sleep, N.H., 1982, Antler orogeny and foreland basin: A model: Geological Society of America Bulletin, v. 93, p. 815-818.

Struik, L.C., 1986, Imbricated terranes of the Cariboo gold belt with correlations and implications for tectonics in southeastern British Columbia: Canadian Journal of Earth Sciences, v. 23, p. 1047-1061.

Tappe, S., and Simonetti, A., Combined U-Pb geochronology and Sr-Nd isotope analysis of the Ice River perovskite standard, with implications for kimberlite and alkaline rock petrogenesis. Chemical Geology, 304-305: 10-17, 2012.

Tafti, R., Mortensen, J.K., Lang, J.R., Rebagliati, M. and Oliver, J.L., 2009, Jurassic U-Pb and Re-Os ages for the newly discovered Xietongmen Cu-Au porphyry district, Tibet, PRC: Implications for metallogenic epochs in the southern Gangdese belt: Economic Geology, v. 104, p. 127-136.

Taylor, G.C., and Stott, D.F., 1973, Tuchodi Lakes map-area, British Columbia (94K): Geological Survey of Canada Memoir 373, 38 p.

Taylor, G.C., 1979, Trutch (94G) and Ware east half (94F, E1/2) map-areas, northeastern British Columbia: Geological Survey of Canada Open File Report 606, scale 1:250,000, 1 sheet.

Taylor, G.C., Cecile, M.P., Jefferson, C.W., and Norford, B.S., 1979, Stratigraphy of Ware (east half) map area, northeastern British Columbia, i*n* Current Research, part A: Geological Survey of Canada Paper 79-1A, p. 227–231.

Thompson, R.I., 1989, Stratigraphy, tectonic evolution and structural analysis of the Halfway River map area (94B), northern Rocky Mountains, British Columbia: Geological Survey of Canada Memoir 425, 119 p.

Wheeler, J.O., and McFeely, P., 1991, Tectonic Assemblage Map of the Canadian Cordillera and Adjacent Parts of the United States of America: Geological Survey of Canada Map 1712A, scale 1:2,000,000, 2 sheets

CHAPTER 4

Conclusions

4.1 Conclusions

The principal contributions of this study are:

(1) Middle Palaeozoic volcanic and sedimentary strata in the Aley region of the western Foreland belt of the Canadian Cordillera record deposition in an active margin characterised by crustal scale nappe formation and syn-kinematic carbonatite magmatism. The westerly derived Late Devonian to Early Mississippian Earn Group that characterizes the western foreland belt to the north of the Aley carbonatite is inferred to consist of syn-orogenic sediments shed from the collision zone.

(2) The Aley carbonatite and associated alkaline intrusives were emplaced at ca. 365 Ma, coeval with the *ca.* 362 Ma Ice River carbonatite complex, and likely coeval with the other four Foreland Belt alkaline-carbonatite complexes which have poorly constrained ages of Late Devonian to Early Mississippian. This temporal association is consistent with interpreting the carbonatite intrusions of the western Foreland Belt as genetically linked components of an alkaline-carbonatitic magmatic province.

(3) Assuming the tectono-stratigraphic record in the Aley area is an accurate proxy for the evolution of the entire western Foreland Belt, syn-magmatic contractional deformation at Aley suggests that the Foreland Belt carbonatite intrusions are magmatic manifestations of a margin-wide Late Devonian orogenic event. The orogenic event was similar in style and timing to the Antler Orogeny, supporting the interpretation of the Antler orogen having

extended the length of Cordilleran margin from the southern United States to Alaska.

(4) Palaeozoic strata of the eastern Foreland Belt lack a record of Late Devonian orogenesis, and are best explained as having been formed at a passive margin. This interpretation requires that the boundary between the eastern and western Foreland Belts, which is mapped as a Paleozoic carbonate to shale facies boundary, is or lies immediately adjacent to a cryptic suture or transform boundary, and that the western Foreland belt is far-travelled and exotic relative to the eastern Foreland belt.

4.2 Recommendations for future work

Investigations in six key areas are recommended to further explore the structural-magmatic evolution of the Aley carbonatite complex and better understand the implications for the tectonic evolution of the eastern Canadian Cordillera:

First, interpreting mid-Paleozoic syn-tectonic alkaline-carbonatite magmatism in the Aley area and related Foreland Belt alkaline-carbonatite complexes to be manifestations of a Late Devonian orogenic event of continental scope rests on the assumptions that: (1) the other five Foreland alkaline-carbonatite complexes contain a record of similar syn-magmatic contractional deformation and related orogenic coarse-clastic sedimentation in their host strata; and (2) the four undated Foreland alkaline-carbonatite complexes are in fact coeval with the Aley and Ice River complexes. Integrated structural, stratigraphic, and geochronological study of each complex is required to further test and confirm the interpretation here presented.

Second, an outstanding problem for employing the Antler arc-continent collision model to explain syn-magmatic contractional deformation in Aley area is the absence of obducted high-pressure subduction zone rocks in the Foreland Belt of the Canadian Cordillera. While such rocks, which are volumetrically minor and areally restricted in most modern collision zone analogues, may have been removed by erosion in the Canadian Cordilleran Foreland Belt, a record of their existence may be preserved in detrital sediments hosted by syn-orogenic strata like the Earn Group. A detailed study of detrital sediments from these rocks could test if ophiolitic sediments (*e.g.* chromite, spinel) exist within the mid-Paleozoic sedimentary record of the western Foreland Belt.

Third, although Earn Group sediments may be interpreted to record disposition in a collisional foreland basin, the lack of Paleozoic detrital zircons, significant volcanic rock fragments, and feldspathic sediments currently recognised in the Earn Group poses a challenge to the Antler arc-continent collision model. Further study and mapping of the Earn Group is necessary to confirm whether all of these collisional indicators are in fact absent from the sedimentary record or are not yet recognised by the limited study of the Earn Group to date.

Fourth, sampling different phases of the carbonatite (calcite, rare-earth bearing ankerite carbonatite dykes) may yield zircons with sufficient radiogenic Pb to date the carbonatite directly via U-Pb methods, thereby providing more robust constraints on the age of syn-carbonatite orogenesis in the western Foreland Belt.

Fifth, paleomagnetic study of mid-Paleozoic volcanic units in the Foreland Belt could help test the final conclusions of this study: that the western Foreland Belt is allochthonous with respect to the eastern Foreland Belt.

Finally, the petrogenetic origin of carbonatite complexes globally is not well understood and models for tectonic controls on their emplacement are varied. Geochemical studies cited within this thesis have attempted to classify the different tectonic environments into which alkaline rock types are emplaced by their isotope and trace-element geochemical signatures. A detailed geochemical study of the Aley carbonatite could help better test the interpretation of the carbonatite being emplaced during a major collisional orogenic event.

APPENDIX A

Geochronology: anlaytical methods and ancillary data

Part 1: U-Pb ID-TIMS titanite analytical methodology

All sample preparation, geochemical separations and mass spectrometry were done at the Pacific Centre for Isotopic and Geochemical Research in the Department of Earth and Ocean Sciences, University of British Columbia. Minerals were separated from samples using conventional crushing, grinding, and Wilfley table techniques, followed by final concentration using heavy liquids and magnetic separations. Mineral fractions for analysis were selected on the basis of grain quality, size, magnetic susceptibility and morphology.

Masses were determined with a Sartorious SE2 ultramicrobalance. Grains were transferred into 300 uL PFA microcapsules (crucibles) and 0.1 mL subboiled 29N HF and 14N HNO_3 in a 10:1 mixture was added. Each fraction was spiked with a $^{233\text{-}235}U$-^{205}Pb tracer solution (typically 2 μg), capped and placed in a 125mL teflon liner (8-13 microcapsules per liner), which in turn went into a Parr-style stainless steel high pressure dissolution device for 7-10 days at 240C. Sample solutions were then dried to salts at ~130°C and residues were redissolved ~1 mL of sub-boiled 6.2 M HCl in oven in high pressure devices for 12 hours at 210°C. These solutions were again dried to salts and were again redissolved in 3.1 N HCl in high pressure devices for at 210C for 12 hours. Purification of Pb and U employed ion exchange column techniques modified slightly from those described by Parrish et al. (1987). Pb was eluted into a PFA beakers and U into a second set of beakers and further purified by passing through columns a second time. U was then eluted into beakers containing Pb. Elutants and dried in 7 mL screwtop PFA beakers on a hotplate at ~120°C in the presence of 2 μL of ultrapure 0.2N phosphoric acid (H_3PO_4).

Samples are loaded onto degassed, zone-refined Re filaments in 2 μL of silicic acid emitter (Gerstenberger and Haase, 1997). Isotopic ratios were measured using a modified single collector VG-54R thermal ionization mass spectrometer equipped with an analogue Daly photomultiplier. Measurements were done in peak-switching mode on the Daly detector.

Analytical blanks during the course of this study were 0.2 pg for U and 8 pg U. Fractionation was determined directly on individual runs using the $^{233\text{-}235}$U tracer, and Pb isotopic ratios were corrected for fractionation of 0.23%/amu, based on replicate analyses of the NBS-982 Pb standard and the values recommended by Thirlwall (2000). Data reduction employed the excel based program of Schmitz and Schoene (2007). Standard concordia diagrams were constructed and regression intercepts, weighted averages calculated with Isoplot (Ludwig, 2003). Unless otherwise noted, all errors are quoted at the 2σ or 95% level of confidence. Isotopic dates are calculated the decay constants λ_{238}=1.55125E-10 and λ_{235}=9.8485E-10 (Jaffey et al. 1971).

References cited

Crowley, J.L., Schoene, B. and Bowring, S.A., 2007. U-Pb dating of zircon in the Bishop Tuff at the millennial scale. Geology, vol. 35, no. 12, pp.1123-1126.

Gerstenberger, H., Haase, G., 1997. A highly effective emitter substance for mass spectrometric Pb isotope ratio determinations. Chem. Geol. 136, 309–312.

Jaffey, A.H., Flynn, K.F., Glendenin, L.E., Bentley, W.C., Essling, A.M.,1971. Precision measurement of half-lives and specific activities of 235U and 238U. Phys. Rev. C4, 1889–1906.

Krogh, T.E, 1982. Improved accuracy of U-Pb zircon ages by the creation of more concordant systems using an air abrasion technique. Geochimica et Cosmochimica Acta, 46, p. 637-649.

Ludwig K.R., 2003. Isoplot 3.00, A Geochronological Toolkit for Microsoft Excel. University of California at Berkely, kludwig@bgc.org.

Parrish, R., Roddick, J.C., Loveridge, W.D., and Sullivan, R.W., 1987, Uranium-lead analytical techniques at the geochronology laboratory, Geological Survey of Canada. *In* Radiogenic Age and Isotopic Studies, Report 1, Geological Survey of Canada, Paper 87-2, p. 3-7.

Schmitz, M. D., and B. Schoene (2007), Derivation of isotope ratios, errors, and error correlations for U-Pb geochronology using 205Pb-235U-(233U)-spiked isotope dilution thermal ionization mass spectrometric data, Geochem. Geophys. Geosyst., 8, Q08006, doi:10.1029/2006GC001492.

Stacey, J.S., and Kramers, J.D. 1975. Approximation of terrestrial lead isotopic evolution by a two-stage model. Earth and Planetary Science Letters, 26: 207–221.

Thirlwall, M.F., 2000. Inter-laboratory and other errors in Pb isotope analyses investigated using a ^{207}Pb–^{204}Pb double spike: Chemical Geology, 163 p. 299–322.

Part 2: U-Pb LA-ICP-MS zircon analytical methodology

Mineral separations were done at the Pacific Centre for Isotopic and Geochemical Research (PCIGR) at the University of British Columbia, using conventional crushing, pulverizing, and wet shaking table concentration methods, followed by heavy liquid and magnetic separation.

Uranium-lead analyses were carried out using laser ablation (LA) ICP-MS methods. Analyses were done using a New Wave UP-213 laser ablation system and a ThermoFinnigan Element2 single collector, double-focusing, magnetic sector ICP-MS. The data acquisition and reduction protocol employed at the PCIGR has been described by Tafti et al. (2009), and is briefly summarized below. The best quality zircons were handpicked from the heavy mineral concentrate and mounted in an epoxy puck along with several grains of the 337 Ma Plešovice zircon standard (Sláma et al., 2007) and a 197 Ma in-house zircon monitor, and brought to a very high polish. The surface of the mount was washed for 10 minutes with dilute nitric acid and rinsed in ultraclean water prior to analysis. High quality portions of each grain, free of alteration, inclusions, or cores, were selected for analysis. Line scans rather than spot analyses were employed in order to minimize elemental fractionation during the analyses (Košler et al., 2008). Backgrounds were measured with the laser shutter closed for ten seconds, followed by data collection with the laser firing for approximately 29 seconds. The time-resolved signals were analyzed using GLITTER software (Van Achterbergh et al., 2001; Griffin et al., 2008), which automatically subtracts background measurements, propagates all analytical errors, and calculates isotopic ratios and ages. Corrections for mass and

elemental fractionation were made by bracketing analyses of unknown grains with replicate analyses of the Plešovice zircon standard.

A typical analytical session at the PCIGR consists of four analyses of the standard zircon, followed by two analyses of the 197 Ma in-house zircon monitor, four analyses of unknown zircons, two standard analyses, four unknown analyses, etc., and finally two analyses of the in-house monitor and four standard analyses. Final interpretation and plotting of the analytical results employs ISOPLOT software (Ludwig, 2003). The amount of radiogenic ^{207}Pb in young zircons is extremely low; hence, counting errors are correspondingly high, and calculated errors for $^{207}Pb/^{235}U$ and $^{207}Pb/^{206}Pb$ ages are also high. Interpreted ages for the samples dating in this study are based on a weighted average of the individual calculated $^{206}Pb/^{238}U$ ages. The amount of measured ^{204}Pb in all but a very small number of the analyses generated during the study is negligible, so no correction was made for contained common Pb.

References cited

Griffin, W.L., Powell, W.J., Pearson, N.J. and O'Reilly, S.Y., 2008, Glitter: Data reduction software for laser ablation ICP-MS; *In* Sylvester, P.J. (ed.), Laser Ablation ICP-MS in the Earth Sciences: Current Practices and Outstanding Issues, Mineralogical Association of Canada Short Course Series, Short Course 40, Vancouver, B.C., pp. 308-311.

Košler, J., Forst, L., Sláma, J., 2008, Lamdate and Lamtool: spreadsheet-based data reduction for laser ablation ICP-MS; *In* Sylvester, P.J. (ed.), Laser Ablation ICP-MS in the Earth Sciences: Current Practices and Outstanding Issues, Mineralogical Association of Canada Short Course Series, Short Course 40, Vancouver, B.C., pp. 315-317.

Ludwig, K., 2003, Isoplot/Ex, version 3: A geochronological toolkit for Microsoft Excel: Berkeley, California, Geochronology Center, Berkeley.

Sláma, J., J., Košler, J., Condon, D.J. Crowley, J.L., Gerdes, A., Hanchar, J.M., Horstwood, M.S.A., Morris, G.A., Nasdala, N., Norberg, N., Schaltegger, U., Schoene, B., Tubrett, M.N. and Whitehouse, M.J., 2007, Plešovice zircon — A new natural reference material for U–Pb and Hf isotopic microanalysis, Chemical Geology, v. 249, pp. 1-35

.

Tafti, R., Mortensen, J.K., Lang, J.R., Rebagliati, M. and Oliver, J.L., 2009, Jurassic U-Pb and Re-Os ages for newly discovered Xietongmen Cu-Au porphyry district, Tibet: Implications for metallogenic epochs in the southern Gangdese Belt; Economic Geology, v. 104, pp. 127–136

Van Achterbergh, E., Ryan, C.G., Jackson, S.E. and Griffin, W.L., 2001, Data reduction software for LA-ICP-MS: appendix; *In* Sylvester, P.J. (ed.), Laser Ablation – ICP-Mass Spectrometry in the Earth Sciences: Principles and Applications, Mineralogical Association of Canada Short Course Series, Ottawa, Ontario, Canada, v. 29, pp. 239-243.

Part 3: Ancillary data

Table A1: U-Th-Pb isotopic data for Ospika pipe ID-TIMS titanite analyses

		Compositional Parameters							Sample (Radiogenic + Initial Pb) Isotope Ratios				
Sample (a)	Wt. mg (b)	U ppm (c)	$\frac{Th}{U}$ (d)	Pb ppm (c)	$^{206}Pb^*$ x10^{-13} mol (e)	mol % $^{206}Pb^*$ (e)	$\frac{Pb^*}{Pb_c}$ (e)	Pb_c (pg) (e)	$\frac{^{206}Pb}{^{204}Pb}$ (f)	$\frac{^{238}U}{^{204}Pb}$ (j)	% err (h)	$\frac{^{206}Pb}{^{204}Pb}$ (j)	% err (h)	corr. coef. 8/4-6/4
MA045A														
T1	0.013	14	0.218	1.7	0.4406	75.89%	0.87	11.68	75	1691.562420	37.995661	117.426984	32.393686	0.999361
T3	0.019	10	0.303	3.2	0.4565	42.86%	0.21	50.62	32	249.178355	5.490588	33.191513	2.550196	0.992225
T4	0.010	23	0.291	3.3	0.5333	70.74%	0.69	18.38	62	1017.579946	18.657768	78.156196	14.372280	0.999709
T5	0.012	12	0.251	2.2	0.3779	62.48%	0.46	18.90	48	693.884851	17.963102	59.057694	12.513442	0.999530

(a)T1, T2 etc. are labels for fractions composed of single titanite grains or fragments of single grains.
(b) Grain masses determined on Sartorious SE2 ultramicrobalance to +/- 1 microgram.
(c) Nominal U and total Pb concentrations subject to uncertainty in mass determinations.
(d) Model Th/U ratio calculated from radiogenic 208Pb/206Pb ratio and 207Pb/235U age.
(e) Pb* and Pbc represent radiogenic and common Pb, respectively; mol % 206Pb* with respect to radiogenic, blank and initial common Pb.
(f) Measured ratio corrected for spike and fractionation only. Mass discrimination of 0.23%/amu based on analysis of NBS-982; all Daly analyses.
(g) Corrected for fractionation, spike, and common Pb; 5 pg of common Pb was assumed to be procedural blank: 206Pb/204Pb = 18.50 ± 1.0%; 207Pb/204Pb = 15.20 ± 1.0%; 208Pb/204Pb = 38.40 ± 1.0% (all uncertainties 1-sigma).
(h) Errors are 2-sigma, propagated using the algorithms of Schmitz and Schoene (2007) and Crowley et al. (2007).
(i) Corrected for fractionation, spike, and blank Pb only.

Table A2: U-Pb isotopic data for zircons from the Skoki Formation volcanic agglomerate tuff (MA062 via LA-ICP-MS)

	Isotopic Ratios							Isotopic Ages						Background corrected mean counts per second							
	207/206	% 1s	207/235	% 1s	206/238	% 1s	rho	207/206	2s	207/235	2s	206/238	2s	202	204	206	207	208	232	235	238
Sample MA-062																					
1	0.05681	0.00074	0.57409	0.00855	0.07402	0.00046	0.42	483.6	28.9	460.7	5.51	460.3	2.79	9	20221	1164	5340	174095	2111	521656	912653
2	0.05669	0.00069	0.57488	0.00795	0.07399	0.00044	0.43	478.9	26.88	461.2	5.13	460.2	2.66	20	20699	1190	5010	167516	2155	535147	3885984
3	0.05602	0.00048	0.58236	0.00564	0.07412	0.00037	0.52	452.6	18.46	466	3.62	460.9	2.22	3	51842	2944	23305	812383	5270	1340442	501308
4	0.05717	0.00059	0.58125	0.00681	0.0741	0.00041	0.47	497.7	22.86	465.3	4.37	460.8	2.44	2	40037	2321	16318	580847	4166	1037467	2427562
5	0.05466	0.00078	0.56406	0.00914	0.07402	0.00049	0.41	398.2	31.22	454.2	5.93	460.3	2.94	0	36736	2036	11099	375843	3773	956452	943733
6	0.05598	0.0007	0.58094	0.00827	0.07517	0.00046	0.43	451.2	27.07	465.1	5.31	467.2	2.76	5	28088	1595	7327	256748	2872	721474	927981
7	0.05522	0.00067	0.55579	0.0077	0.07409	0.00045	0.44	420.9	26.84	448.8	5.02	460.7	2.68	0	28550	1599	8056	281843	3012	745400	2710321
8	0.05721	0.00107	0.564	0.01203	0.07409	0.00061	0.39	499	40.61	454.1	7.81	460.8	3.65	0	11243	652	2070	69067	1212	294081	1779879
9	0.05618	0.00089	0.56433	0.01022	0.07411	0.00054	0.40	458.8	35.09	454.3	6.64	460.9	3.21	0	21519	1226	5576	191623	2280	563760	179560
10	0.05728	0.00076	0.57391	0.00863	0.07408	0.00047	0.42	501.8	28.87	460.5	5.57	460.7	2.85	5	21246	1234	4977	174218	2258	557870	3823929
11	0.05649	0.00066	0.56572	0.00752	0.07234	0.00043	0.45	470.9	25.94	455.2	4.88	450.2	2.58	0	24780	1420	3504	125570	2641	668826	1458974
12	0.06095	0.00261	0.58996	0.02891	0.07391	0.00129	0.36	637.4	89.47	470.8	18.47	459.7	7.76	12	5415	334	1665	53740	597	143326	1035232
13	0.05533	0.00168	0.60859	0.02139	0.07721	0.00094	0.35	425.3	66.08	482.7	13.5	479.5	5.64	2	6872	385	2279	74272	668	174435	1072736
14	0.05449	0.00129	0.56189	0.01519	0.07424	0.00073	0.36	391.4	52	452.8	9.87	461.7	4.36	0	9337	516	2965	100635	969	246951	730576
15	0.05704	0.00103	0.56095	0.01143	0.07387	0.00059	0.39	492.5	39.3	452.1	7.44	459.4	3.51	0	8843	512	2780	95311	963	235507	131258
16	0.05525	0.00116	0.56704	0.01358	0.07367	0.00066	0.37	422.3	45.59	456.1	8.8	458.2	3.95	0	21749	1220	4241	146290	2275	582975	215538
17	0.05606	0.00109	0.58144	0.01293	0.07424	0.00062	0.38	454.4	42.5	465.4	8.3	461.7	3.74	0	10894	620	2518	84501	1128	290303	451113
18	0.05563	0.00145	0.53888	0.01598	0.07423	0.0008	0.36	437.3	56.9	437.7	10.54	461.6	4.83	0	16103	909	6228	218778	1788	429995	245040
19	0.05629	0.0008	0.57275	0.00926	0.07428	0.0005	0.42	463.2	31.38	459.8	5.98	461.9	2.99	4	14985	856	5741	203499	1586	400635	590518
20	0.0551	0.00109	0.57201	0.01288	0.07398	0.00063	0.38	416	42.79	459.3	8.32	460.1	3.77	41	11727	656	3374	115039	1217	315397	351513

Table A-33: U-Pb isotopic data for detrital zircons from the basal Kechika Formation (MA076 and MA190 via LA-ICP-MS). Preferred ages for zircons with <10% discordance are highlighted in yellow.

	Isotopic Ratios							Isotopic Ages						Preferred Ages			Background corrected mean counts per second						
Analysis_#	Pb207/Pb206		Pb207/U235		Pb206/U238		Rho	Pb207/Pb206		Pb207/U235		Pb206/U238		Discordance	Preferred Age	2s	202	204	206	207	208	232	235	238
MA076(f)	0.1144	0.0013	4.17453	0.07263	0.28005	0.00196	0.40	1870.4	20.37	1669	14.25	1591.6	9.85	14.9	1870.4	20.37	0	8	109006	12312	10873	122141	3434	912653
2	0.10653	0.00124	1.82415	0.02676	0.12748	0.00088	0.47	1741	21.16	1054.2	9.62	773.5	5.06	55.6	1741	21.16	0	253	211867	22343	26904	488768	14213	3885984
3	0.19696	0.00234	13.6755	0.36141	0.50999	0.0041	0.30	2801.2	19.26	2727.5	25.01	2656.6	17.49	5.2	2801.2	19.26	0	0	109651	21433	13138	87385	1812	501308
4	0.09838	0.00123	2.71611	0.04829	0.20631	0.0015	0.41	1593.6	23.24	1332.9	13.2	1209.1	8	24.1	1593.6	23.24	0	24	215395	21083	10897	185662	8945	2427562
5	0.1105	0.00122	4.1186	0.0682	0.29671	0.00201	0.41	1807.6	20.01	1658	13.53	1675	9.99	7.3	1807.6	20.01	66	0	120765	13310	7995	80574	3711	943733
6	0.11155	0.00137	5.09523	0.1042	0.33108	0.00243	0.36	1824.8	22.11	1835.3	17.36	1843.6	11.74	-1.0	1824.8	22.11	0	0	133241	14900	5958	55283	3335	927981
7	0.15825	0.00155	6.3913	0.09071	0.32278	0.00204	0.45	2437.1	16.52	2031.1	12.46	1803.3	9.93	26.0	2437.1	16.52	85	17	380442	60508	39881	428500	10762	2710321
8	0.12753	0.00164	3.99675	0.07917	0.23187	0.00178	0.39	2064.2	22.52	1633.5	16.09	1344.3	9.33	34.9	2064.2	22.52	0	27	179963	23123	20635	325414	6554	1779879
9	0.12164	0.00258	5.30451	0.21566	0.35344	0.00429	0.30	1980.4	37.25	1869.6	34.73	1951	20.42	1.5	1980.4	37.25	14	0	27750	3409	4313	34696	725	179560
10	0.10202	0.00113	2.33528	0.03306	0.17079	0.00112	0.46	1661.2	20.39	1223.1	10.06	1016.5	6.14	38.8	1661.2	20.39	0	78	286351	29582	12685	216502	14255	3823929
11	0.11335	0.00115	4.76083	0.06599	0.32698	0.00202	0.45	1853.8	18.3	1778	11.63	1823.7	9.82	1.6	1853.8	18.3	0	34	210306	24259	24147	231798	5696	1458974
12	0.10507	0.00155	3.16712	0.07047	0.23945	0.00197	0.37	1715.6	26.93	1449.2	17.17	1383.8	10.27	19.3	1715.6	26.93	80	14	109576	11745	17845	201071	4131	1035232
MA076©	0.16244	0.00137	10.2662	0.11455	0.46801	0.00278		2481.3	14.1	2459.1	10.32	2474.8	12.23	0.3	2481.3	14.1	39	0	204405	33818	1990	7629	3879	1072736
MA190(f)	0.15613	0.00173	9.36984	0.16088	0.44997	0.00296	0.38	2414.1	18.67	2374.9	15.75	2395.1	13.16	0.8	2414.1	18.67	37	71	147675	23870	13078	86114	2782	730576
b	0.15821	0.00222	9.36614	0.25988	0.46646	0.00398	0.31	2436.6	23.6	2374.5	25.46	2468	17.51	-1.3	2436.6	23.6	15	7	27577	4528	3511	16390	526	131258
c	0.15694	0.00215	9.57011	0.25285	0.46488	0.00383	0.31	2422.9	23.03	2394.3	24.29	2461.1	16.84	-1.6	2422.9	23.03	1	29	45251	7388	5597	33646	837	215538
d	0.1144	0.00201	4.4431	0.13265	0.30033	0.00294	0.33	1870.4	31.39	1720.4	24.74	1692.9	14.57	9.5	1870.4	31.39	67	18	61346	7319	4861	32411	1782	451113
e	0.10702	0.00155	4.95209	0.11771	0.33465	0.00267	0.34	1749.3	26.27	1811.2	20.08	1860.9	12.9	-6.4	1749.3	26.27	38	0	37229	4165	5373	46811	906	245040
f	0.17591	0.002	11.8253	0.19338	0.49616	0.0032	0.39	2614.7	18.77	2590.7	15.31	2597.3	13.78	0.7	2614.7	18.77	0	18	133719	24709	6711	32369	2238	590518
g	0.10424	0.00137	4.47608	0.08482	0.31555	0.00224	0.37	1700.9	24.02	1726.5	15.73	1768	11	-3.9	1700.9	24.02	1	0	50756	5571	4264	37704	1329	351513
h	0.14048	0.00195	5.70417	0.12307	0.3111	0.00243	0.36	2233.2	23.82	1932	18.64	1746.1	11.93	21.8	2233.2	23.82	0	0	95240	14122	13230	98330	2635	667282
i	0.10638	0.00163	4.52967	0.10973	0.3146	0.00259	0.34	1738.3	27.74	1736.4	20.15	1763.3	12.68	-1.4	1738.3	27.74	12	0	57768	6502	17475	177206	1523	399198
j	0.15907	0.00225	7.59929	0.17852	0.36468	0.00293	0.34	2445.8	23.71	2184.8	21.08	2004.3	13.86	18.1	2445.8	23.71	48	10	139957	23611	27794	239409	3286	832180
k	0.09408	0.00132	2.80631	0.051	0.22075	0.0016	0.40	1509.7	26.2	1357.2	13.61	1285.8	8.42	14.8	1509.7	26.2	25	0	207340	20785	244	2086	7786	2026125
l	0.10311	0.00141	4.0922	0.07623	0.28659	0.00205	0.38	1680.8	25.08	1652.7	15.2	1624.5	10.26	3.3	1680.8	25.08	12	11	119935	13208	16207	159108	3382	900426
m	0.10083	0.00129	2.96009	0.04503	0.21059	0.00139	0.43	1639.4	23.63	1397.4	11.55	1232	7.4	24.9	1639.4	23.63	15	0	278721	30088	12906	181052	10619	2840380
n	0.17129	0.00228	10.7868	0.22112	0.46934	0.0034	0.35	2570.3	22.1	2504.9	19.05	2480.6	14.9	3.5	2570.3	22.1	0	0	218451	40156	40742	279770	3877	996337
o	0.1452	0.00183	7.57608	0.11773	0.39294	0.00256	0.42	2290.1	21.57	2182	13.94	2136.4	11.86	6.7	2290.1	21.57	56	0	302148	47191	14455	110592	6467	1641814
MA190©	0.12915	0.00336	6.64141	0.36062	0.38308	0.00578		2086.4	45.11	2064.9	47.92	2090.6	26.96	-0.2	2086.4	45.11	5	3	15493	2028	3194	17804	356	97208
b	0.1177	0.00369	6.22125	0.40517	0.41483	0.00732		1921.6	55.11	2007.4	56.97	2237	33.35	-16.4	1921.6	55.11	0	0	8534	1017	2441	12597	190	49183
c	0.14087	0.00178	6.88133	0.1327	0.36963	0.00272		2238	21.67	2096.3	17.1	2027.6	12.8	9.4	2238	21.67	19	29	207274	29527	4177	33567	4990	1333455

Table A-4: 40Ar/39Ar step heating analytical results for MA045A Run 1

Laser	*Isotope Ratios*												
	MA045a biotite Run 1			*(sample/mineral)*									
Power(%)	*40Ar/39Ar*	*1σ*	*37Ar/39Ar*	*1σ*	*36Ar/39Ar*	*1σ*	*Ca/K*	*Cl/K*	*%40Ar atm*	*f 39Ar*	*40Ar*/39ArK*	*Age*	*2σ*
2.00 W	77.83	1.17	0.17	0.08	0.261	0.012	0.31		98.97	0.05	0.801	15.85	± 133.44
2.30 W	22.50	0.17	1.08	0.03	0.040	0.001	1.99		52.28	0.39	10.746	201.98	± 13.51
2.70 W	17.50	0.09	0.20	0.00	0.007	0.000	0.38		11.19	3.45	15.546	285.39	± 3.14
2.90 W	18.92	0.10	0.03	0.00	0.002	0.000	0.05		3.40	9.49	18.272	331.09	± 3.14
3.10 W	18.26	0.09	0.01	0.00	0.001	0.000	0.02		2.40	10.02	17.826	323.70	± 3.03
3.20 W	18.76	0.10	0.01	0.00	0.000	0.000	0.01		0.89	9.07	18.596	336.46	± 3.19
3.30 W	18.76	0.10	0.01	0.00	0.000	0.000	0.02		0.66	6.05	18.632	337.05	± 3.26
3.40 W	18.84	0.10	0.01	0.00	0.000	0.000	0.02		0.91	6.17	18.670	337.68	± 3.33
3.50 W	19.19	0.10	0.01	0.00	0.000	0.000	0.01		0.73	6.12	19.051	343.96	± 3.46
3.60 W	19.34	0.10	0.01	0.00	0.001	0.000	0.01		1.08	6.84	19.135	345.33	± 3.26
3.70 W	19.33	0.10	0.00	0.00	0.000	0.000	0.01		0.67	12.86	19.200	346.40	± 3.24
3.80 W	19.69	0.10	0.00	0.00	0.000	0.000	0.00		0.77	7.71	19.535	351.90	± 3.38
3.90 W	20.01	0.10	0.00	0.00	0.001	0.000	0.01		1.07	10.24	19.792	356.09	± 3.32
4.00 W	19.98	0.11	0.01	0.00	0.001	0.000	0.01		1.05	3.47	19.767	355.69	± 3.70
4.20 W	20.14	0.11	0.00	0.00	0.001	0.000	0.00		0.99	3.12	19.946	358.60	± 3.65
4.60 W	20.12	0.11	0.00	0.00	0.000	0.000	0.00		0.63	4.80	19.993	359.37	± 3.44
5.10 W	19.57	0.31	0.02	0.03	0.016	0.001	0.04		24.39	0.15	14.797	272.62	± 11.26
Power(%)	*40Ar/39Ar*	*1σ*	*37Ar/39Ar*	*1σ*	*36Ar/39Ar*	*1σ*	*Ca/K*	*Cl/K*	*%40Ar atm*	*f 39Ar*	*40Ar*/39ArK*	*1σ*	
Total/Average	19.242	0.026	0.006	0.000	0.0006	0.0000				100.00	18.682	0.027	
J = 0.0109966 ± 0.0000550			Volume 39ArK =	1.766	Integrated Date =	340.33	± 3.24	Ma					
Plateau Age = no plateau													
Inverse isochron (correlation age) results, plateau steps: Model 1 Solution (±95%-conf.) on1 6 points							Age = not resolved						

Table A-5: 40Ar/39Ar step heating analytical results for MA045A Run 2

Laser	*Isotope Ratios*												
	MA45a biotite Run 2			*(sample/mineral)*									
Power(%)	*40Ar/39Ar*	*1σ*	*37Ar/39Ar*	*1σ*	*36Ar/39Ar*	*1σ*	*Ca/K*	*Cl/K*	*%40Ar atm*	*f 39Ar*	*40Ar*/39ArK*	*Age*	*2σ*
2.00 W	81.35	1.61	0.88	0.17	0.261	0.009	1.62		94.79	0.06	4.240	82.40	± 80.94
2.30 W	24.55	0.18	2.53	0.12	0.054	0.003	4.65		64.81	0.26	8.657	164.44	± 28.44
2.80 W	17.35	0.15	2.98	0.06	0.005	0.000	5.47		7.85	6.64	16.020	293.42	± 5.10
3.00 W	17.40	0.10	2.26	0.05	0.004	0.000	4.15		5.61	6.89	16.453	300.73	± 3.24
3.10 W	17.02	0.09	2.26	0.05	0.003	0.003	4.14		4.81	2.70	16.226	296.91	± 34.43
3.20 W	16.57	0.13	0.19	0.01	0.001	0.000	0.36		1.91	4.29	16.256	297.40	± 4.26
3.30 W	16.89	0.12	0.03	0.00	0.001	0.000	0.05		1.81	5.78	16.580	302.87	± 4.14
3.40 W	16.79	0.09	0.03	0.00	0.001	0.000	0.05		1.15	6.77	16.592	303.07	± 2.92
3.50 W	16.87	0.18	0.03	0.00	0.001	0.000	0.05		1.14	6.93	16.675	304.45	± 6.01
3.60 W	16.91	0.10	0.02	0.00	0.001	0.000	0.03		1.30	7.56	16.688	304.68	± 3.45
3.70 W	17.10	0.18	0.01	0.00	0.001	0.000	0.02		1.11	10.84	16.909	308.38	± 6.12
3.80 W	17.27	0.15	0.01	0.00	0.000	0.000	0.01		0.82	7.50	17.128	312.06	± 5.00
3.90 W	17.22	0.22	0.01	0.00	0.000	0.000	0.02		0.84	6.41	17.079	311.23	± 7.42
4.00 W	17.70	0.09	0.01	0.00	0.000	0.000	0.01		0.90	5.64	17.539	318.93	± 3.01
4.20 W	17.86	0.12	0.01	0.01	0.001	0.000	0.02		1.89	5.28	17.523	318.65	± 4.35
4.40 W	19.02	0.10	0.01	0.00	0.000	0.000	0.01		0.90	9.06	18.848	340.60	± 3.35
4.70 W	18.87	0.10	0.01	0.00	0.000	0.000	0.01		0.67	5.76	18.746	338.93	± 3.31
5.20 W	16.40	0.10	0.01	0.01	0.001	0.000	0.01		2.75	1.39	15.946	292.17	± 3.43
6.00 W	14.68	0.11	0.01	0.07	0.005	0.001	0.02		9.76	0.23	13.248	245.94	± 11.31
Power(%)	*40Ar/39Ar*	*1σ*	*37Ar/39Ar*	*1σ*	*36Ar/39Ar*	*1σ*	*Ca/K*	*Cl/K*	*%40Ar atm*	*f 39Ar*	*40Ar*/39ArK*	*1σ*	
Total/Average	17.389	0.027	0.014	0.001	0.0006	0.0000				100.00	17.026	0.030	

J = 0.0109967 ± 0.0000550 Volume 39ArK = 2.257 Integrated Date = 310.6 ± 1.00 Ma

No plateau

Inverse isochron (correlation age) results, plateau steps: Model 1 Solution (±95%-conf.) on 19 points No Model 1 solution

Table A-6: $^{40}Ar/^{39}Ar$ step heating analytical results for MA045D Run 1

Laser *Isotope Ratios*

	MA045d biotite Run 1						*(sample/mineral)*						
Power(%)	*40Ar/39Ar*	*1σ*	*37Ar/39Ar*	*1σ*	*36Ar/39Ar*	*1σ*	*Ca/K*	*Cl/K*	*%40Ar atm*	*f 39Ar*	*40Ar*/39ArK*	*Age*	*2s*
2.00 W	42.52	0.73	0.22	0.06	0.136	0.008	0.40		94.40	0.09	2.384	46.79	± 84.24
2.30 W	11.32	0.06	0.51	0.01	0.010	0.000	0.93		25.00	1.47	8.494	161.48	± 4.83
2.60 W	14.90	0.08	0.05	0.00	0.004	0.000	0.09		7.52	5.00	13.783	255.20	± 2.78
2.80 W	17.67	0.10	0.01	0.00	0.001	0.000	0.02		2.48	4.63	17.233	313.81	± 3.43
3.00 W	18.14	0.09	0.01	0.00	0.001	0.000	0.01		2.06	8.95	17.764	322.66	± 3.09
3.20 W	18.20	0.25	0.00	0.00	0.001	0.000	0.01		1.65	14.10	17.896	324.86	± 8.28
3.30 W	18.35	0.11	0.00	0.00	0.001	0.000	0.01		1.33	16.13	18.110	328.41	± 3.59
3.40 W	18.47	0.09	0.00	0.00	0.000	0.000	0.00		0.81	10.06	18.320	331.89	± 3.09
3.50 W	19.06	0.12	0.00	0.00	0.000	0.000	0.00		0.90	13.70	18.893	341.35	± 3.79
3.70 W	19.53	0.10	0.00	0.00	0.001	0.000	0.01		1.04	6.19	19.326	348.46	± 3.36
3.80 W	19.65	0.10	0.00	0.00	0.000	0.000	0.00		0.76	7.20	19.502	351.35	± 3.33
3.90 W	19.71	0.12	0.00	0.00	0.000	0.000	0.00		0.67	4.89	19.577	352.58	± 3.83
4.00 W	19.77	0.11	0.00	0.00	0.000	0.000	0.00		0.76	4.16	19.620	353.28	± 3.63
4.20 W	19.85	0.13	0.00	0.00	0.001	0.000	0.01		1.27	1.54	19.603	353.00	± 5.08
4.50 W	19.54	0.11	0.00	0.00	0.001	0.000	0.01		1.32	1.59	19.285	347.80	± 4.48
5.50 W	17.92	0.10	0.01	0.02	0.000	0.002	0.02		0.82	0.32	17.770	322.77	± 15.70
Power(%)	*40Ar/39Ar*	*1σ*	*37Ar/39Ar*	*1σ*	*36Ar/39Ar*	*1σ*	*Ca/K*	*Cl/K*	*%40Ar atm*	*f 39Ar*	*40Ar*/39ArK*	*1s*	
Total/Average	17.268	0.026	0.003	0.000	0.0008	0.0000				100.00	17.542	0.029	

J = 0.0109967 ± 0.0000550 Volume 39ArK = 1.849 Integrated Date = 328.49 ± 3.38 Ma

Plateau Age = no plateau

Inverse isochron (correlation age) results, plateau steps: Model 1 Solution (±95%-conf.) on 16 points Age = not resolved

Table A-7: $^{40}Ar/^{39}Ar$ step heating analytical results for MA045D Run 2

Laser *Isotope Ratios*

MA045d biotite Run 2 *(sample/mineral)*

Power(%)	*40Ar/39Ar*	*1s*	*37Ar/39Ar*	*1s*	*36Ar/39Ar*	*1s*	*Ca/K*	*Cl/K*	*%40Ar atm*	*f 39Ar*	*40Ar*/39ArK*	*Age*	*2s*
2.00 W	129.00	3.36	1.07	0.39	0.406	0.020	1.95		93.03	0.02	8.995	170.60	± 178.27
2.30 W	33.18	0.28	0.68	0.17	0.085	0.002	1.24		76.00	0.15	7.967	151.90	± 22.55
2.80 W	12.88	0.07	2.00	0.04	0.010	0.000	3.66		21.17	2.25	10.170	191.75	± 3.00
3.10 W	15.12	0.08	0.11	0.01	0.006	0.000	0.21		11.60	4.06	13.368	248.06	± 2.85
3.20 W	15.58	0.08	0.09	0.00	0.002	0.000	0.17		3.97	2.88	14.960	275.46	± 2.90
3.30 W	15.55	0.08	0.12	0.01	0.002	0.000	0.22		4.03	2.17	14.928	274.91	± 2.81
3.50 W	16.93	0.09	0.06	0.00	0.002	0.000	0.11		3.17	4.84	16.397	299.84	± 2.92
3.70 W	17.99	0.09	0.01	0.00	0.001	0.000	0.03		1.78	9.22	17.668	321.14	± 3.06
3.80 W	18.00	0.09	0.02	0.00	0.001	0.000	0.03		1.19	7.95	17.782	323.04	± 3.03
3.90 W	18.21	0.09	0.02	0.00	0.001	0.000	0.03		1.12	4.12	18.002	326.68	± 3.12
4.00 W	18.93	0.10	0.01	0.00	0.000	0.000	0.02		0.85	7.79	18.774	339.46	± 3.18
4.20 W	18.48	0.09	0.03	0.00	0.001	0.000	0.06		0.96	4.51	18.301	331.64	± 3.07
4.40 W	18.51	0.10	0.07	0.00	0.000	0.000	0.13		0.87	4.80	18.348	332.43	± 3.18
4.60 W	18.44	0.09	0.07	0.01	0.001	0.000	0.13		0.95	6.00	18.263	331.01	± 3.06
4.80 W	18.20	0.10	0.03	0.00	0.000	0.000	0.06		0.94	5.07	18.026	327.09	± 3.28
5.00 W	18.27	0.09	0.03	0.00	0.000	0.000	0.05		0.85	7.74	18.116	328.57	± 3.08
5.20 W	18.88	0.10	0.05	0.00	0.000	0.000	0.08		0.76	8.21	18.740	338.89	± 3.16
5.40 W	19.19	0.10	0.06	0.00	0.000	0.000	0.10		0.78	5.64	19.046	343.94	± 3.29
5.60 W	19.30	0.10	0.06	0.00	0.000	0.000	0.10		0.65	3.65	19.178	346.10	± 3.41
5.80 W	19.49	0.10	0.03	0.00	0.000	0.000	0.05		0.69	2.59	19.355	349.01	± 3.44
6.10 W	19.53	0.10	0.01	0.00	0.000	0.000	0.03		0.67	3.28	19.396	349.67	± 3.28
6.40 W	19.76	0.11	0.01	0.01	0.001	0.000	0.02		0.96	1.71	19.575	352.61	± 3.52
6.80 W	19.28	0.11	0.03	0.01	0.001	0.000	0.05		1.22	1.34	19.049	343.98	± 3.82

Power(%)	*40Ar/39Ar*	*1s*	*37Ar/39Ar*	*1s*	*36Ar/39Ar*	*1s*	*Ca/K*	*Cl/K*	*%40Ar atm*	*f 39Ar*	*40Ar*/39ArK*	*1s*
Total/Average	17.562	0.020	0.033	0.001	0.0005	0.0000				96.95	17.157	0.020

J = 0.0109990 ± 0.0000550 Volume 39ArK = 3.147 Integrated Date = 314.01 ± 0.68 Ma

No Plateau

Inverse isochron (correlation age) results, plateau steps: Model 1 Solution (±95%-conf.) on 23 points No solution

Part 4: Cathode-luminescence imaging of zircons from the Aley carbonatite

Cathode-luminescence (CL) imagining was conducted on Aley carbonatite zircons by the author in spring of 2010 at Simon Fraser University's NanoImaging Facility (4D Labs). The objective was to map growth/resorption zonation patterns which could facilitate a search for areas within zircon grains with sufficient radiogenic Pb to date. Later analyses revealed that these zircons had uniform near-zero counts of radiogenic lead across the entire grain; further planned work on CL grain mapping was abandoned. Equipment used was a Bausch & Lomb LE 2100 Nanolab SEM retrofitted with a cathode-luminescence detector.

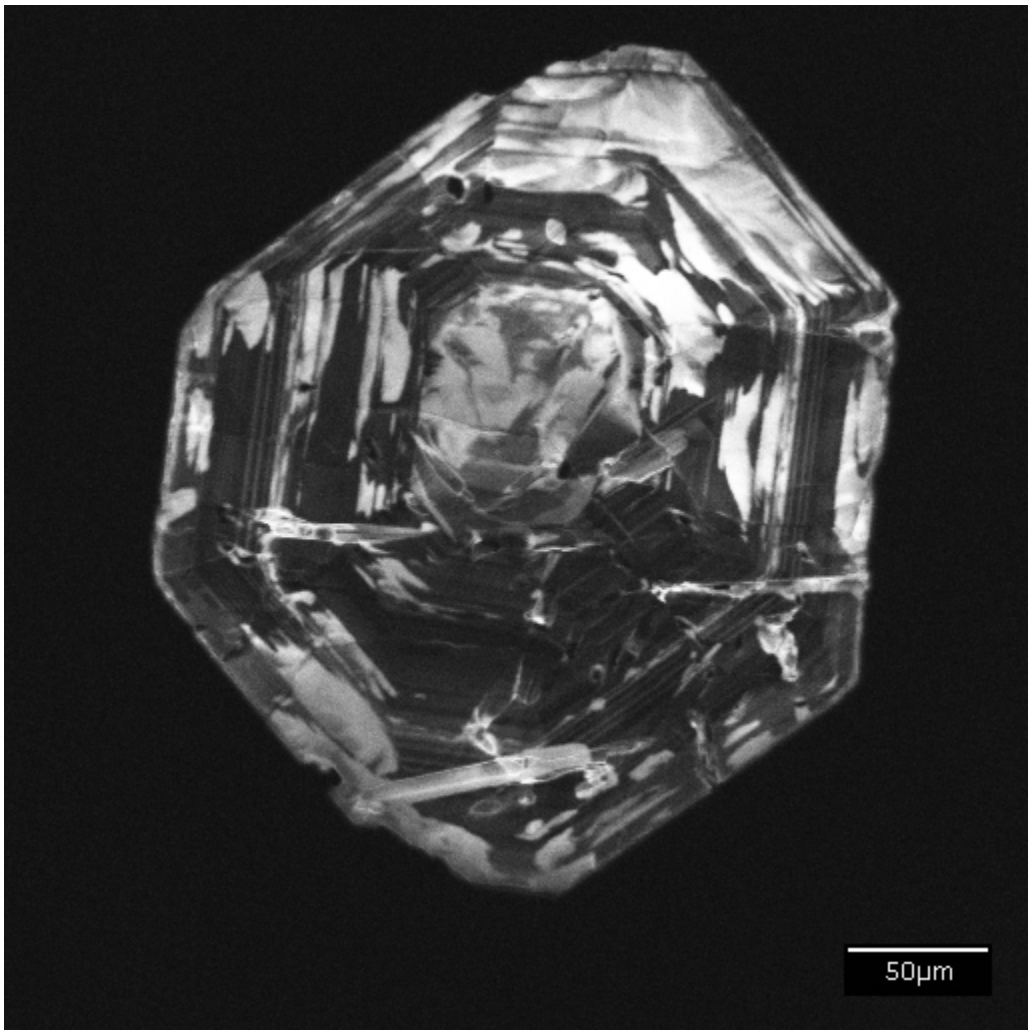

Figure A-1: Zircon grain #8 from MA096 (dolomite carbonatite) displaying significant resorption textures.

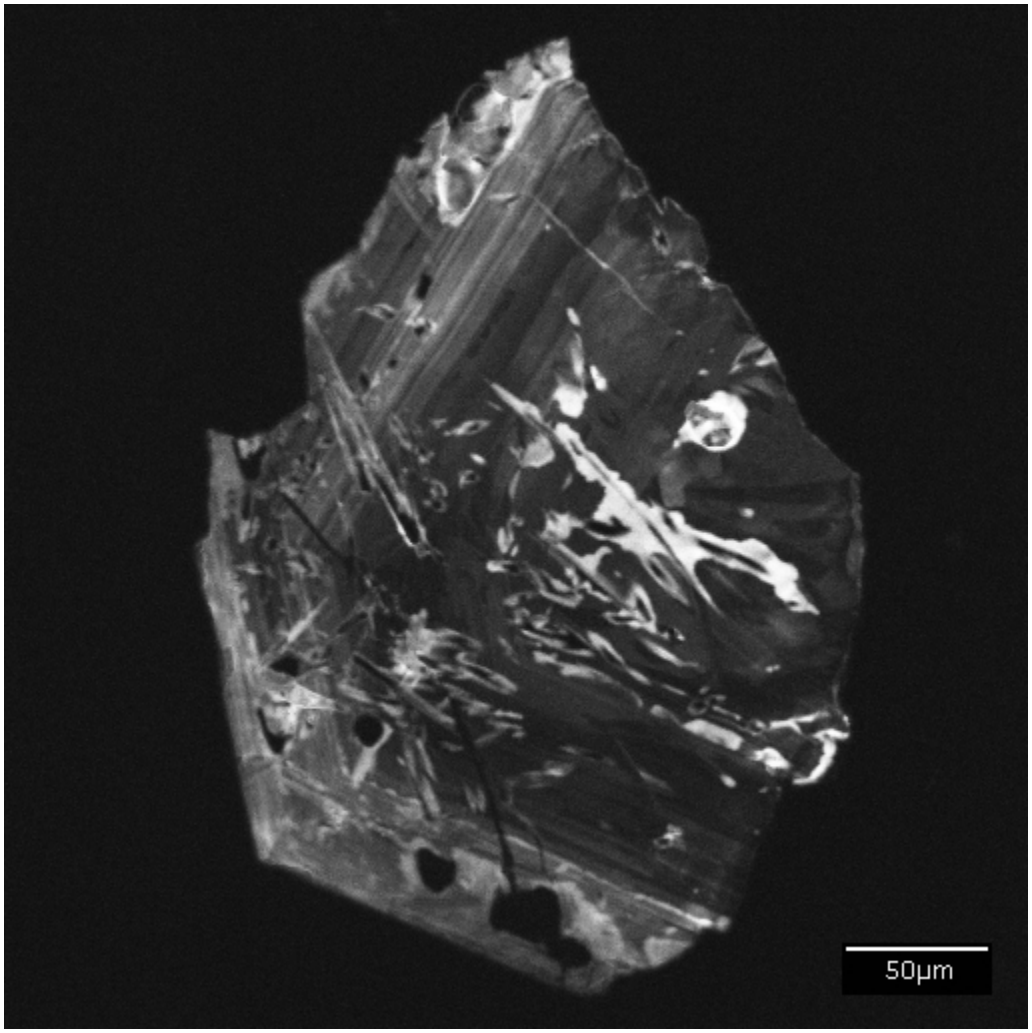

Figure A-2: Zircon grain #5 from MA096 displaying moderately-well preserved growth zonation.

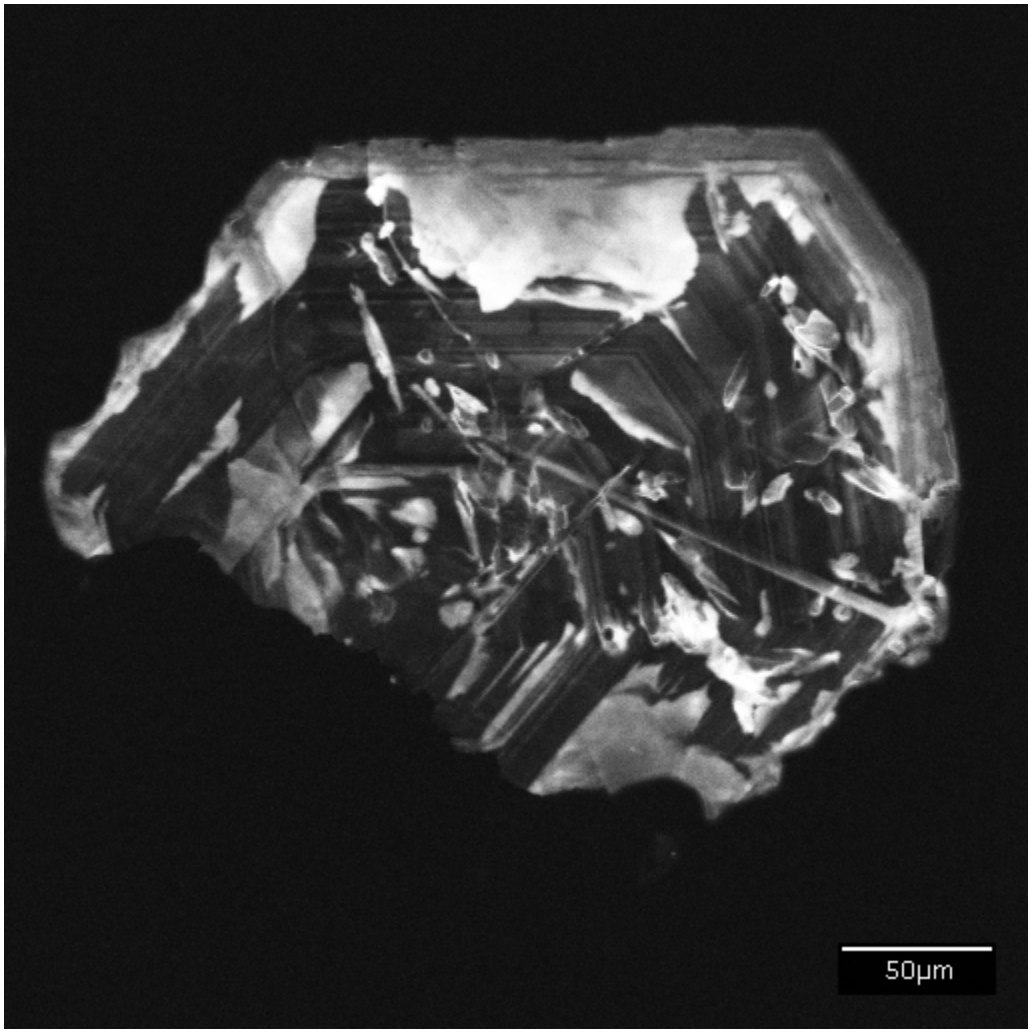

Figure A-3: Zircon grain #4 from MA096. Strong resorption textures around grain rims appears to locally obliterate growth zonation.

APPENDIX B

Structural data

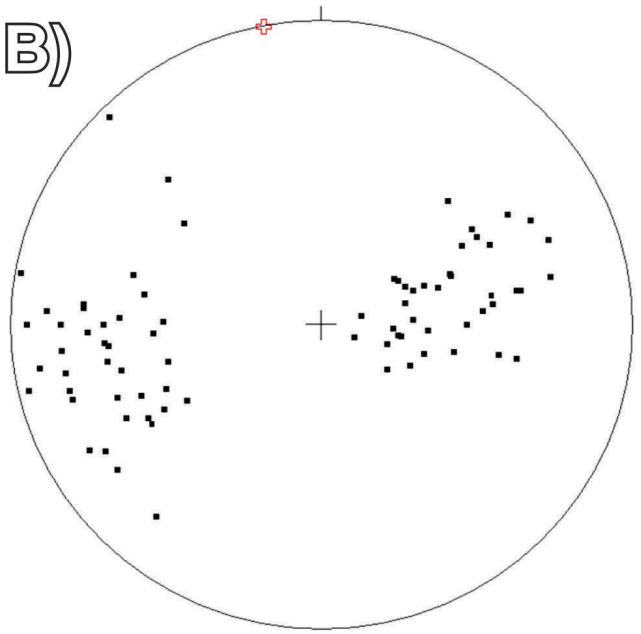

No. of Data = 77
Mean Principal Orientation = 169/80
Mean Resultant dir'n = 14-092
Mean Resultant length = 0.50
(Variance = 0.50)
Calculated. girdle: 79/90
Calculated beta axis: 0-349

Figure B-1: (A) F_2 fold in outcrop of fenitized Kechika Formation with concordant dolomite carbonatite vein (red arrow) in centre. (B) Composite equal-angle stereonet plot of poles to bedding from cross-section transect of map area showing F_2 fold morphology for comparison. The calculated beta axis is depicted as a red cross.

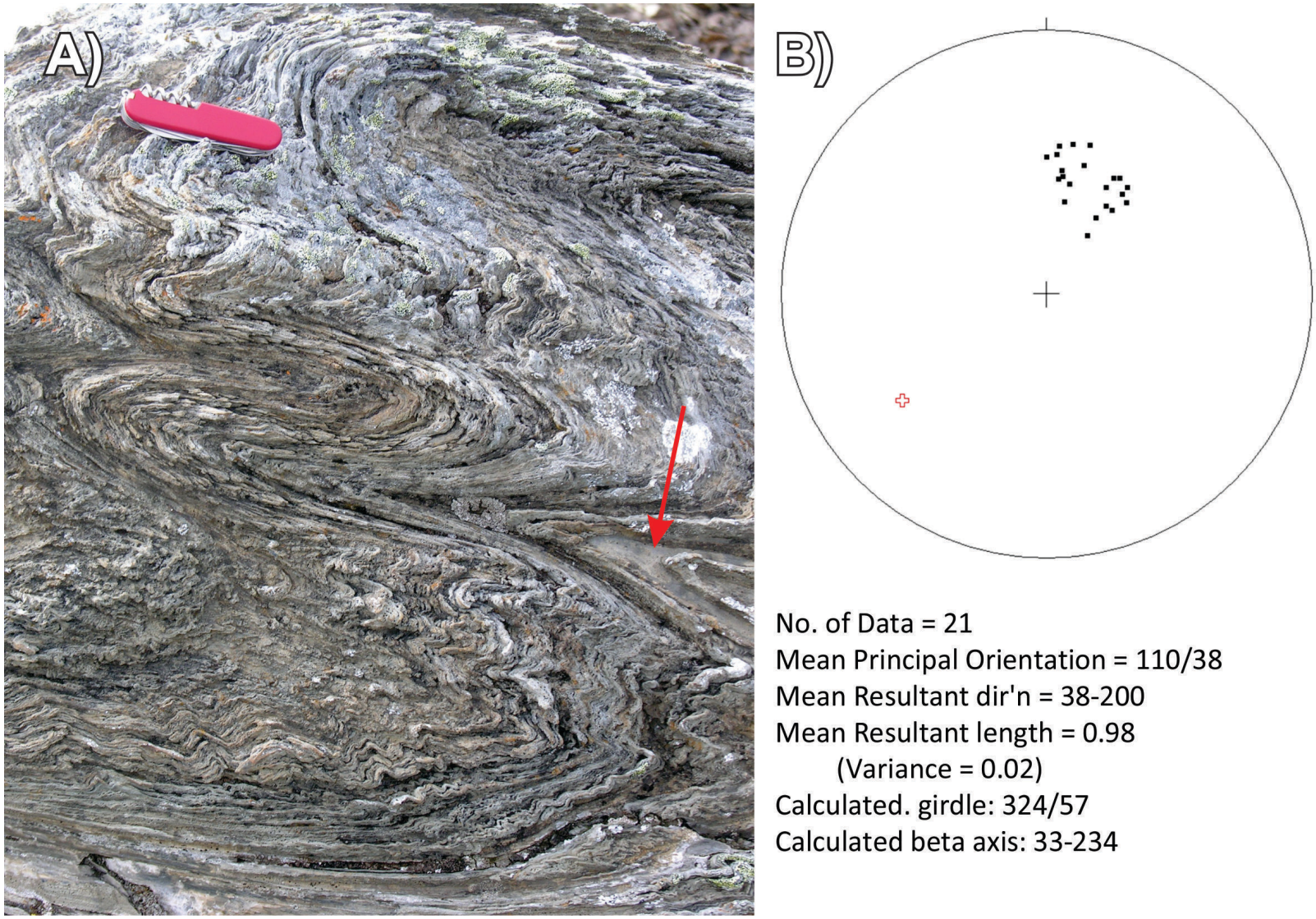

Figure B-2: (A) F_1 isoclinal fold in outcrop of fenitized Kechika Formation with concordant calcite carbonatite vein (red arrow) at right (B) Composite equal-angle stereonet plot of poles to bedding from photo location (eastern carbonatite-Kechika contact) for comparison. The calculated beta axis is depicted as a red cross.

Table C-1: Raw structural and field sample data georeferenced by field station.

STN Name	Position	Orientation (Dip/ Dip Direction, Plunge/ Trend)	Type	Sample
Mapper: Ambrose *All NAD83 Z10N				
AA001	10 V 454699 6257457	70/000	foliation	
AA002	10 V 454883 6257483	35/315	foliation	
		38/290	fold hinge	
AA003	10 V 455086 6257211	55/150	foliation	
AA004	10 V 455121 6257151	65/225	foliation	
		35/110	fold hinge	
AA005	10 V 455195 6257033	80/155	foliation	
		70/185	foliation	
AA006	10 V 455539 6257149	80/190	foliation	
AA007	10 V 455544 6257196	65/015	foliation	
AA008	10 V 455576 6257380			
AA009	10 V 455598 6257450			AA009
AA010	10 V 455727 6257679	50/230	foliation	
AA011	10 V 455745 6257721	60/190	foliation	
AA012	10 V 455811 6257849	75/225	bdg	
		85/215	bdg 10m to north	
AA013	10 V 455893 6257887	75/220	bdg	
AA014	10 V 453079 6258159	35/50		
		85/230		
		80/228		
AA015	10 V 453151 6258194	32/043	bedding	
		40/050	bedding	
		12/091	bedding	
		31/110	bedding	
		66/259	bedding	
		73/259	bedding	
		45/070	hinge on smaller fold	
AA016	10 V 453182 6258176	60/086	bdg	
		47/132	bdg	
		46/285	bdg	
AA017	10 V 453020 6258145	82/084	clv	
		26/254	clv	
		33/288	bdg	
		57/267	bdg	
		44/265	bdg	
		85/72	clv	
AA018	10 V 452931 6258134	60/070	bdg	
		32/045	bdg	
AA019	10 V 452881 6258125	68/258	bdg	
		38/268	bdg	
		54/276	bdg	
AA020	10 V 452853 6258134	83/75	bdg	
AA021	10 V 452771 6258141	64/066	bdg	
AA022	10 V 452685 6258149	81/061	bdg	
		57/087	bdg	
		56/092	bdg	
AA023	10 V 452622 6258187	46/093	bdg	

STN Name	Position	Orientation (Dip/ Dip Direction, Plunge/ Trend)	Type	Sample
Mapper: Ambrose				
AA023		88/115	bdg	
		88/260	bdg	
		53/275	bdg	
AA024	10 V 452361 6258259	65/042	bdg	
AA025	10 V 452105 6258355	78/050	bdg	AA025 A B
		79/054	bdg	
		44/278	clv	
		88/067	bdg	
AA026	10 V 452001 6258382	28/278	bdg	
		54/090	bdg	
		07/195	bdg to the west	

STN Name	Position	Orientation (Dip/ Dip Direction, Plunge/ Trend)	Type	Sample
Mapper: McLeish				
MA001	10 V 451173 6258004	65/240	bedding/foliation	MA001
		55/050	crenulation cleavage	
MA002	10 V 451506 6258037	65/245	S1	
		50/060	S2	
MA003	10 V 451741 6258189	60/050		
MA004	10 V 451919 6258260	65/085		MA005
MA005	10 V 452004 6258381	45/270		
MA006	10 V 452182 6258328			MA006A, MA, 006B
MA007	10 V 452527 6258210	trending 160		
MA008	10 V 452772 6258145	trending 160		
		80/250		
MA009	10 V 454393 6257580			MA009
MA010	10 V 454641 6257419	60/355	S1	MA010A, MA010B, MA010C
MA011	10 V 454113 6257035			MA011
MA012	10 V 453866 6256952	40/290	layering/banding	
		75/140	joint	
		65/265	joint	
MA013	10 V 453603 6256812			MA013A, MA013B, MA013C
MA014	10 V 453536 6256790	80/110	joint	
		80/310	bedding	MA014
MA015	10 V 453389 6256791	80/090	bedding	MA015A, MA015B
MA016	10 V 453284 6256791	60/245	foliation	MA016
		50/210	lineation	
MA017	10 V 453200 6256805	70/240	bdg	MA017
MA018	10 V 452970 6256857	85/075	bdg	
MA019	10 V 452792 6256804	60/280	bdg	
MA020	10 V 453690 6256845			MA020A, MA020B
MA021	10 V 454453 6257333	70/350	weak foliation	
		45/20	weak foliation	
		90/360	joint	
MA022	10 V 454372 6257932	30/170		MA022A,MA022B, MA022C
		60/270		
MA023	10 V 453831 6258170	45/130	MA024	
MA024	10 V 453999 6258074	70/145	bdg	

STN Name	Position	Orientation (Dip/ Dip Direction, Plunge/ Trend)	Type	Sample
Mapper: McLeish				
MA025	10 V 454771 6257455			MA025A, MA025B, MA025C
MA026	10 V 454815 6257427			MA026
MA027	10 V 454942 6257345			
MA028	10 V 455111 6257188	70/280	joint	
		90/100	foliation	
MA029	10 V 455530 6257065	90/170	joint	
MA030	10 V 454642 6257334	60/020	foliation	MA030
MA031	10 V 455546 6257223	75/170	foliation	MA031
MA032	10 V 455578 6257380	65/260	mineral lineation	
MA033	10 V 455622 6257496	65/260	prominent joint	MA033
		90/170	joint	
		70/220	joint	
MA035	10 V 455808 6257821	85/200	main foliation	
		70/240	lineation	
MA036	10 V 455836 6257863	80/190	contact	MA036 A B C D E F
MA037	10 V 453677 6256731	70/320	banding	MA037 A B
MA038	10 V 453780 6256592	80/250	veins	MA038
MA039	10 V 453868 6256485			MA039 A B
MA040	10 V 453852 6255958			
MA041	10 V 453691 6255948	70/040	Foliation	
MA042	10 V 453442 6256148	60/050	bedding	
MA043	10 V 453463 6256220	65/250	foliation	MA043
		65/250	lineation	
MA044	10 V 453420 6256211	70/230	foliation	
MA045	10 V 453370 6256125			MA045 A B C D
MA046	10 V 454458 6257330	38/318	foliation	
		60/243	folitaion	
		20/270	folds hinge	
MA047	10 V 454646 6257422	50/295	lineation	
		60/340	foliation	MA047 A B C
MA048	10 V 454418 6257621	51/344	foliation	
		48/003	foliation	
MA049	10 V 454333 6257942	56/272	foliation	
		82/255	foliation 10m to W	
		79/271	foliation 15m to W	MA049 A B
MA050	10 V 454201 6257972	70/150	foliation	MA050
		70/140	foliation	
		78/149	foliation	
MA051	10 V 454081 6258024	58/218	fault	MA051 A B
		65/262	fold axis	
		44/171	foliation	

STN Name	Position	Orientation (Dip/ Dip Direction, Plunge/ Trend)	Type	Sample
Mapper: McLeish				
MA052	10 V 453998 6258701	38/310	foliation	
MA052		35/250		
		58/130	cleavage	
MA053	10 V 453874 6258140	41/224		MA053
		41/224		
		50/230		
		60/290	bdg	
		70/305	bdg	
MA054	10 V 453674 6258380	83/083	bdg	
MA055	10 V 453169 6258012	80/070	bdg	
		88/247	bdg	
		84/255	cleavage	
		90/140	quartz veins	
		80/235	quartz veins	
		15/310	fibers in cone qtz	
MA056	10 V 453215 6258120	77/088	paleoflow	MA056
		73/256	bdg	
		82/250	cleavage	
		78/250	cleavage	
		66/265	Crenulation	
MA057	10 V 453250 9258130			
MA058	10 V 453315 9258160	70/260	bdg	
		20/165	fold axis	
MA059	10 V 453470 625880?	025/330	fold hinge	
MA060	10 V 453763 6259160	43/253	fold hinge	
		60/218	bdg	
		80/250	axial surface	
		65/280	fold hinge	
MA061	10 V 453573 6259395?	72/248	bdg	MA061A
MA062	10 V 453754 6259405			MA062
MA063	10 V 453827 6259530			
MA064	10 V 453856 6259510?	74/225	bdg	MA064
		?/310	paleoflow	
MA065	10 V 453485 6259830		bdg	
MA066	10 V 452675 6259557	65/245	bdg	
MA067	10 V 452777 6257955	80/045	bdg	
		80/090	bdg	
		70/065	cleavage	
		10/182	Fold Axis	
MA068	10 V 454984 6237107	84/195	mineral fabric	MA068
MA069	10 V 455623 6257010	42/240	mineral lineation	
		28/236	fold	
		55/190	mineral foliation	
MA070	10 V 455730 6256986	41/219		

STN Name	Position	Orientation (Dip/ Dip Direction, Plunge/ Trend)	Type	Sample
Mapper: McLeish				
		40/240	fold axis	
MA071	10 V 456120 6256738	60/310	limb	071A-F
		40/350	limb	
MA072	10 V 456174 6256763	20-40/330	fold axis	
		17/239	lineation	
MA073	10 V 456331 6256821	22/059	Axial plane	
		35/260	bedding	
		20/350	bedding	
MA074	10 V 456538 6256807	68/263	foliation	
MA075	10 V 456784 6256766	38/296	foliation	
MA076	10 V 456909 6256809	15/279	bedding	
MA077	10 V 455150 6256585			MA077
MA078	10 V 456596 6256790			
MA079	10 V 456615 6256723	65/060	E Limb	
		30/330	E Limb	
		70/060	W Limb	
		20/045	W Limb	
		40/300	W Limb	
		55/100	W Limb	
		50/230	W Limb	
		60/265	W Limb	
MA080	10 V 456000 6256440	55/255	bdg	
		65/260	bdg	
MA081	10 V 455875 6256383	45/215	fabric	
		60/310	dyke	
MA082	10 V 455027 6256350	87/225	bedding	
		40/310	fold hinge	
MA083	10 V 455730 6256275	40/306	bdg	
		65/110	bdg	
MA084	10 V 455650 6256184	85/172	dyke	
		80/270	bedding	
MA085	10 V 455620 6256127	10/220	fold hinge	
MA086	10 V 454070 6256940	86/320	fabric	
MA087	10 V 454030 6256940	46/255	mineral lineation	
MA088	10 V 453877 6256875	60/330	fabric	
		70/270	fold	
MA089	10 V 453786 6256730	40/290		MA089
MA090	10 V 453755 6256618	70/170	fabric (mineral lineation)	
MA091	10 V 453772 6256532	70/290	mineral lineation	
MA092	10 V 453792 6256495	65/290		
MA093	10 V 453880 6256486	35/308	contact	
		25/005	lineation	
MA094	10 V 453796 6256345	70/310	fabric	
MA095	10 V 453362 6256124			MA095
MA096	10 V 453653 6257427			MA096

STN Name	Position	Orientation (Dip/ Dip Direction, Plunge/ Trend)	Type	Sample
Mapper: McLeish				
MA097	10 V 458347 6255014	0-63/237		
MA098	10 V 458204 6255006	69/085	fold bedding	
		80/069	fold bedding	
MA099	10 V 458110 6255038	47/282	bdg/clv	
MA100	10 V 458049 6255023	66/223	limb	
		75/290	limb	
MA101	10 V 457857 6254999	74/258	bedding	
MA102	10 V 457745 6254931	74/243	bdg	
		34/068	bdg	
MA103	10 V 457540 6254889	63/270		
MA104	10 V 456913 6254875	43/252	bdg	
MA105	10 V 456437 6255048	48/243	bdg	
		53/236	clv	
MA106	10 V 456246 6255062	60/237	bdg	
MA107	10 V 453300 6258179	45/090	bdg	MA107 A B
		80/276	contact	
MA108	10 V 453217 6258455			MA108
MA109	10 V 453735 6259553	72/239	foliated volcanics	
MA110	10 V 453798 6259498	59/228	foliated volcanics	
MA111	10 V 453914 6259581	69/233	foliated volcanics	
MA112	10 V 453822 6259645	73/248	foliated volcanics	
MA113	10 V 453768 6259708	80/230	foliated volcanics	
		74/234	foliated volcanics	
MA114	10 V 453639 6259368	75/250	contact	
MA115	10 V 452958 6258701			
MA116	10 V 452814 6258700	80/090	bdg	
		75/070	bdg	
		50/220	bdg	
MA117	10 V 452714 6258706			
MA118	10 V 453663 6256652	65/240	mineral lineation	
		30/350	small fold limb	
		50/050	small fold hinge	
MA119	10 V 453623 6256638	65/265	foliation	
MA120	10 V 453450 6256626	70/275	foliation	
MA121	10 V 453446 6256585	70/310	foliation	
MA122	10 V 453447 6256541	55/320	lineation	
MA123	10 V 453444 6256525	55/315	West Limb	
		65/260	East Limb	

STN Name	Position	Orientation (Dip/ Dip Direction, Plunge/ Trend)	Type	Sample
Mapper: McLeish				
MA124	10 V 453565 6256451	71/330	SW Limb	
		60/270	NE Limb	
MA125	10 V 453472 6256364	55/270	contact	
MA126	10 V 453434 6256641	45/335	lineation?	
MA127	10 V 453412 6256782	70/320	contact	
MA128	10 V 453589 6256777	75/352	lineation	
MA129	10 V 453708 6256838			MA129 A B
MA130	10 V 454758 6257435	70/000	foliation	
		50/040	foliation	
		55/030	foliation	
		75/340	foliation	
		45/355	foliation	
		60/070	foliation	
MA131	10 V 454936 6257545			
MA132	10 V 455552 6256665			
MA133	10 V 455038 6256954			
MA134	10 V 454680 6257332	45/350	contact	
		65/320	contact	
		60/330	contact	
MA135	10 V 454508 6257161	55/330	foliation	
		52/335	foliation	
		65/310	foliation	
		41/340	foliation	
MA136	10 V 454562 6257348			MA136
MA137	10 V 454417 6257627	54/339	contact	
MA138	10 V 454417 6257740	60/309	contact	
		75/242	contact	
		60/310	contact	
MA139	10 V 454446 6257855	65/194	contact	
MA140	10 V 454438 6257881	64/211	fabric/foliation	
MA141	10 V 454208 6257970			MA141
MA142	10 V 453592 6258326	~80/254	clv	
		67/074	bdg	
		44/076	bdg	
MA143	10 V 453554 6258306	~76/240		
		~54/062		
MA144	10 V 453515 6258304	67/084	bdg	
MA145	10 V 453470 6258297	76/249	bdg	
		70/080	bdg	
MA147	10 V 454003 6257530	61/339	foliation	
		66/002		
MA148	10 V 453941 6257528	76/330	clv/foliation	
MA149	10 V 453879 6257523	67/358	foliation	
MA150	10 V 453740 6257618	88/306	foliation	
MA151	10 V 453674 6257677	74/329	foliation	
MA152	10 V 453601 6257672	88/288	bdg/foliation	
MA153	10 V 453596 6257520	69/308	foliation	

STN Name	Position	Orientation (Dip/ Dip Direction, Plunge/ Trend)	Type	Sample
Mapper: McLeish				
MA154	10 V 453731 6257564	76/338	foliation	
MA155	10 V 453655 6257440	87/311	foliation	
MA156	10 V 453608 6257362	67/308	foliation	
MA157	10 V 453642 6257338	159/311	foliation	
MA158	10 V 453683 6257325	63/331	contact	
MA159	10 V 453633 6257260	49/315	contact	
MA160	10 V 453551 6257204	69/295	contact	
MA161	10 V 453508 6257226	88/286	contact	
MA162	10 V 453436 6257274	74/269	clv/bdg	
MA163	10 V 453400 6257399	84/350	bdg	
MA164	10 V 453457 6257436	54/199	bdg	
MA165	10 V 453483 6257422	72/171	clv/bdg	
MA166	10 V 453502 6257528	86/298	clv/bdg	

STN Name	Position	Orientation (Dip/ Dip Direction, Plunge/ Trend)	Type	Sample
Mapper: Mihalynuk				
MMI09-6-1	10 V 453638 6257251	68/300	joint	
MMI09-6-2	Mihalynuk GPS	75/270	overturned bdg	
MMI09-7-1	10 V 454571 6257138	20/280	fold axis	
MMI09-7-2	10 V 454741 6257221	50/280	mineral lineation	
MMI09-7-3	Mihalynuk GPS	72/262	foliation	
		52/255	mineral lineation	
MMI09-7-4	10 V 454240 6257786	65/142	bdg	
MMI09-7-5	10 V 454207 6257802			
MMI09-7-6	10 V 453692 6258122	53/060	bdg	
		78/290	clv	
		37/057	bdg	
		76/111	clv	
		38/038	intersection lineation	
MMI09-7-7	10 V 453371 6257946			
MMI09-8-1	Mihalynuk GPS			
MMI09-8-2	10 V 452627 6258010			
MMI09-8-3	10 V 452981 6257925			
MMI09-9-1	10 V 454173 6256757	82/345	foliation	
		10/075	fold axis	
MMI09-9-2	10 V 453741 6256370	53/015	foliation	
		20/110	mineral lineation	
		27/020	fold axis	
		80/298	clv	
MMI09-9-3	10 V 453725 6256340	37/025	fold hinge	
		80/107	axial surface	
		15/050	hinge	
		40/010	clv	
		53/000	hinge	
		00/060	hinge	
		50/340	clv	
		22/225	hinge	
MMI09-9-4	Mihalynuk GPS	40/235	hinge	
		48/288	foliation	
MMI09-9-5	10 V 453485 6256467	38/165	foliation	
MMI09-9-6		73/276	bdg	
MMI09-9-7	10 V 453400 6256585	62/185	hinge	
		66/260	foliation	
MMI09-9-8	10 V 453163 6256641			
MMI09-9-9	10 V 453034 6256640	22/140	clv	
MMI09-9-10	10 V 452973 6256617	60/240	bdg	
		48/290	bdg	
MMI09-9-11	10 V 452813 6250537	18/003	hinge	

STN Name	Position	Orientation (Dip/ Dip Direction, Plunge/ Trend)	Type	Sample
Mapper: Mihalynuk				
MMI09-9-12	10 V 452740 6256500	02/070	bdg	
		80/072	clv	
MMI09-9-13	10 V 452680 6256507	80/040	contact	
MMI09-9-14	10 V 452660 6256504	63/240	bdg	
		80/240	clv	
MMI09-9-15	10 V 452300 6256558	90/190	large qtz vein	
		45/275	bdg	
		45/180	vein in trees	
MMI09-9-16	10 V 452166 6256548	23/275	clv	
MMI09-9-17	10 V 452473 6256900	~50/270	bdg	
MMI09-9-18	10 V 452685 6256992	89/044	clv	
		87/044	bdg	
		65/040	bdg 50m to E	
MMI09-9-19	10 V 452883 6257050	85/235	foliation	
MMI09-9-20	10 V 452886 6257050			
MMI09-10-1	10 V 456585 6256650	72/355	hinge	
		60/055	hinge	
		55/310	hinge	
MMI09-10-2	10 V 456440 6256581	60/275	bdg	
MMI09-11-1	10 V 453457 6256456	42/350	hinge	
		60/305	foliation	
		50/015	foliation	
MMI09-11-2	Mihalynuk GPS	52/065	foliation	
MMI09-11-3	10 V 453300 6256835	73/267	bdg	
MMI09-11-4	10 V 453400 6256950	55/050	foliation	
MA026	10 V 454815 6257427	32/005	foliation	
		60/006	foliation	
		38/341	cleavage	
		51/344	foliation	
		55/012	foliation	
		82/255	foliation	
		79/011	foliation	
		72/125	foliation, bdg?	
		83/146	foliation, bdg?	
		48/173	lamprophyre dyke	
		88/142	bdg	
		19/248	clv bdg intersect	
		58/218	fault	
		66/171	bdg	

STN Name	Position	Orientation (Dip/ Dip Direction, Plunge/ Trend)	Type	Sample
Mapper: Mihalynuk				
		71/274	STJ notes illegible	
		77/325	foliation	
		37/229	mineral lineation	
		67/168	bdg	
		43/299?	bdg	
		68/320	bdg	
		03/038	lineation	
		76/305	bdg	
		73/083	bdg	

STN Name	Position	Orientation (Dip/ Dip Direction, Plunge/ Trend)	Type	Sample
Mapper: Johnston				
AA001	10 V 454699 6257457	71/007	foliation	
		69/005	foliation	
AA002	10 V 454883 6257483	47/311	foliation	
		38/329	foliation	
		42/305	fold axis	
		42/281	fold axis	
		38/289	fold axis	
		43/290	fold axis	
		45/332	foliation	
		46/346	foliation	
		84/337	fabric between 002 and 003	
AA003	10 V 455086 6257211	69/156	foliation	
		74/169	foliation	
		79/160	foliation	
AA004	10 V 455121 6257151	85/039	foliation	
		71/209	foliation	
		89/186	foliation	
		35/113	fold axis	
AA005	10 V 455195 6257033	76/179	foliation	
		67/170	foliation	
		77/179	foliation	
		45/186	foliation between AA005 and AA006	
		47/208	SF	
		40/221	lineation enroute to AA006	
AA006	10 V 455539 6257149	64/161	foliation	
		65/175	SF	
AA007	10 V 455544 6257196	75/030	foliation	
		81/028	foliation	
AA008	10 V 455576 6257380			
AA009	10 V 455598 6257450	68/291	bdg	
		57/162	bdg	
		83/092	foliation	
AA010	10 V 455727 6257679	46/219	foliation	
		60/214	foliation	
		51/322	foliation	
AA011	10 V 455745 6257721	70/201	bdg	
		68/195	bdg	
		67/209	bdg	
AA012	10 V 455811 6257849	59/225	bdg	
		54/220	bdg	

STN Name	Position	Orientation (Dip/ Dip Direction, Plunge/ Trend)	Type	Sample
Mapper: Johnston				
		29/243	fold axis just down hill	
		82/196	bdg	
AA013	10 V 455893 6257887	77/231	bdg	
		64/228	bdg	
MA068	10 V 454984 6237107	87/31	foliation	
		80/211	foliation	
		84/195	foliation	
		88/217	foliation	
MA069	10 V 455623 6257010	28/236	foliation	
		41/217	foliation	
		51/187	foliation	
		42/240	lineation	
		63/185	foliation	
MA070	10 V 455730 6256986	36/219	foliation	
		28/175	foliation	
		42/200	foliation	
MA071	10 V 456120 6256738	54/304	foliation	
		68/314	foliation	
		86/359	foliation	
		79/340	foliation	
		65/285	foliation	
		79/280	bdg	
		62/277	bdg	
		76/271	bdg	
		72/344	bdg	
		78/347	bdg	
MA072	10 V 456174 6256763	39/309	bdg	
		29/340	Fold Axis	
		20/321	Fold Axs	
		33/318	fold axis	
		41/323	bdg	
		29/305	bdg	
		17/239	lineation	
		67/215	bdg	
		24/235	lineation	
MA073	10 V 456331 6256821	22/059	bdg	
		19/046	bdg	
		24/028	bdg	
MA074	10 V 456538 6256807	46/219	foliation	
		68/303	foliation	
		62/292	foliation	
		60/300	foliation	
MA075	10 V 456784 6256766	38/296	bdg	
		39/289	bdg	
		31/278	bdg	
		48/272	bdg	
		29/299	bdg (down hill)	

STN Name	Position	Orientation (Dip/ Dip Direction, Plunge/ Trend)	Type	Sample
Mapper: Johnston				
MA076	10 V 456909 6256809	24/334	bdg	
		15/280	bdg	
		26/296	bdg	
		13/325	bdg	
AA014	10 V 453079 6258159	33/065	bdg	
		30/040	bdg	
		89/240	bdg	
		84/241	bdg	
		81/228	clv	
		75/228	clv	
		31/143	lineation	
		24/146	lineation	
AA015	10 V 453151 6258194	30/045	bdg	
		29/040	bdg	
		76/262	bdg	
		74/005	bdg	
		76/238	clv	
		82/230	clv	
		72/243	clv	
		28/042	bdg	
		12/106	bdg	
AA016	10 V 453182 6258176	36/089	bdg	
		55/120	bdg	
		42/093	bdg	
		50/280	bdg	
		34/279	clv	
		11/019	lineation	
		14/016	lineation	
		36/307	bdg	
AA017	10 V 453020 6258145	25/306	bdg	
		26/286	bdg	
		29/018	clv	
		9/002	lineation	
		59/063	bdg	
		34/008	clv	
AA018	10 V 452931 6258134	64/070	bdg	
		67/072	bdg	
AA019	10 V 452881 6258125	36/239	bdg	
		43/244	bdg	
		57/262	bdg	
AA020	10 V 452853 6258134	64/255	bdg	
		82/076	bdg	
AA021	10 V 452771 6258141	61/061	bdg	
		64/116	bdg	
		66/259	bdg	
		44/241	bdg	
AA022	10 V 452685 6258149	59/083	bdg	
		53/087	bdg	
		8/351	bdg	

STN Name	Position	Orientation (Dip/ Dip Direction, Plunge/ Trend)	Type	Sample
Mapper: Johnston				
		42/110	bdg	
		39/063	clv	
		58/088	bdg	
AA023	10 V 452622 6258187	55/002	bdg	
		70/277	bdg	
		53/268	bdg	
		88/260	bdg	
		83/090	bdg	
		45/086	bdg	
		57/086	bdg	
AA024	10 V 452361 6258259	86/041	bdg	
		82/040	bdg	
		77/344	bdg	
		84/058	bdg	
		71/236	bdg	
AA025	10 V 452105 6258355	84/044	bdg	
		79/073	foliation	
		55/001	clv	
		84/073	bdg	
		66/254	clv	
AA026	10 V 452001 6258382	46/004	bdg	
		64/006	bdg	
		70/074	bdg	
		60/079	bdg	
		82/075	bdg	

APPENDIX C

Petrography: thin section images

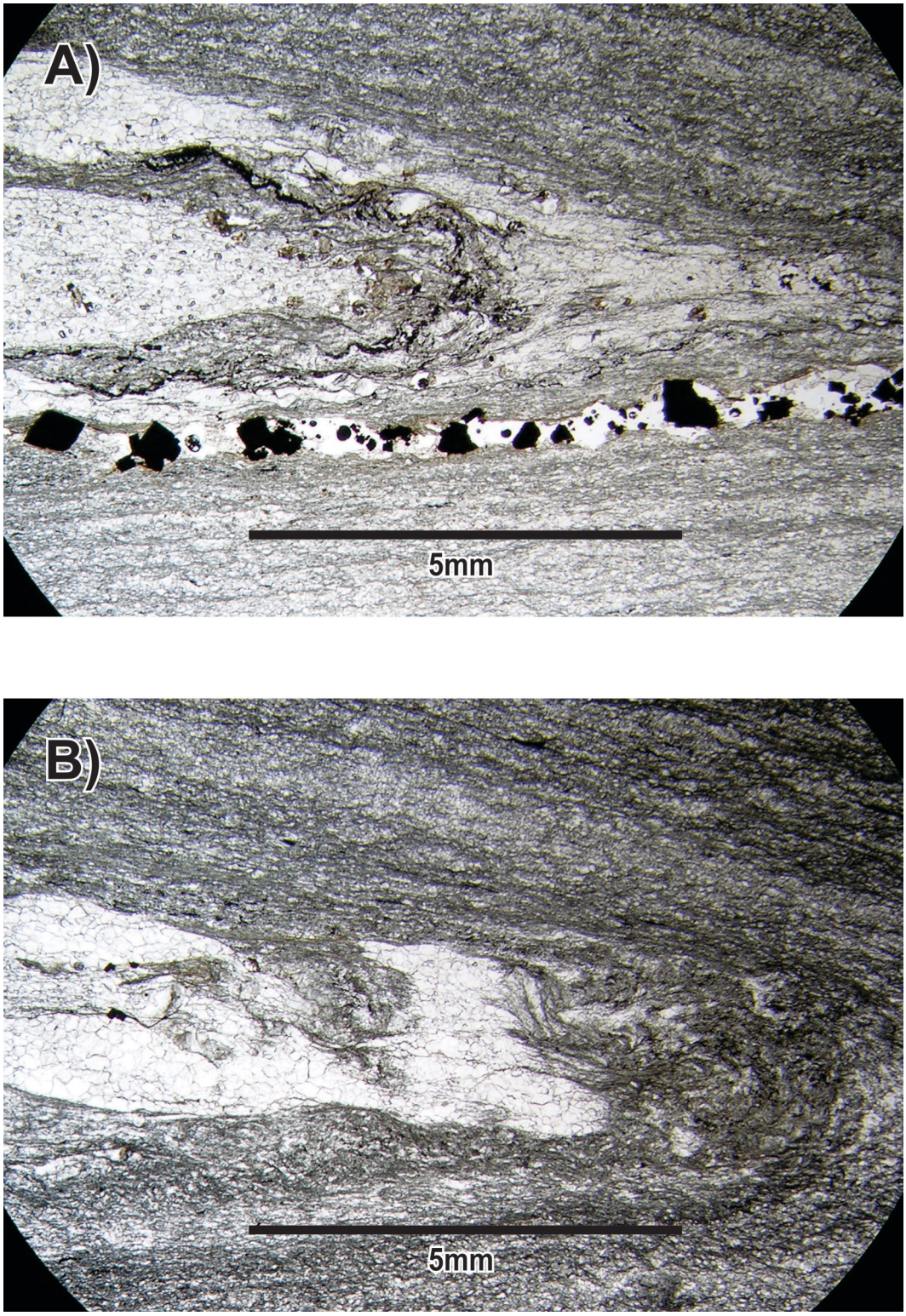

Figure C-1: (A & B) Calcite carbonatite veinlets intrude along axial planes of near-isoclinal F_1 folds in the Kechika Formation. Sample MA071. Images taken in PPL.

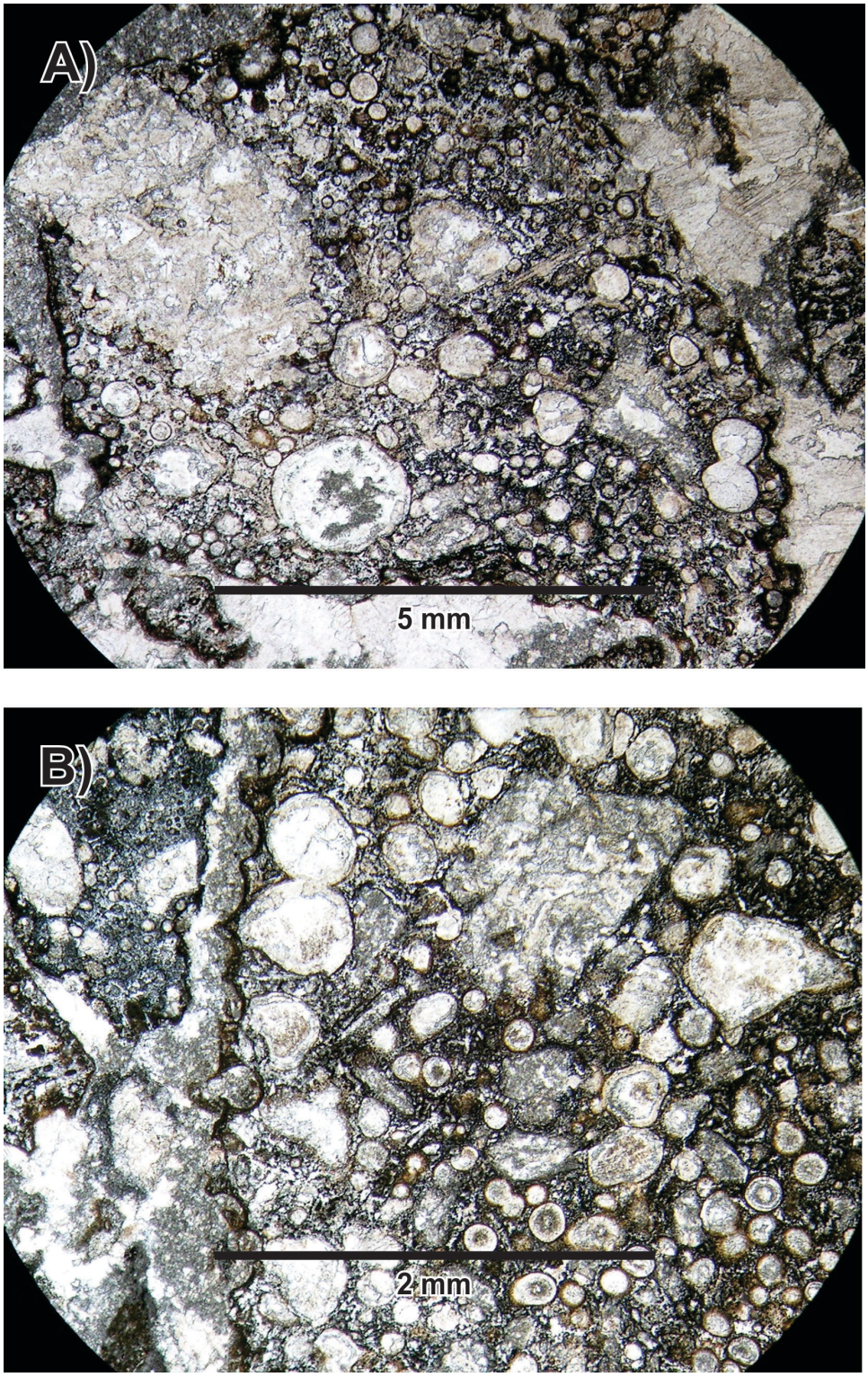

Figure C-2: (A & B) Lapilli-sized volcanic fragments in tuffaceous layers of the middle volcanic member of the Skoki Formation. The volcanic lapilli contain carbonate globules which may have an igneous origin (note fused margins) as carbonatite ocelli. Samples MA062 & MA064. Images taken in PPL.

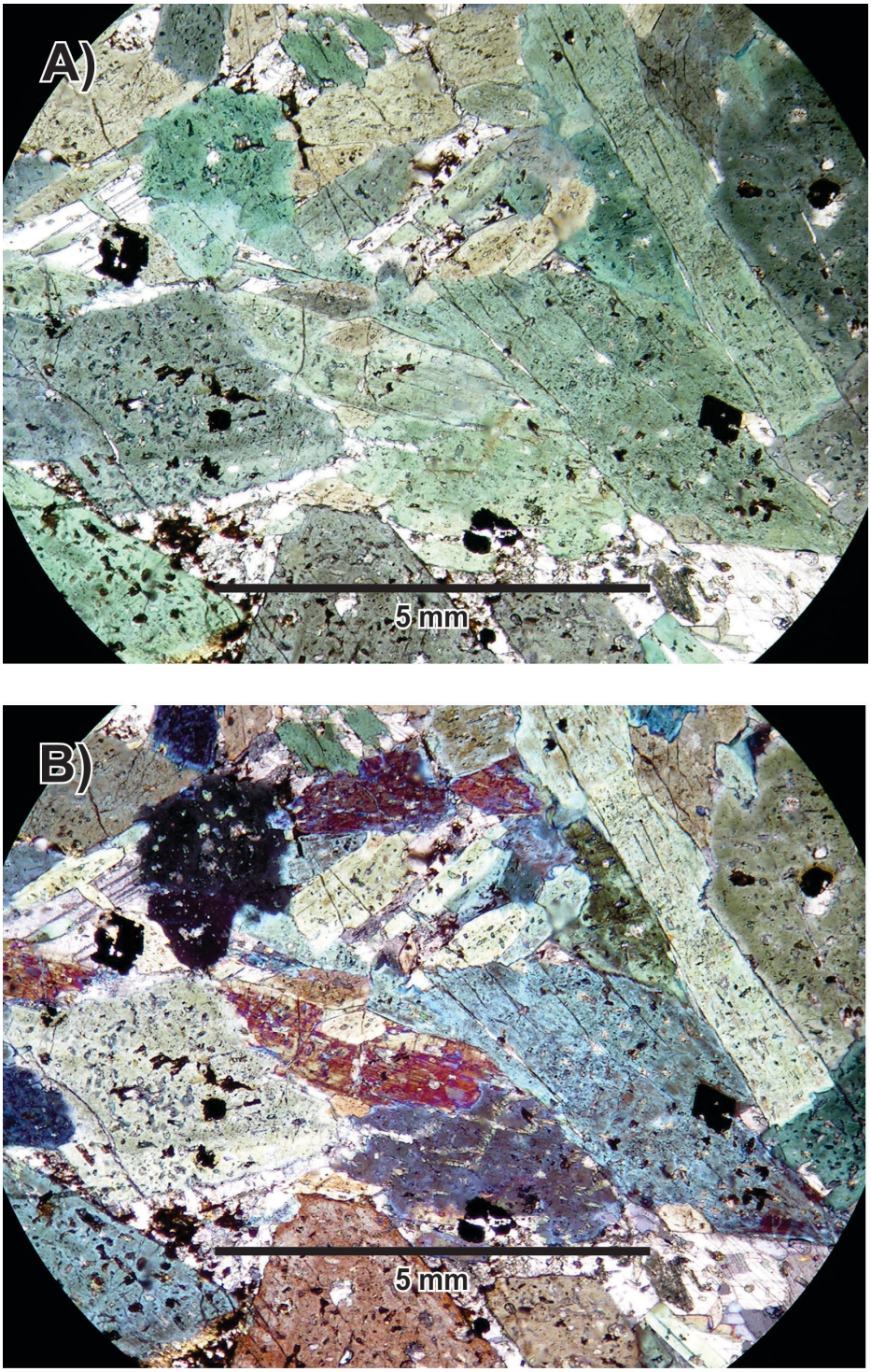

Figure C-3: (A & B) Lower volcano-sedimentary member of the Kechika Formation near the contact with the calcite carbonatite unit. Sodic metasomatism has resulted in the near complete replacement of the original sedimentary matrix by sodic pyroxenes (mostly arfvedsonite according to Mader, 1986). Sample MA089. Image (A) taken in PPL; (B) taken in XPL.

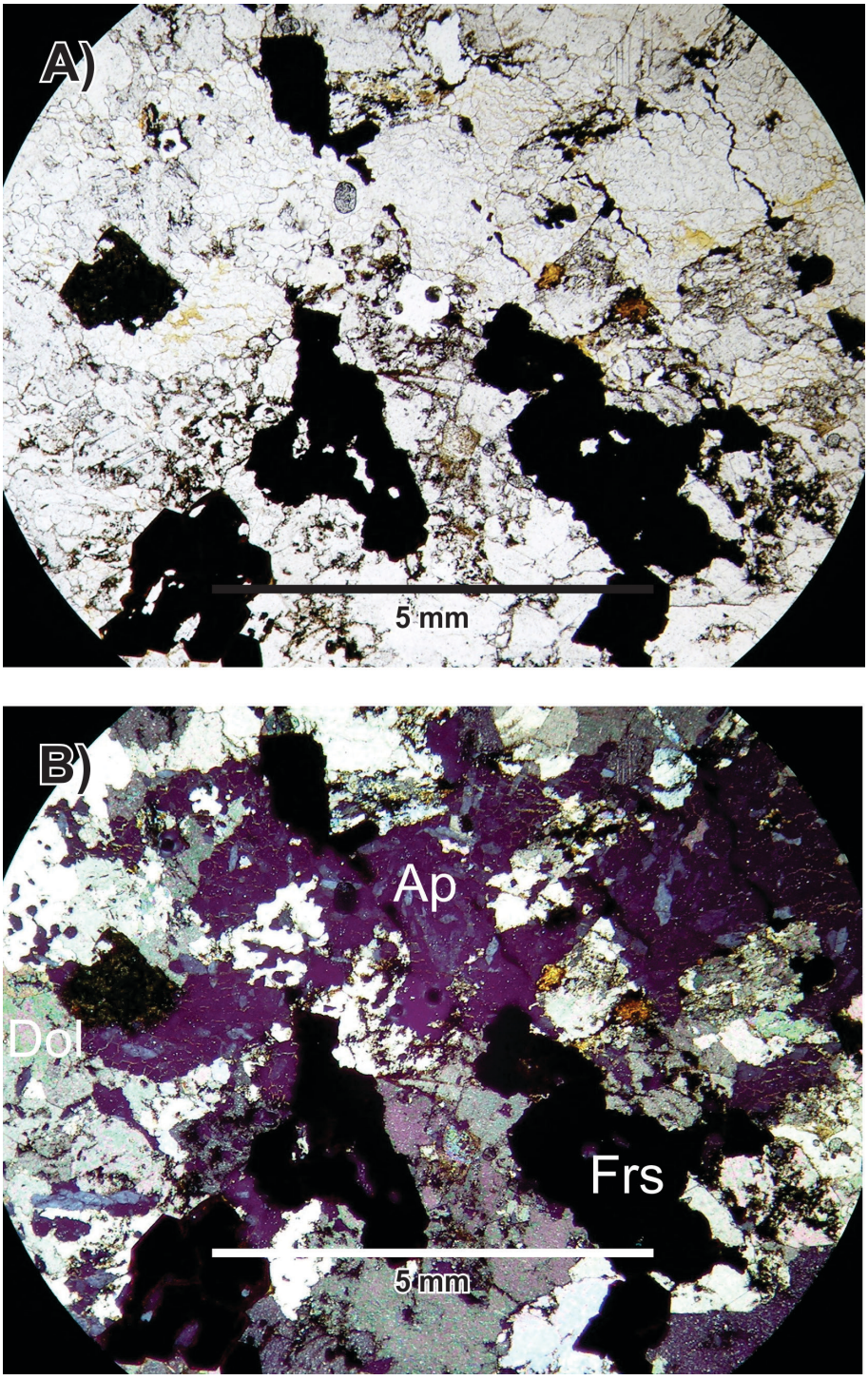

Figure C-4: (A & B) Massive (unfoliated) dolomite carbonatite near the centre of the intrusion displaying typical modal composition of the unit. Dolomite (Dol) and apatite (Ap) dominate the matrix with trace phlogopite present. Work by Kressall et al. (2010) has shown the opaque mineral to be pyrochlore +/- columbite totally or near totally pseudomorphed by acicular fersmite. Sample MA096. Image (A) taken in PPL; (B) taken in XPL.

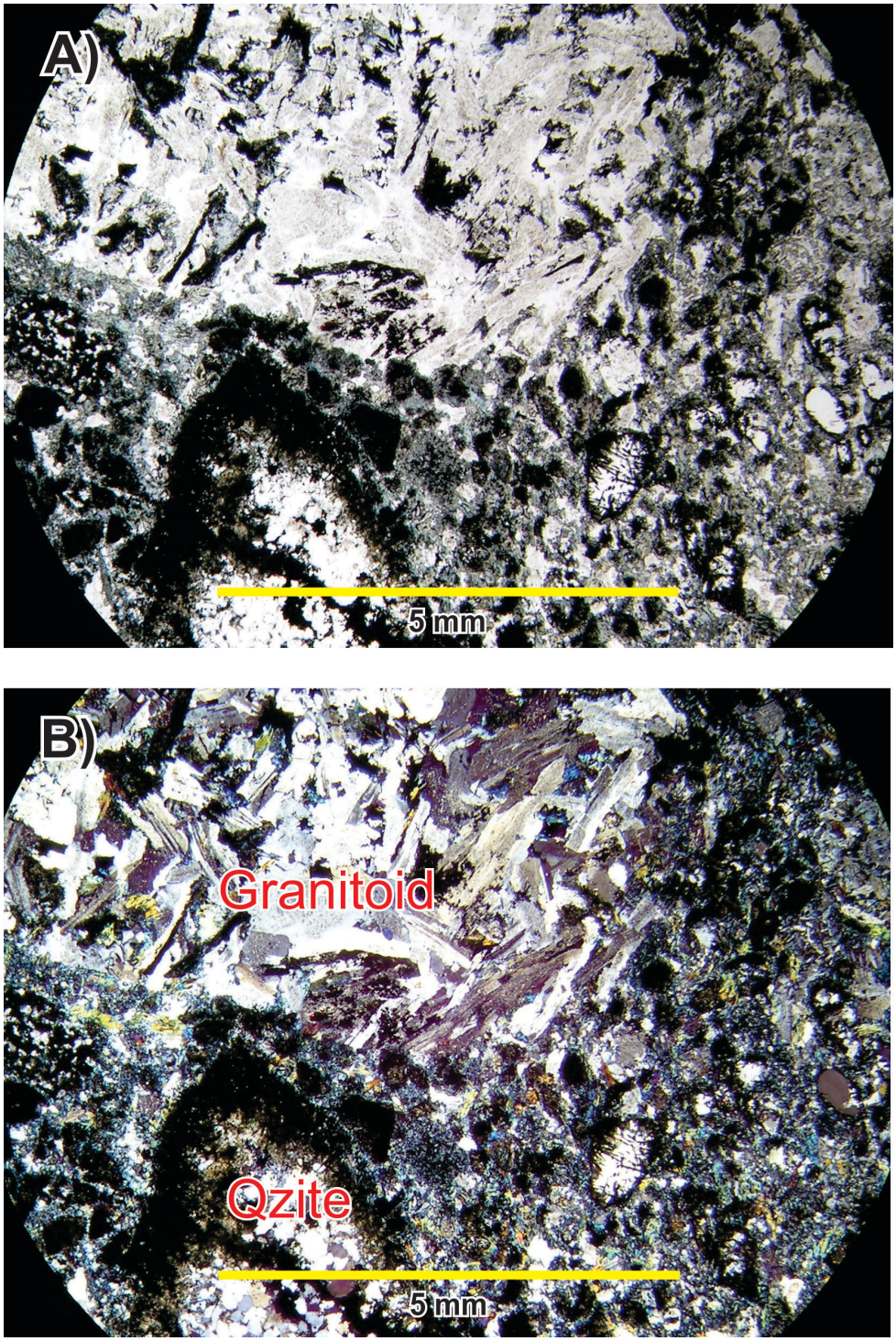

Figure C-5: (A & B) Conglomerate unit from the lower volcano-sedimentary member of the Kechika Formation hosting two distinct clasts types: (1) quartzite and (2) albite-rich granitoid. Both are of unknown origin. Strong fenitization is evidenced by near complete arfvedsonite +/- aegirine replacement of an original quartz-carbonate sedimentary matrix; chlorite alteration may also be present. Sample MA190. Image (A) taken in PPL; (B) taken in XPL.

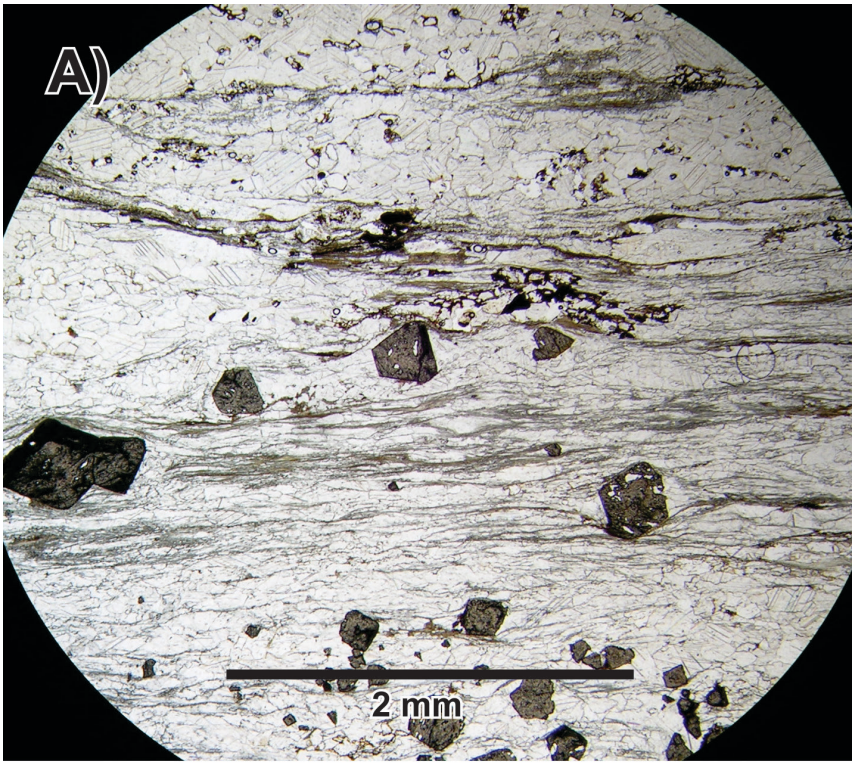

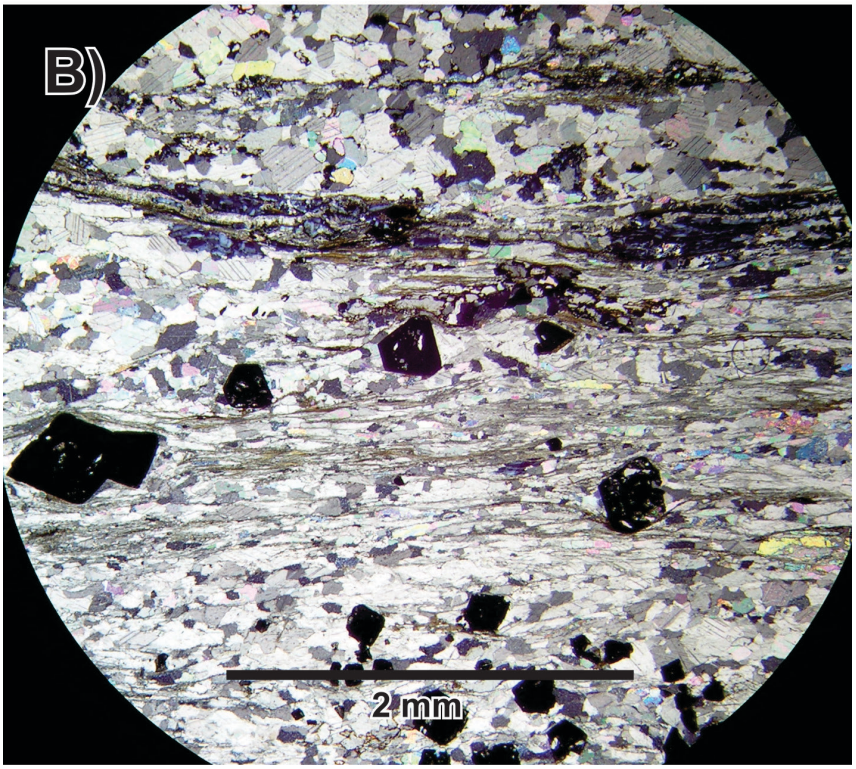

Figure C-6: (A & B) Foliated calcite carbonatite near western Kechika Formation-carbonatite contact. Dark grey to opaque dipyramidal grains are suspect metamict zircons. Sample MA049. Image (A) taken in PPL; (B) taken in XPL.

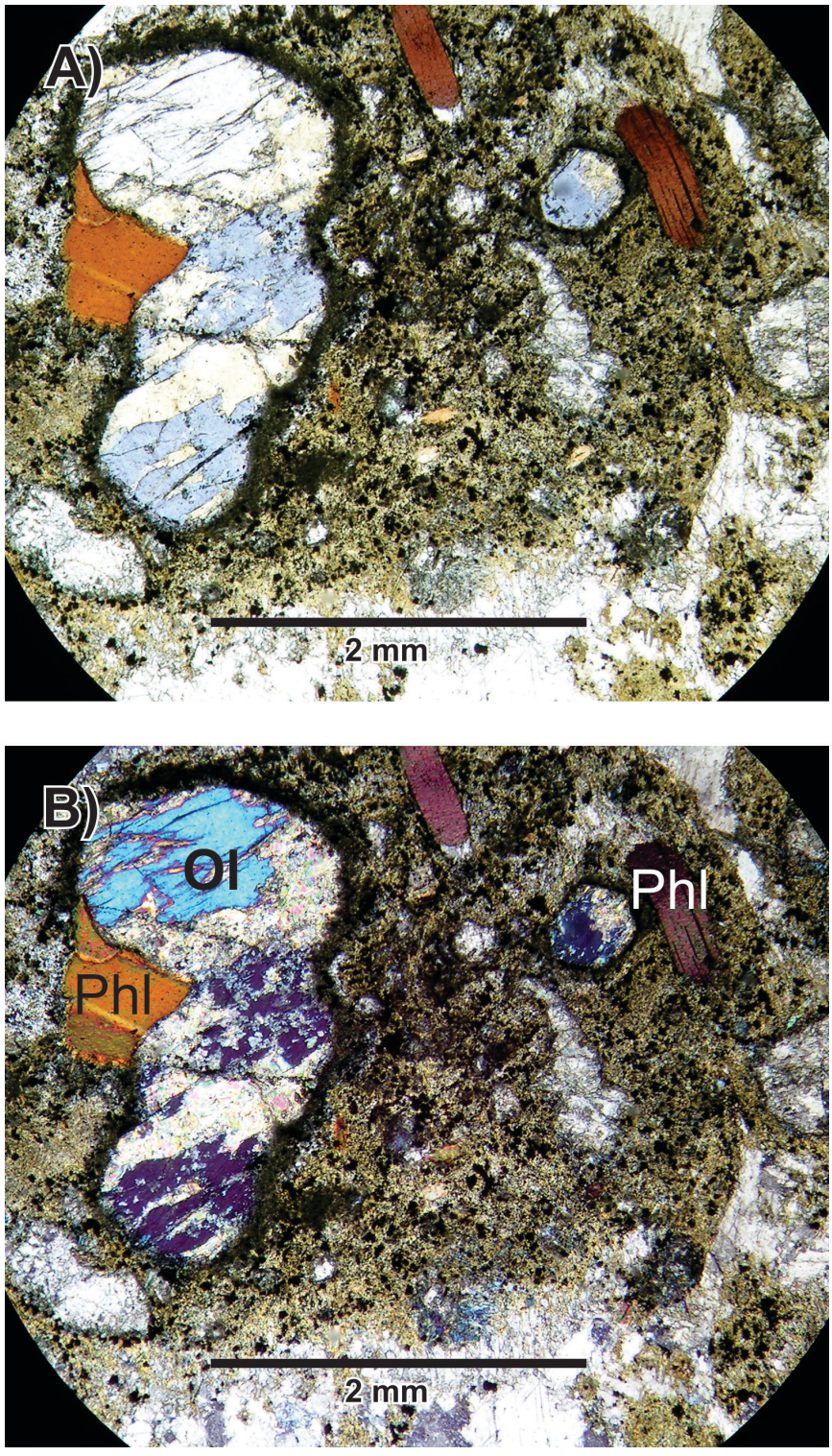

Figure C-7: (A & B) Massive phase of the Ospika pipe diatreme showing phlogopite-olivine (Phl-Ol) macrocrysts set in a very fine-grained to cryptocrystalline, hypidiomorphic dolomite-chlorite matrix. Sample MA045A. Image (A) taken in PPL; (B) taken in XPL.

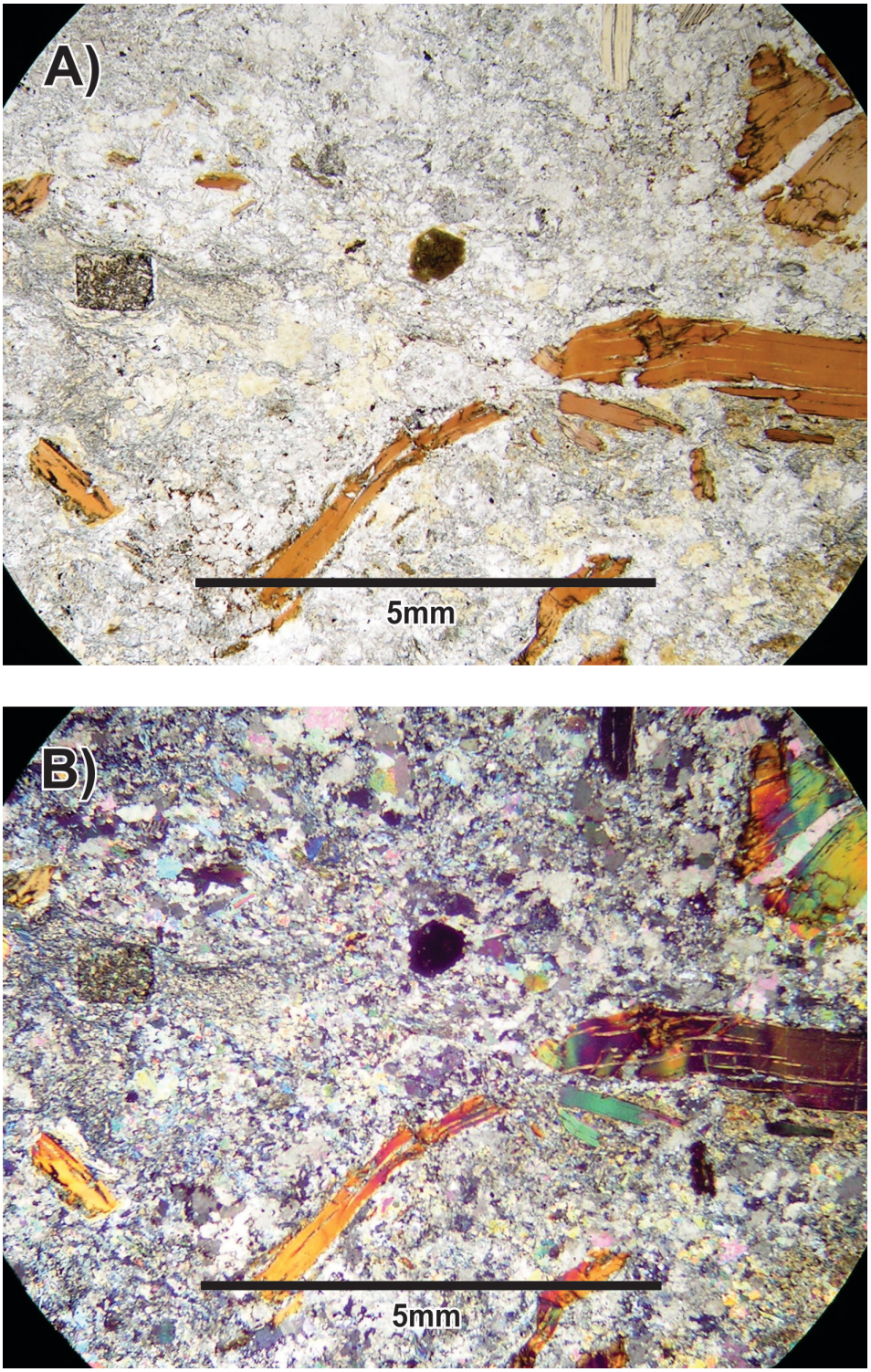

Figure C-8: (A & B) Weakly-foliated, phlogopite-rich calcite carbonatite adjacent to contact with Kechika Formation. Phlogopite content of carbonatite phases appears to increase towards contact and may be controlled by carbonatite-wallrock interactions. Sample MA012. Image (A) taken in PPL; (B) taken in XPL.

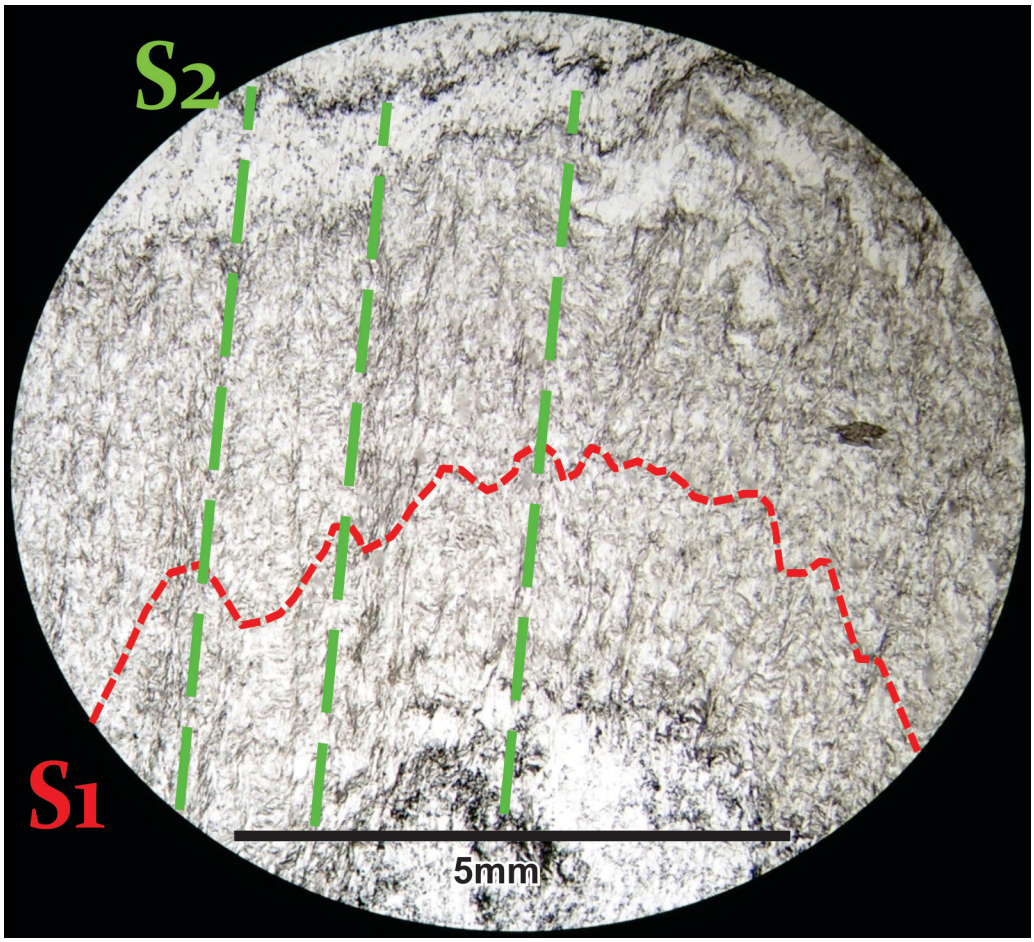

Figure C-9: Polyphase deformation in the Kechika Formation. The S_1 bedding parallel cleavage is crenulated about a later S_2 cleavage which is axial planar to Rocky Mountain (Laramide) orogen related folds in the map area. Sample MA071. Image taken in PPL.

APPENDIX D

Supplementary field photographs

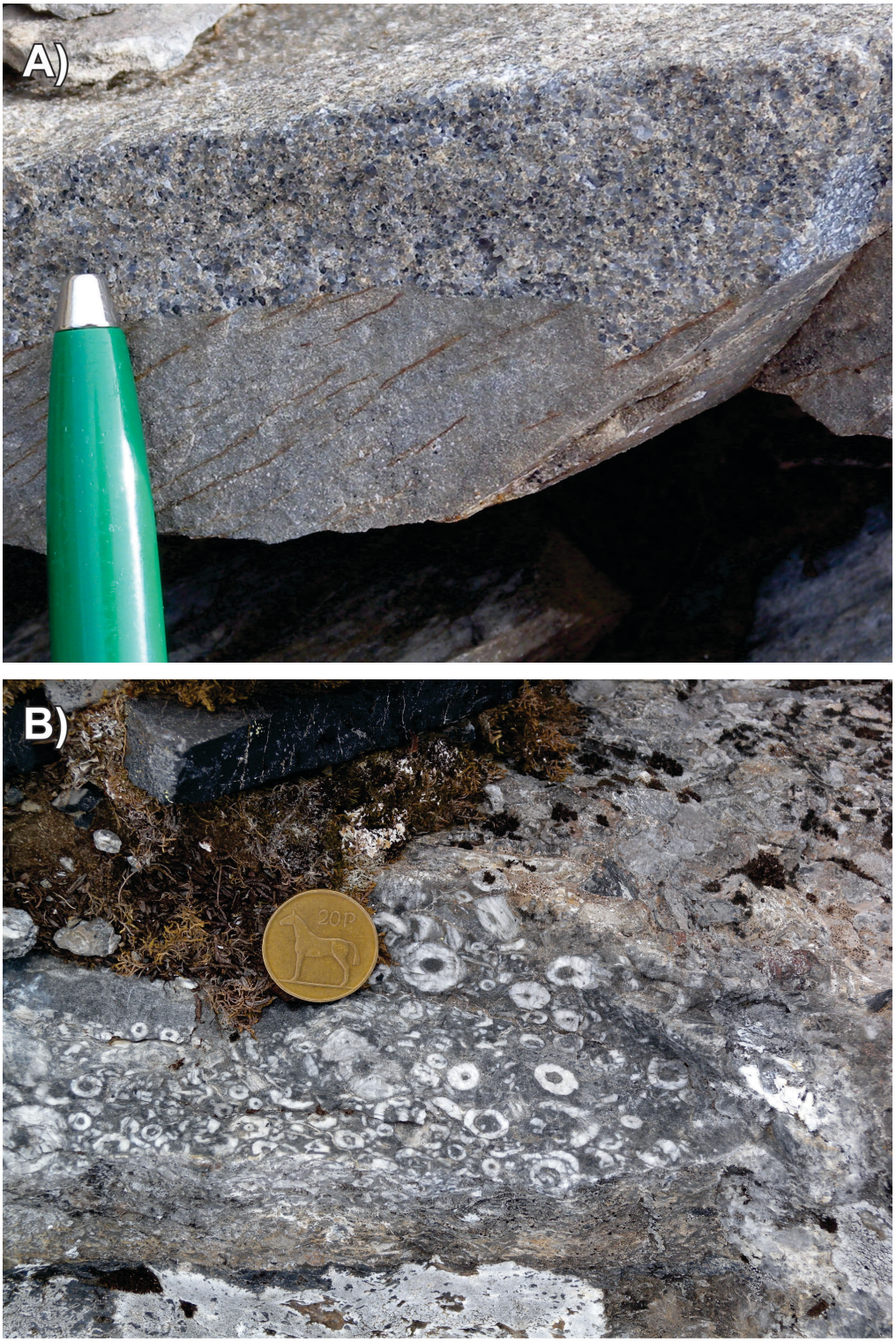

Figure D-1: (A) Medium- to coarse-grained quartz and lithic arenite beds, Devonian Road River Group. (B) Graded crinoid ossicle rich layers in fossiliferous dolostone beds, Devonian Road River Group. Cross-beds, load structures, and graded-bedding indicate that the strata are overturned.

Figure D-2: Pillow basalt textures in suspect flows from the basal Kechika Formation.

Figure D-3: Fenite haloes around xenoliths of Road River Group siltstone and argillaceous dolostone in the Ospika pipe. The groundmass consists of phlogopite-clinopyroxene-olivine macrocryst mineral assemblage hosted in a very fine-grained to cryptocrystalline, hypidiomorphic dolomite-chlorite matrix.

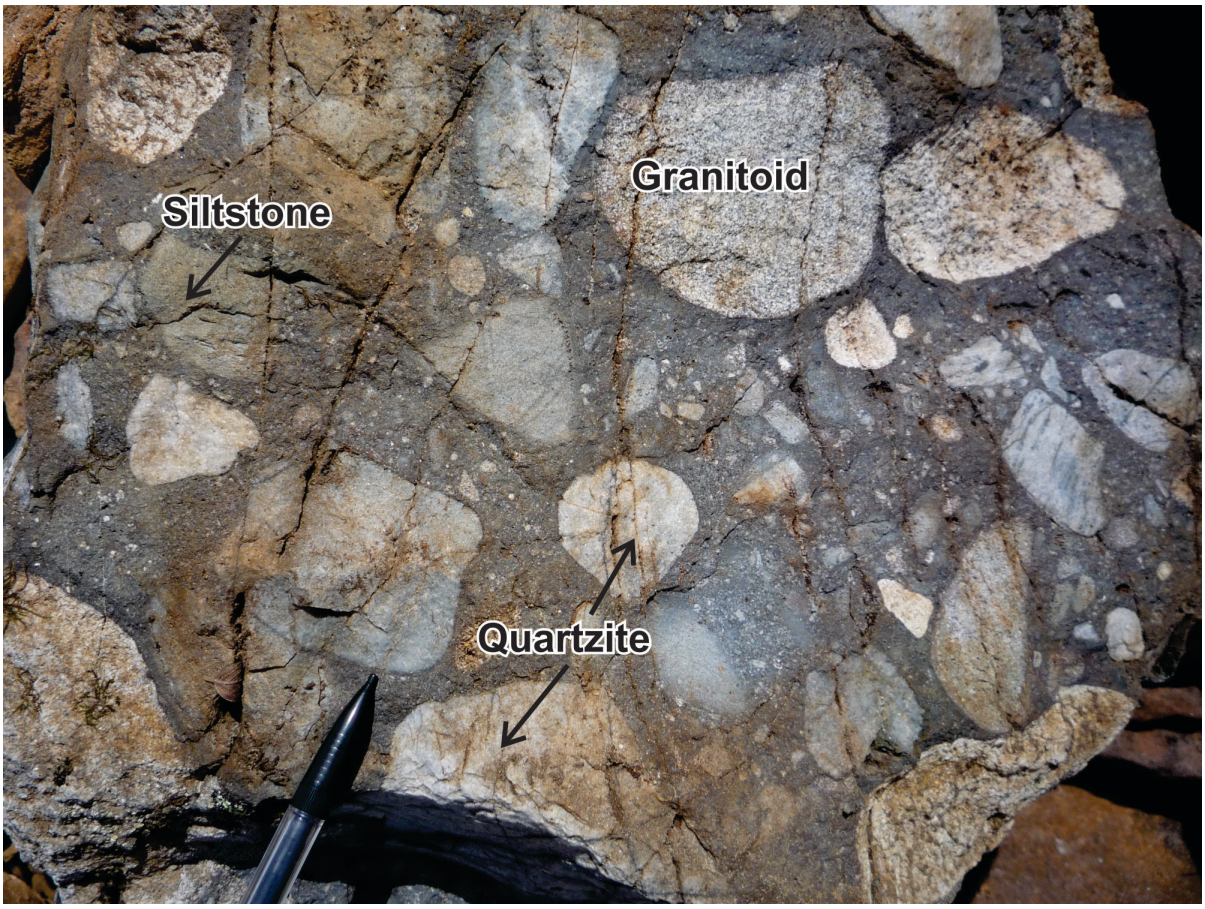

Figure D-4: Conglomerate unit from the lower volcano-sedimentary member of the Kechika Formation hosting quartzite, granitoid, and siltstone clast types. All are of unknown origin. See appendix figure C-5 for thin section images of this unit.

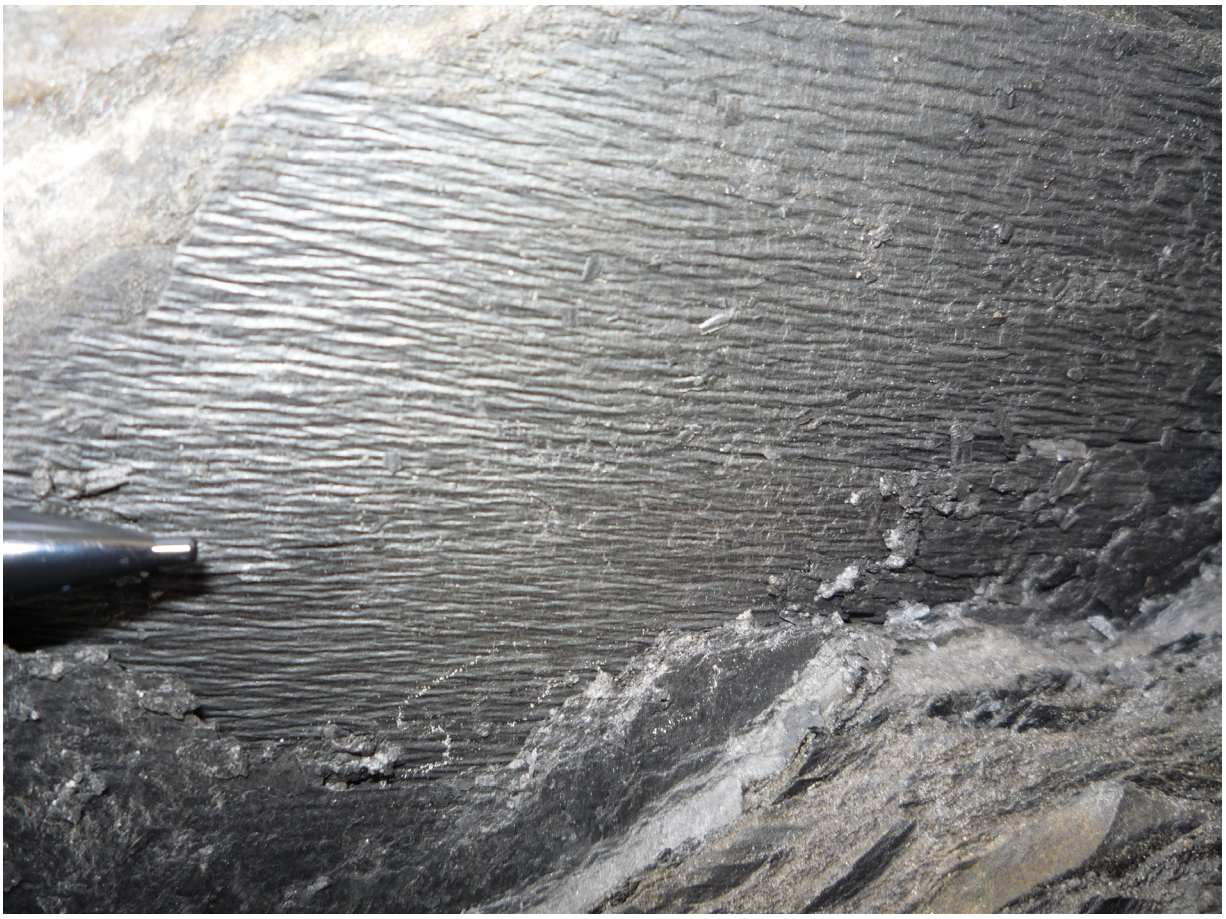

Figure D-5: S_2-S_1 cleavage intersection lineation in mudstone-siltstone layers of the Road River Group. The N-S trending, sub-horizontal orientation of this lineation is in agreement with the calculated beta-axis for F_2 folds (*cf*. stereonet in Fig. B-1). Photo credit: M. Mihalynuk.

Figure D-6: Weathered outcrop of calcite carbonatite proximal to contact with fenitized Kechika Formation (just outside of photo at right). Planar, greyish-white apatite bands are distinctly resistive relative to the calcite dominated carbonatite matrix. The fabric defined by the apatite bands is parallel to the contact, bedding, and S_1 in the Kechika Formation.

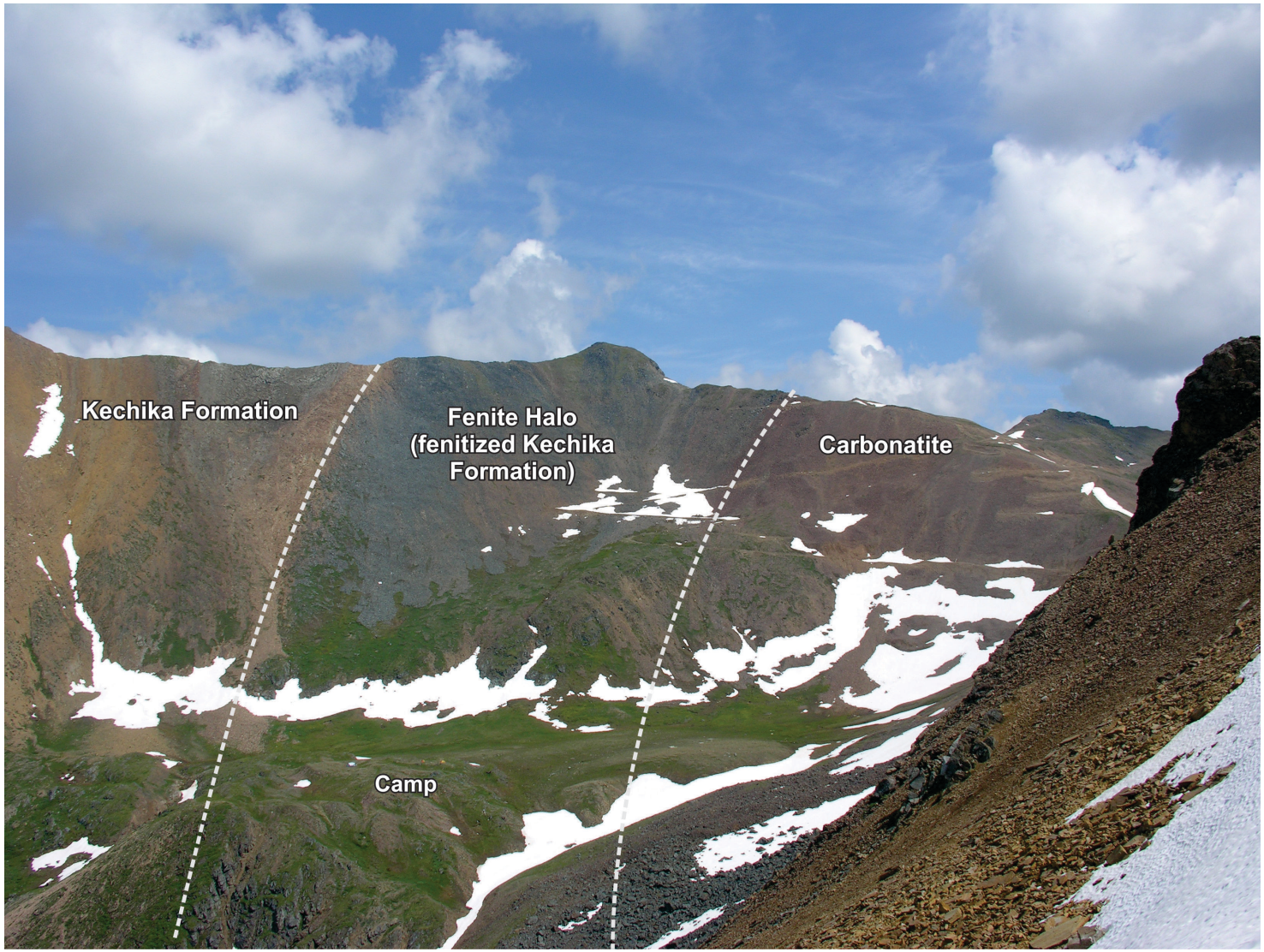

Figure D-7: View from the west-central margin of the carbonatite looking northeast showing contact relationships and alteration halo that typify the margins of the intrusion.

Figure D-8: View from north of the carbonatite intrusion looking south towards resistant, cliff-forming fenitized Kechika Formation (dark grey cliffs and scree). The small glacier in the centre of the photo is covered with orange-maroon coloured carbonatite scree being preferentially eroded from the cirque at the back of the central ridge in the photo. Person for scale.

Figure D-9: View from camp looking south towards the west-central margin of the carbonatite. Dark grey cliffs at right of photo are resistant fenitized Kechika Formation. Orange-maroon scree-cover to the left of the cliffs is eroded material from the recessive central dolomite phase of the carbonatite. Photo credit: M. Mihalynuk.

APPENDIX E

Geological maps: 1:5k field master sheets

LEGEND

ROCK UNITS

INTRUSIVE ROCKS

DEVONIAN

Aley Carbonatite Complex

Ddc — **Dolomite carbonatite**
Medium to coarse-grained, pyrite- and fersmite-bearing dolomite-apatite carbonatite, generally containing ~90% dolomite, 5-10% apatite, 2-5% pyrite, and 1-2% niobates. Weathered surfaces display a distinct orange-maroon colour; fresh surfaces are light-pink to beige. Texture varies from moderate- to weakly-foliated along intrusion margins to massive (granoblastic) in the core.

Dcc — **Calcite carbonatite**
Fine- to locally medium-grained, magnetite, pyrochlore, phlogopite-bearing calcite-apatite carbonatite, generally containing ~50-90% calcite, 2-15% apatite, 0-15% magnetite, 0-10% phlogopite, and 1-2% niobates. Weathered surfaces display grey- to chocolate-brown colour; fresh surfaces are light-grey to beige to locally white. Weak- to strongly-foliated texture defined by apatite bands.

Ospika Pipe

Dop — **Ultramafic diatreme**
Maroon-brown weathering ultramafic diatreme containing phlogopite-clinopyroxene-olivine macrocrysts set in a very fine-grained hypidiomorphic dolomite-chlorite matrix. Contains a breccia phase bearing 5-30% subangular to subrounded, randomly-oriented xenoliths of siltstone from the underlying Road River Group.

STRATIFIED ROCKS

ORDOVICIAN, SILURIAN, AND DEVONIAN

OSDr — **Road River Group**
Fissile, graptolitic shale and planar-laminated to locally cross-bedded grey weathering calcareous siltstone and argillaceous limestone. Massive, fine- to medium-grained quartzite and quartz-lithic arenite interbeds are present near middle of exposed section in map area. Metre thick dolostone beds with chert lenses occur near top of exposed section in map area.

ORDOVICIAN

Os — **Skoki Formation**
Massive to cross-bedded dolostone and bioclastic limestone containing crinoid ossicles and gastropods; chert lenses and oncolite rich layers occur near upper contact with the Road River Group. Contains a middle volcanic member composed of fine grained, marine ash-crystal tuff and flows that pass upward into agglomerates and coarser-grained volcaniclastic layers.

CAMBRIAN AND ORDOVICIAN

COk — **Kechika Formation**
Tan-brown and grey planar laminated argillaceous limestone; wavy, banded orange-brown calcareous siltstone; and massive, cream-coloured dolostone. Includes a basal volcano-sedimentary member (undifferentiated), consisting of intercalated conglomerate, pillow basalt, tuff, volcaniclastic rocks and fragmental volcanic layers.

COkf — **Fenitized Kechika Formation**
Sodic metasomatic altered rocks mostly belonging to the basal member of the Kechika Formation. Metasomatism is manifest by the development of sodic amphiboles and pyroxenes in marls, siltstones, and volcaniclastic rocks near the contact with the carbonatite, and decreases gradationally in intensity outwards from the contact.

MAP SYMBOLS

- REE-enriched lamprophyre dyke (defined, inferred)
- Bedding, unknown facing (inclined, vertical)
- Bedding, known facing (overturned)
- Mineral lamination (Scc and Scd)
- Synform (overturned anticline)
- Antiform (overturned syncline)
- F1 Fault (defined, inferred)
- Fault trace (defined, inferred)
- Stratigraphic contact (defined, inferred)
- Intrusive contact (defined, inferred)
- Extent of metasomatic contact aureole (defined, inferred)
- Mapped outcrop
- U — U-Pb isotopic date sample locality (outcrop sample)
- Ar — Ar-Ar isotopic date sample locality (outcrop sample)
- U — U-Pb detrital zircon sample locality (float sample)
- Petrographic study sample locality (outcrop sample)
- Diamond drill hole

Notes: All map data from McLeish and Johnston (2013) and McLeish et al. (2013) except - (1) carbonatite-wallrock contacts south of 6,256,000 mN and select northern areas with limited mapping coverage (from Mader, 1986); and (2) DDH data (from Cominco Ltd. and Taseko Mines Ltd. assessment reports). See reference sections in thesis text for full citation information. Diamond drill holes with no drill trace shown were drilled vertically. Geochronology and petrography samples on map correspond to samples discussed in thesis text. Mapping to date has not been sufficiently detailed to differentiate the banded magnetite-apatite cumulate unit (see thesis text and Kressall et al., 2010) documented within the dolomite carbonatite core from the dolomite carbonatite unit itself.

N

Aley Carbonatite Complex

Geology with Orthophoto

BCGS: 094B.042	NTS: 94B/05
Date: April, 2013	Scale: 1:5,000
UTM NAD83, Zone 10 N	Plotted by: DFM

LEGEND

ROCK UNITS

INTRUSIVE ROCKS

DEVONIAN

Aley Carbonatite Complex

Ddc — **Dolomite carbonatite**
Medium to coarse-grained, pyrite- and fersmite-bearing dolomite-apatite carbonatite, generally containing ~90% dolomite, 5-10% apatite, 2-5% pyrite, and 1-2% niobates. Weathered surfaces display a distinct orange-maroon colour; fresh surfaces are light-pink to beige. Texture varies from moderate- to weakly-foliated along intrusion margins to massive (granoblastic) in the core.

Dcc — **Calcite carbonatite**
Fine- to locally medium-grained, magnetite, pyrochlore, phlogopite-bearing calcite-apatite carbonatite, generally containing ~50-90% calcite, 2-15% apatite, 0-15% magnetite, 0-10% phlogopite, and 1-2% niobates. Weathered surfaces display grey- to chocolate-brown colour; fresh surfaces are light-grey to beige to locally white. Weak- to strongly-foliated texture defined by apatite bands.

Ospika Pipe

Dop — **Ultramafic diatreme**
Maroon-brown weathering ultramafic diatreme containing phlogopite-clinopyroxene-olivine macrocrysts set in a very fine-grained hypidiomorphic dolomite-chlorite matrix. Contains a breccia phase bearing 5-30% subangular to subrounded, randomly-oriented xenoliths of siltstone from the underlying Road River Group.

STRATIFIED ROCKS

ORDOVICIAN, SILURIAN, AND DEVONIAN

OSDr — **Road River Group**
Fissile, graptolitic shale and planar-laminated to locally cross-bedded grey weathering calcareous siltstone and argillaceous limestone. Massive, fine- to medium-grained quartzite and quartz-lithic arenite interbeds are present near middle of exposed section in map area. Metre thick dolostone beds with chert lenses occur near top of exposed section in map area.

ORDOVICIAN

Os — **Skoki Formation**
Massive to cross-bedded dolostone and bioclastic limestone containing crinoid ossicles and gastropods; chert lenses and oncolite rich layers occur near upper contact with the Road River Group. Contains a middle volcanic member composed of fine grained, marine ash-crystal tuff and flows that pass upward into agglomerates and coarser-grained volcaniclastic layers.

CAMBRIAN AND ORDOVICIAN

COk — **Kechika Formation**
Tan-brown and grey planar laminated argillaceous limestone; wavy, banded orange-brown calcareous siltstone; and massive, cream-coloured dolostone. Includes a basal volcano-sedimentary member (undifferentiated), consisting of intercalated conglomerate, pillow basalt, tuff, volcaniclastic rocks and fragmental volcanic layers.

COkf — **Fenitized Kechika Formation**
Sodic metasomatic altered rocks mostly belonging to the basal member of the Kechika Formation. Metasomatism is manifest by the development of sodic amphiboles and pyroxenes in marls, siltstones, and volcaniclastic rocks near the contact with the carbonatite, and decreases gradationally in intensity outwards from the contact.

MAP SYMBOLS

- REE-enriched lamprophyre dyke (defined, inferred)
- Bedding, unknown facing (inclined, vertical)
- Bedding, known facing (overturned)
- Mineral lamination (Scc and Scd)
- Synform (overturned anticline)
- Antiform (overturned syncline)
- F1 Fault (defined, inferred)
- Fault trace (defined, inferred)
- Stratigraphic contact (defined, inferred)
- Intrusive contact (defined, inferred)
- Extent of metasomatic contact aureole (defined, inferred)
- Mapped outcrop
- (U) U-Pb isotopic date sample locality (outcrop sample)
- (Ar) Ar-Ar isotopic date sample locality (outcrop sample)
- (U) U-Pb detrital zircon sample locality (float sample)
- Petrographic study sample locality (outcrop sample)
- Diamond drill hole

Notes: All map data from McLeish and Johnston (2013) and McLeish et al. (2013) except - (1) carbonatite-wallrock contacts south of 6,256,000 mN and select northern areas with limited mapping coverage (from Mader, 1986); and (2) DDH data (from Cominco Ltd. and Taseko Mines Ltd. assessment reports). See reference sections in thesis text for full citation information. Diamond drill holes with no drill trace shown were drilled vertically. Geochronology and petrography samples on map correspond to samples discussed in thesis text. Mapping to date has not been sufficiently detailed to differentiate the banded magnetite-apatite cumulate unit (see thesis text and Kressall et al., 2010) documented within the dolomite carbonatite core from the dolomite carbonatite unit itself.

N

Aley Carbonatite Complex

Geology

BCGS: 094B.042	NTS: 94B/05
Date: April, 2013	Scale: 1:5,000
UTM NAD83, Zone 10 N	Plotted by: DFM